ANNALS OF PHYSICS: 53, 439–520 (1969)

Studies of Small-Polaron Motion IV. Adiabatic Theory of the Hall Effect*†

DAVID EMIN‡§

Department of Physics, University of Pittsburgh, Pittsburgh, Pennsylvania 15213

AND

T. HOLSTEIN

Department of Physics, University of California, Los Angeles, California 90024

The two-dimensional molecular crystal model of Friedman and Holstein describing the motion of a small polaron in the presence of a magnetic field is studied in the adiabatic approximation. Upon averaging over the electronic coordinates, according to the standard prescription, one finds that the vibrational Hamiltonian contains (in addition to the usual terms, namely the carrier-free vibrational Hamiltonian supplemented by the energy of the excess electron expressed as a function of vibrational coordinates) a term which is linearly dependent on the lattice momentum and proportional to the magnetic field. In the adiabatic theory the effect of the magnetic field on the motion of the small polaron is found by studying the influence of the magnetic term of the vibrational Hamiltonian on the particular vibrational motions which correspond to the passage of the excess carrier from one site to a particular neighbor.

In the present work, concerned only with the high temperature regime (in practice, temperatures above $\frac{1}{2}\theta_{\text{Debye}}$) within which the small polaron moves through the lattice by a succession of incoherent jumps between neighboring sites, the vibrational motion is treated classically, as is appropriate at sufficiently high temperatures.

It is found that although the temperature dependence of the drift mobility that is herein calculated differs little from that derived in the Friedman–Holstein perturbation calculation, the Hall mobility temperature dependence (for reasonable choices of the physical parameters) differs markedly from the perturbation result. In particular, for appropriate choices of the physical parameters, the adiabatic Hall mobility can be a decreasing function of temperature. Thus the absence of an activated Hall mobility is not in itself evidence against small polaron motion.

* Supported in part by the U. S. Office of Aerospace Research, U. S. Air Force, AFOSR Grant No. 196–66 and by the National Science Foundation.

† Based in part on a thesis submitted to the faculty of the University of Pittsburgh in partial fulfillment of the requirements for the Ph.D. degree.

‡ NASA Predoctoral Trainee 1963-1966.

§ Present address: Division 5113, Sandia Laboratories, Albuquerque, New Mexico.

INTRODUCTION

This paper constitutes a continuation of a series of theoretical studies of the small polaron[1] which find application to low mobility materials. In these materials —specifically in materials in which the interaction between the lattice vibrations and the carrier is sufficiently strong and the carrier bandwidth is sufficiently small— an excess charge carrier will find it energetically favorable to remain localized at one of an infinite number of equivalent sites of the crystal, the electron-lattice interaction giving rise to an "induced" lattice distortion in the immediate vicinity of the carrier. The potential well produced by this distortion, in turn, acts as a trapping center for the carrier. The *self-trapped* unit consisting of the excess carrier with its induced lattice deformation is called a *small polaron.*

The theory developed in I and II predicts that with the existence of a nonvanishing electronic bandwidth the small polaron will be able to move through the lattice. In fact there are two distinct types of small polaron motion, one of which prevails in each of the two complementary temperature regimes above and below a certain transition temperature (estimated to be of the order of $\theta_{\text{Debye}}/2$). At temperatures below this transition temperature, small polaron motion is describable in terms of a band picture in which the polaron bandwidth is an exponentially decreasing function of temperature. Above this transition temperature the small polaron moves through the lattice by a succession of mutually incoherent thermally activated jumps between neighboring sites. The present work will be concerned solely with the high temperature regime in which the thermally activated hopping motion predominates.

Much of the theoretical knowledge of the effect of the hopping of small polarons on the transport properties of low mobility materials has resulted from investigating the molecular-crystal model of references I, II, and III[2] with perturbation-schemes, the validity of which requires that the physical parameters satisfy the inequality[3]

$$J^2 \ll \left(\frac{\epsilon_2 kT}{\pi}\right)^{1/2} \left(\frac{\hbar\omega_0}{\pi}\right),$$

where J is the electron transfer integral, i.e., the bandwidth parameter of conventional tight-binding theory, ϵ_2 is the activation energy associated with the thermally

[1] T. Holstein, *Ann. Phys.* (N.Y.) **8**, 325 (1959); **8**, 343 (1959) (to be referred to as I and II, respectively); L. Friedman and T. Holstein, *Ann. Phys.* (N.Y.) **21**, 494 (1963) (to be referred to as III).

[2] The two-dimensional molecular-crystal model developed in III is a generalization of the one-dimensional molecular-crystal model introduced in I.

[3] A derivation of this condition is found in Sec. VI and Appendix III of II.

activated drift mobility, and ω_0 is the longitudinal optical vibration frequency.[4] The calculations in this small-J limit yield drift and Hall mobilities which are thermally activated with the activation energy of the Hall mobility being about one-third that of the drift mobility. Since it is quite possible that the above condition is not fulfilled in many substances, we have been led to the present task of calculating the Hall and drift mobilities in the complementary regime (the adiabatic regime):

$$J^2 \gg \left(\frac{\epsilon_2 kT}{\pi}\right)^{1/2} \left(\frac{\hbar\omega_0}{\pi}\right).$$

The principal results of our investigation of the drift and Hall mobilities within the adiabatic approximation[5] may be stated simply as follows. Although the expression for the drift mobility is formally different, it still possesses the thermally-activated behavior which is predicted by the small-J theory. However, for reasonable choices of the parameters ϵ_2 and J, the temperature dependence of the Hall mobility may be quite different from the thermally-activated behavior of the small-J theory. In fact the Hall mobility may even be a decreasing function of temperature over a significant temperature range.

Thus, while the absence of a thermally activated drift mobility may be interpreted as evidence of the absence of small polaron hopping, the failure of the Hall mobility to be thermally activated may not be so simply interpreted. This situation points up the importance of unambiguous measurements of the drift mobility in low-mobility materials.

In Section I of this paper, preceding the development of the adiabatic theory, we review the basic features of the two-dimensional molecular-crystal model of Ref. III. In Section II the adiabatic approximation is introduced and the Hamiltonian governing the lattice motion is derived. It is shown that this Hamiltonian is the sum of three terms: the Hamiltonian of the carrier-free lattice, an additional potential energy term due to the presence of the excess carrier (expressed as a function of the lattice displacements), and a term which to first order in the magnetic field has the form

$$\frac{e}{Mc} \sum_{\mathbf{g}} \{A_{\mathbf{g}} P_{\mathbf{g}} + P_{\mathbf{g}} A_{\mathbf{g}}\},$$

where M is the reduced mass of a molecule of the molecular crystal, $P_{\mathbf{g}}$ is the momentum operator associated with the vibration of the $\mathbf{g}$th molecule, and $A_{\mathbf{g}}$ is

[4] Throughout the present work we shall assume that the dispersion of the longitudinal optical frequencies is sufficiently small to justify the common approximation of replacing the band of longitudinal optical frequencies by a single frequency ω_0.

[5] A systematic discussion of the results of the adiabatic theory is found in Sec. IX of this paper.

a function of the lattice coordinates and the magnetic field which vanishes in the absence of the magnetic field. Furthermore we show that for the three-site configuration of III,[6] the relevant terms in the Hamiltonian depend on only two independent lattice-displacement variables (denoted by x and y) and the corresponding momenta, p_x and p_y. In fact we describe the relevant lattice motion as the motion of a fictitious particle in the x–y plane under the influence of a field-independent force (derived from the field-independent terms of the Hamiltonian) and a field-dependent force which has the form of the Lorentz force. The fictitious "magnetic field" appearing in this term is perpendicular to the x–y plane; it, in contrast to the real field, is a function of the vibrational coordinates, x and y.

We proceed in Section III to show that the nonmagnetic potential in the reduced Hamiltonian is composed of three mutually adjacent harmonic oscillator wells,[7] the occupation by the fictitious particle of a given potential well corresponding to the occupation of one of the three lattice sites by the small polaron. Section III also contains various details concerning the x–y dependence of the inhomogeneous effective magnetic field (as well as details of the potential energy surface).

In Section IV the effect of the magnetic field on the rate at which the fictitious particle moves classically from one well to a particular neighboring well is considered and a formal expression for the magnetic field-dependent contribution to the rate at which small polarons hop from a given site to a particular neighboring site is derived.

In Section V we use the Hamilton–Jacobi theory to prove theorems that are utilized in Section VI to relate the field-dependent portion of the jump rate at a given energy to the magnetic flux associated with the passage of the inhomogeneous magnetic field through a characteristic area. Sections VII and VIII are devoted to a study of various essential features of this flux, in particular its energy dependence.

In Section IX the results of the previous sections are used to obtain final expressions for the Hall and drift mobilities. These expressions are then compared to the formulae derived in the perturbation theory of II and III. We conclude Section IX with a discussion of the significance of the results for the interpretation of Hall-effect measurements.

[6] In III, Friedman and Holstein showed that the magnetic field dependence of the jump rate (which ultimately gives rise to a Hall effect) arises from the interference between the quantum mechanical amplitude for a direct hop between two neighboring sites and the amplitude for an indirect hop involving intermediate occupancy of a third site. An appropriate geometry for the investigation of such a process is one in which the three sites involved are mutually nearest neighbors. This basic arrangement, studied in the present paper as well as in III, is illustrated in Fig. 1.

[7] The location in the $x - y$ plane of the minima of the three oscillator wells is indicated by the crosses of Fig. 2.

I. REVIEW OF THE MOLECULAR CRYSTAL MODEL

In this section let us briefly review the essential features of the molecular crystal model as used in III. The lattice is taken to be two-dimensional with the magnetic field perpendicular to the plane. Each site is taken to be a linear diatomic molecule whose orientation and center of gravity are fixed but whose internuclear separation is allowed to vary. The Hamiltonian for the lattice when no carrier is present is

$$H_L = \sum_{\mathbf{g}} \left(\frac{-\hbar^2}{2M} \frac{\partial^2}{\partial x_{\mathbf{g}}^2} + \frac{M}{2} \omega_0^2 x_{\mathbf{g}}^2 + \frac{M}{2} \sum_{\mathbf{h}} \omega_1^2 x_{\mathbf{g}} x_{\mathbf{g}+\mathbf{h}} \right), \tag{1.1}$$

where $\mathbf{g}$ is the position vector of each site and $x_{\mathbf{g}}$ is the deviation from equilibrium of the internuclear separation of site $\mathbf{g}$. Without the last term, the Hamiltonian is just that of a lattice of uncoupled harmonic oscillators. The final term provides coupling between various nearest neighbor sites, giving rise to dispersion of the vibrational frequencies.

The problem of carrier motion through this lattice is formulated in terms of the tight binding approximation. The total state of the system is written as

$$\Psi(\mathbf{r}, \cdots x_{\mathbf{g}} \cdots) = \sum_{\mathbf{g}} a_{\mathbf{g}}(\cdots x_{\mathbf{g}} \cdots) \, \phi_{\mathbf{g}}(\mathbf{r}, x_{\mathbf{g}}), \tag{1.2}$$

where $\phi_{\mathbf{g}}$, the electronic wave function, satisfies the equation

$$\left[\frac{1}{2m} \left(\frac{\hbar}{i} \operatorname{grad}_{\mathbf{r}} + \frac{e\mathbf{A}}{c} \right)^2 + U(\mathbf{r} - \mathbf{g}, x_{\mathbf{g}}) \right] \phi_{\mathbf{g}}(\mathbf{r}, x_{\mathbf{g}}) = E(x_{\mathbf{g}}) \, \phi_{\mathbf{g}}(\mathbf{r}, x_{\mathbf{g}}), \tag{1.3}$$

where $U(\mathbf{r} - \mathbf{g}, x_{\mathbf{g}})$ is the contribution of molecule $\mathbf{g}$ to the effective one electron potential, $E(x_{\mathbf{g}})$ generally depends on $x_{\mathbf{g}}$, and the gauge is taken so that

$$\mathbf{A} = \tfrac{1}{2}\mathbf{H} \times \mathbf{r}. \tag{1.4}$$

Using the relations (1.1)–(1.3), and making the approximations which are appropriate to the tight binding case, equations may be found for the $a_{\mathbf{g}}(\cdots x_{\mathbf{g}} \cdots)$. Additional simplifying assumptions are now introduced. These are:

a) The local electronic energy $E(x_{\mathbf{g}})$ is taken to be linear in $x_{\mathbf{g}}$ (dropping the additive constant $E(0)$ for convenience): $E = -Ax_{\mathbf{g}}$.

b) The energy terms which appear added to $E(x_{\mathbf{g}})$ and take account of the dependence of the electronic energy on the lattice displacements of neighboring sites are neglected.

c) The dependence of transfer type integrals on $x_{\mathbf{g}}$ is neglected. Hence all transfer integrals are written as $-J$, a constant.

d) The vibrational axes of the diatomic molecules and the magnetic field are taken parallel, both being perpendicular to the plane of the lattice. Discussion of these approximations are found in the three earlier works. In addition to the arbitrarily small magnetic field, a small electric field, **F**, is also applied. The set of equations which is found for the $a_{\mathbf{g}}(\cdots x_{\mathbf{g}} \cdots)$ is: [cf. Eq. (1.29) of Ref. III]

$$i\hbar(\partial a_{\mathbf{g}}/\partial t) = (H_{\mathrm{L}} - Ax_{\mathbf{g}} + e\mathbf{F}\cdot\mathbf{g})a_{\mathbf{g}} - J\sum_{\mathbf{h}} a_{\mathbf{g}+\mathbf{h}} \exp(i\alpha_{\mathbf{g},\mathbf{g}+\mathbf{h}}), \tag{1.5}$$

where

$$\alpha_{\mathbf{g},\mathbf{g}+\mathbf{h}} \equiv -\frac{e}{\hbar c}\mathbf{H}\cdot\mathbf{A}_{\mathbf{g},\mathbf{g}+\mathbf{h}}\,; \qquad A_{\mathbf{g},\mathbf{g}+\mathbf{h}} \equiv \frac{1}{2}[(\mathbf{g}+\mathbf{h})\times\mathbf{g}]. \tag{1.6}$$

The magnetic phase factors $a_{\mathbf{g},\mathbf{g}+\mathbf{h}}$ are not unique since the origin is arbitrary; however, the sum of three or more phase factors corresponding to a closed path is uniquely determined. For a triangular path

$$\alpha_{\mathbf{g}_1,\mathbf{g}_2} + \alpha_{\mathbf{g}_2,\mathbf{g}_3} + \alpha_{\mathbf{g}_3,\mathbf{g}_1} = \frac{e}{\hbar c}\mathbf{H}\cdot\mathbf{A}_{321} \equiv \alpha, \tag{1.7}$$

where $\mathbf{A}_{321} = \frac{1}{2}(\mathbf{h}_{21}\times\mathbf{h}_{31})$, the area of the enclosed triangle.

The calculation will be concerned with a lattice which has three mutually near neighbor sites as shown in Fig. 1. In the absence of the external fields, symmetry dictates that the probabilities of hops from site 1 to either site 2 or 3 be equal. When a magnetic field is applied perpendicular to the plane of the paper, this equality will be destroyed. If the change in the jump rate due to the magnetic field is proportional to the magnetic field strength, a Hall effect will result.

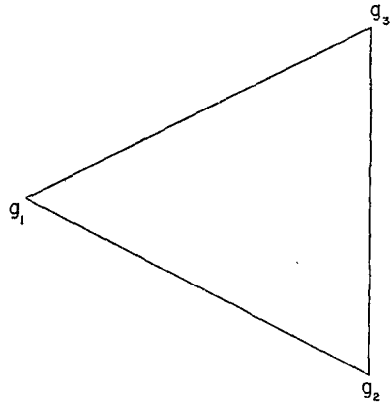

FIG. 1. The location of the three basic sites labeled by their site vectors.

For convenience, the electric field term will be dropped from the electronic energy. It can be reinserted whenever necessary by the prescription

$$-Ax_{\mathbf{g}} \rightarrow -Ax_{\mathbf{g}} + e\mathbf{F}\cdot\mathbf{g}.$$

II. DERIVATION OF THE VIBRATIONAL HAMILTONIAN

Let us begin by assuming that site 1 is occupied by the carrier (i.e., $|a_1| \gg |a_2|$, $|a_3|$). If a hop is to take place to site 2 or 3, $|a_2|$ and/or $|a_3|$ will increase and $|a_1|$ will decrease. During the time of a single hop only the $a_{\mathbf{g}}$'s of the three mutual nearest neighbors can be large. Hence we are led to the consideration of the following coupled equations:

$$\begin{aligned}
i\hbar\frac{\partial a_1}{\partial t} &= (H_{\mathrm{L}} - Ax_1)a_1 - J[\exp(i\alpha_{12})a_2 + \exp(i\alpha_{13})a_3] \\
i\hbar\frac{\partial a_2}{\partial t} &= (H_{\mathrm{L}} - Ax_2)a_2 - J[\exp(i\alpha_{23})a_3 + \exp(i\alpha_{21})a_1 \\
i\hbar\frac{\partial a_3}{\partial t} &= (H_{\mathrm{L}} - Ax_3)a_3 - J[\exp(i\alpha_{31})a_1 + \exp(i\alpha_{32})a_2].
\end{aligned} \tag{2.1}$$

In the adiabatic approach, one approximates the "wave function" $a_{\mathbf{p}}(\cdots x_{\mathbf{g}}\cdots)$ by the *Product-Ansatz*

$$a_{\mathbf{p}}(\cdots x_{\mathbf{g}}\cdots) = C_{\mathbf{p}}(\cdots x_{\mathbf{g}}\cdots)\,\chi(\cdots x_{\mathbf{g}}\cdots). \tag{2.2}$$

Here the "electronic" wave function is an eigenfunction of the "electronic" Hamiltonian; in particular, the $C_p(\cdots x_{\mathbf{g}}\cdots)$'s are normalized solutions of the equations

$$\begin{aligned}
WC_1 &= -Ax_1C_1 - J[\exp(i\alpha_{12})C_2 + \exp(i\alpha_{13})C_3] \\
WC_2 &= -Ax_2C_2 - J[\exp(i\alpha_{23})C_3 + \exp(i\alpha_{21})C_1] \\
WC_3 &= -Ax_3C_3 - J[\exp(i\alpha_{31})C_1 + \exp(i\alpha_{32})C_2]
\end{aligned} \tag{2.3}$$

gotten from (2.1) by discarding the lattice Hamiltonian.[8]

At this point it should be remarked that, while (2.3) possesses three solutions, the one of interest to us is the (nondegenerate) one pertaining to the lowest eigenvalue of W.

[8] The crucial step is actually to drop the kinetic energy term, $(-\hbar^2/2M)\sum_{\mathbf{g}}\partial^2/\partial x_{\mathbf{g}}^2$ of H_{L}, whereupon the vibrational coordinates $x_{\mathbf{g}}$ become simply parameters in (2.3). The potential energy term of H_{L} is then simply a number and may also be discarded.

Substituting (2.2) into (2.1) [with concomitant use of (2.3)], and multiplying by C_1^*, C_2^*, and C_3^*, respectively, one obtains (with $\sum_p | C_p |^2 = 1$):

$$\left[H_L + W + \frac{\hbar}{i}\sum_g\sum_p C_p^* \frac{\partial C_p}{\partial x_g}\left(\frac{\hbar}{iM}\frac{\partial}{\partial x_g}\right) + \frac{1}{2M}\left(\frac{\hbar}{i}\right)^2 \sum_g\sum_p C_p^* \frac{\partial^2 C_p}{\partial x_g^2}\right]\chi(\cdots x_g \cdots)$$

$$= i\hbar \frac{\partial}{\partial t}\chi(\cdots x_g \cdots). \tag{2.4}$$

It is noted that in the absence of a magnetic field the C_p's, as determined from (2.3), can be chosen real and

$$\sum_p C_p^* \frac{\partial C_p}{\partial x_g} = \sum_p C_p \frac{\partial C_p}{\partial x_g} = \frac{1}{2}\sum_p \frac{\partial C_p^2}{\partial x_g} = \frac{1}{2}\frac{\partial}{\partial x_g}\left(\sum_p C_p^2\right) = 0. \tag{2.5}$$

It is this term which, as will be seen below, manifests the influence of the magnetic field on the system.

The eigenvalue equation for χ may be rewritten by noting the following relation (derived in Appendix A)

$$i\left(\mathrm{Im}\sum_p C_p^* \frac{\partial^2 C_p}{\partial x_g^2}\right) = \frac{\partial}{\partial x_g}\left(\sum_p C_p^* \frac{\partial C_p}{\partial x_g}\right). \tag{2.6}$$

Hence we have

$$\left\{H_L + W + \frac{1}{M}\sum_g\sum_p\left[\frac{\hbar}{i} C_p^* \frac{\partial C_p}{\partial x_g} P_g + \frac{\hbar}{2i}\frac{\partial}{\partial x_g}\left(\frac{\hbar}{i} C_p^* \frac{\partial C_p}{\partial x_g}\right)\right.\right.$$

$$\left.\left. + \frac{1}{2}\left(\frac{h}{i}\right)^2 \mathrm{Re}\left(C_p^* \frac{\partial^2 C_p}{\partial x_g}\right)\right]\right\}\chi = ih\frac{\partial}{\partial t}\chi. \tag{2.7}$$

It is further noted that

$$\left(\sum_p \frac{\hbar}{i} C_p^* \frac{\partial C_p}{\partial x_g}\right) P_g + \frac{\hbar}{2i}\frac{\partial}{\partial x_g}\left(\sum_p \frac{\hbar}{i} C_p^* \frac{\partial C_p}{\partial x_g}\right)$$

$$= \left(\sum_p \frac{\hbar}{i} C_p^* \frac{\partial C_p}{\partial x_g}\right) P_g + \frac{1}{2} P_g \left(\sum_p \frac{\hbar}{i} C_p^* \frac{\partial C_p}{\partial x_g}\right) - \frac{1}{2}\left(\sum_g \frac{\hbar}{i} C_p^* \frac{\partial C_p}{\partial x_g}\right) P_g$$

$$= \frac{1}{2}\left[\left(\frac{\hbar}{i}\sum_p C_p^* \frac{\partial C_p}{\partial x_g}\right) P_g + P_g\left(\frac{\hbar}{i}\sum_p C_p^* \frac{\partial C_p}{\partial x_g}\right)\right]. \tag{2.8}$$

Finally the Hamiltonian for the lattice motion (adiabatic motion) is given by

$$\mathscr{H} = H_{\mathrm{L}} + W(\cdots x_{\mathrm{g}} \cdots) + \frac{1}{2M}\left[\sum_{\mathrm{g}}\left(\frac{\hbar}{i}\sum_{p} C_p^* \frac{\partial C_p}{\partial x_{\mathrm{g}}}\right) P_{\mathrm{g}} + P_{\mathrm{g}}\left(\frac{\hbar}{i}\sum_{p} C_p^* \frac{\partial C_p}{\partial x_{\mathrm{g}}}\right)\right]$$
$$- \frac{\hbar^2}{2M}\,\mathrm{Re}\left[\sum_{\mathrm{g}}\sum_{p} C_p^* \frac{\partial^2 C_p}{\partial x_{\mathrm{g}}^2}\right]. \tag{2.9}$$

The first term is just the Hamiltonian for the lattice without a carrier being present; the second represents the characteristic potential energy term of the adiabatic theory, i.e., the potential energy arising from the dependence of the electron energy on the vibrational coordinates. The third term is the crucial one of the present treatment; it represents the effect of the magnetic field on the vibrational motion via its effect on the carrier.[9] Finally, the fourth term of (2.9), which is negligibly small within the range of validity of the theory, will be discarded.

[To clarify this point let us first observe that the reality of this term implies an even magnetic field dependence. Therefore the magnetic field dependence of this term is irrelevant for considerations of the Hall effect and can safely be neglected. To obtain an estimate of the magnitude of this term let us remark, as will be shown in Sec. 3, that the x_{g} variation of the C_{g}'s [as determined by solving Eqs. (2.3)] is on a scale of $4\,J/A$, so that differentiation with respect to the x's is equivalent (in order of magnitude) to multiplication by $A/4J$. The fourth term of (12.9), H_4, is then $\sim(\hbar^2/2M)(A^2/16J^2)$. Furthermore we shall see in Sec. III that for the variation of the x_{g}'s over which the C_{g}'s change, the change in the remaining potential energy term of (2.9) is of order of J. Therefore the fourth term may be neglected if $H_4 \ll J$, that is, if

$$\frac{H_4}{J} \sim \frac{(\hbar\omega_0)^2}{J^2}\,\frac{(A^2/4M\omega_0^2)}{8J} \sim \frac{(\hbar\omega_0)^2\,\epsilon_2}{8J^3} \ll 1,$$

where $\epsilon_2 = (A^2/4M\omega_0^2)$. To show that the above condition is satisfied within the framework of the classical adiabatic theory (i.e., in which the vibrational motion is treated classically, as in the present treatment) one notes that a condition for the validity of the classical theory is that the relative variation of the deBroglie wavelength within a wavelength be small, i.e.,

$$\lambda\,\frac{d}{dx}\ln\lambda = \frac{d\lambda}{dx} \ll 1.$$

[9] It should be noted that the term is of the form $(e/2Mc)\,\Sigma_{\mathrm{g}}\,(A_{\mathrm{g}}P_{\mathrm{g}} + P_{\mathrm{g}}A_{\mathrm{g}})$. It is then evident, as will be seen explicitly below, that it gives rise to an effective magnetic field, obtainable by appropriate differentiations of the A_{g} with respect to the x_{g}.

Let us apply this condition to the region of vibrational coordinates x_1, x_2, x_3, situated about the "triple coincidence," $x_1 = x_2 = x_3$ (specifically $x_1 - x_2$, $x_2 - x_3$, $x_3 - x_1 \sim J/A$ within which, as will be shown in Sec. III, the potential energy varies by an amount of the order of J). Furthermore, at temperatures which will be of interest to us ($kT \lesssim J$) a characteristic value of the momentum in the vicinity of the triple coincidence is $\sqrt{2MJ}$. Thus a necessary condition for the validity of this classical adiabatic theory is

$$1 \gg \frac{d\lambda}{dx} \sim \frac{\hbar/\sqrt{2MJ}}{2J/A} = \left[\frac{(\hbar\omega_0)^2\,(A^2/4M\omega_0^2)}{2J^3}\right]^{1/2} = 2(H_4/J)^{1/2},$$

i.e., $H_4/J \ll 1$.] Q.E.D.

Let us now obtain expressions for the C_p's. For this purpose it is convenient to introduce new parameters:

$$\begin{aligned} X &\equiv W + Ax_1 - Je^{-i\alpha} \\ Y &\equiv W + Ax_2 - Je^{-i\alpha} \\ Z &\equiv W + Ax_3 - Je^{-i\alpha}, \end{aligned} \tag{2.10}$$

where α is defined by (1.7). One then obtains[10] from (2.3)

$$\begin{aligned} \frac{C_2}{C_1} &= \frac{X}{Y^*}\frac{\exp(i\alpha_{23})}{\exp(i\alpha_{13})} \\ \frac{C_3}{C_1} &= \frac{X^*}{Z}\frac{\exp(i\alpha_{32})}{\exp(i\alpha_{12})}. \end{aligned} \tag{2.11}$$

In order to proceed further, the lowest eigenvalue of (2.3), W, must be examined. This involves finding the solution to the cubic:

$$\begin{aligned} W^3 + W^2[A(x_1 + x_2 + x_3)] + W[A^2(x_1x_2 + x_2x_3 + x_3x_1) - 3J^2] + A^3x_1x_2x_3 \\ -J^2A(x_1 + x_2 + x_3) + 2J^3\cos\alpha = 0. \end{aligned} \tag{2.12}$$

In that α is infinitesimally small and enters (2.12) as an even function we may set $\cos\alpha = 1$; the lowest order correction to W will be proportional to H^2, and hence is ignorable.

Making the orthogonal transformation to the coordinates

$$\begin{aligned} x &= (x_2 + x_3 - 2x_1)/\sqrt{6} \\ y &= (x_3 - x_2)/\sqrt{2} \\ z &= (x_1 + x_2 + x_3)/\sqrt{3} \end{aligned} \tag{2.13}$$

[10] The equation for C_2/C_1 is obtained by eliminating C_3 from the first and second equations of (2.3); that for C_3/C_1, by eliminating C_2 from the first and third equations of (2.3).

and the substitution

$$W = \epsilon - \frac{Az}{\sqrt{3}} \tag{2.14}$$

we find the following cubic for ϵ:

$$\epsilon^3 - 3\epsilon[(A/\sqrt{6})^2 (x^2 + y^2) + J^2] + 2[(A/\sqrt{6})^3 (3y^2 - x^2)x + J^3] = 0. \tag{2.15}$$

The important fact to note is that ϵ will only be a function of x and y, and not of z. Noting the inverse transformations

$$\begin{aligned} x_1 &= z/\sqrt{3} - 2x/\sqrt{6} \\ x_2 &= z/\sqrt{3} + (x - \sqrt{3}y)/\sqrt{6} \\ x_3 &= z/\sqrt{3} + (x + \sqrt{3}y)/\sqrt{6}, \end{aligned} \tag{2.16}$$

it becomes apparent that

$$\begin{aligned} W + Ax_1 &= \epsilon(x, y) - 2Ax/\sqrt{6} \\ W + Ax_2 &= \epsilon(x, y) + A(x - \sqrt{3}y)/\sqrt{6} \\ W + Ax_3 &= \epsilon(x, y) + A(x + \sqrt{3}y)/\sqrt{6}. \end{aligned} \tag{2.17}$$

Therefore we see that the C_p's, as shown by (2.11), will be independent of z. This is a manifestation of the fact that only the *relative* site coordinates determine the probability of a site being occupied. Within the framework of classical adiabatic theory, the problem is then to study the time variation of these coordinates in terms of appropriate initial conditions (i.e., corresponding to a given site, say site 1, being occupied at $t = -\infty$). To this end it is first necessary to derive classical equations of motion for the coordinates x and y.

In the interest of simplicity, it is at this point desirable to introduce the (previously employed) approximation[11] of neglecting the so-called dispersion terms of H_L (i.e., those terms in (1.1) which are proportional to ω_1^2). With this approximation, one may write H_L in the form

$$H_L = H_L^{(3)} + H_L^{(N-3)}, \tag{2.18a}$$

[11] Cf., T. Holstein, Studies II, especially pp. 363–366, 370–374, 389; also FH Studies III, pp. 508–510. As shown in these works, this neglect does not introduce any substantial physical modifications provided one disregards, as we shall do, the circumstance in which the hop of an electron from one site to its neighbor is followed by an immediate return hop. The role of dispersion in such a process is discussed below (cf., the first bracketed insert of Sec. IV).

where $H_L^{(N-3)}$ depends on all the vibrational coordinates other than those pertaining to the three sites under consideration (i.e., other than g_1, g_2, and g_3) and where

$$H_L^{(3)} = \sum_{g=1,2,3} \left(-\frac{\hbar^2}{2M} \frac{\partial^2}{\partial x_g^2} + \frac{M}{2} \omega_0^2 (x_g^2) \right)$$

$$= -\frac{\hbar^2}{2M} \left(\frac{\partial^2}{\partial x^2} + \frac{\partial^2}{\partial y^2} + \frac{\partial^2}{\partial z^2} \right) + \frac{M}{2} \omega_0^2 (x^2 + y^2 + z^2) \quad (2.18b)$$

[the second equality being obtained by use of (2.16)]. Introducing (2.18a) and (2.18b) into (2.9), and discarding both $H_L^{(N-3)}$ and the z-dependent terms of (2.18b) and (2.14) (which, with the above-introduced neglect of the dispersion terms, are clearly seen to play no role in the dynamics of the x and y coordinates) one has

$$\mathscr{H} = \frac{1}{2M} (p_x^2 + p_y^2) + \frac{M}{2} \omega_0^2 (x^2 + y^2) + \epsilon(x, y) + \frac{e}{2Mc} (\mathbf{A} \cdot \mathbf{p} + \mathbf{p} \cdot \mathbf{A}), \quad (2.19)$$

where[12]

$$\frac{e\mathbf{A}}{c} \equiv (\hbar/i) \sum_{p=1}^{3} C_p^*(x, y) \operatorname{grad}_r C_p(x, y) \quad (2.20)$$

and

$$\operatorname{grad}_r \equiv \frac{\partial}{\partial x} \mathbf{i} + \frac{\partial}{\partial y} \mathbf{j} + \frac{\partial}{\partial z} \mathbf{k}; \qquad \mathbf{p} = \frac{\hbar}{i} \operatorname{grad}_r .$$

From (2.19) one obtains by standard procedures the vector equation of motion

$$M\ddot{\mathbf{r}} = -M\omega_0^2 \mathbf{r} - \operatorname{grad}_r \epsilon(x, y) - \frac{e}{c} [\dot{\mathbf{r}} \times \mathbf{k} H(x, y)], \quad (2.21)$$

where the inhomogeneous magnetic field $H(x, y)$ is given by

$$H(x, y) = \frac{\partial A_y}{\partial x} - \frac{\partial A_x}{\partial y} . \quad (2.22)$$

Equation (2.21), together with certain statistical specifications of initial conditions (to be developed in Sec. IV) constitutes the basis of the treatment of the present paper.

[12] Henceforth all reference to the vector potential shall refer to the quantity defined by (2.20) and should not be confused with that defined in (1.4). It should here be remarked that (as will be shown in Appendix D) (2.20) can be chosen to be proportional to the magnetic field. Hence terms quadratic in A have been ignored in deriving (2.21).

III. BASIC PROPERTIES OF THE POTENTIAL $V(x, y)$ AND THE FIELD $H(x, y)$

In order to proceed further in our discussion of the Hamiltonian (2.19) we must evaluate the potential energy term $V(x, y) = (M/2)\,\omega_0^2(x^2 + y^2) + \epsilon(x, y)$ and the magnetic field expression (2.22).

Let us first note that $\epsilon(x, y)$ is the lowest energy solution of the cubic (2.15). Explicitly this solution is given by the standard formula[13]

$$\epsilon(x, y) = 2\sqrt{a}\cos\left(\frac{\phi}{3} + \frac{2\pi}{3}\right), \tag{3.1}$$

where

$$\cos\phi = -\frac{b}{a^{3/2}}, \qquad 0 < \phi \leqslant \pi \tag{3.2}$$

and

$$a \equiv J^2\left[\left(\frac{A}{J\sqrt{6}}\right)^2(x^2 + y^2) + 1\right]$$

$$b \equiv J^3\left[\left(\frac{A}{J\sqrt{6}}\right)^3(3y^2 - x^2)x + 1\right]. \tag{3.3}$$

$\epsilon(x, y)$ can be described as a triangular pyramid which has its peak at the origin and its edges rounded within the characteristic distance $(J\sqrt{6}/A)$.[14] The edges of

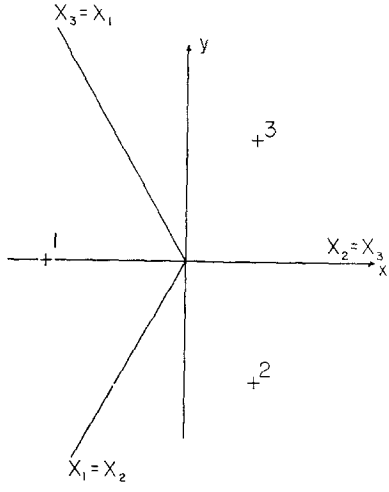

FIG. 2. The coincidence lines $x_1 = x_2$, $x_2 = x_3$, $x_3 = x_1$, and the regions which they bound are shown above. Crosses mark the minima of the potential energy.

[13] "Handbook of Chemistry and Physics," 48th ed., p. A-245.

[14] The description of $\epsilon(x, y)$ in this section is based on the study of (3.1)–(3.3) which is carried out in Appendix B.

the pyramid, shown in Fig. 2, lie along the lines $y = \sqrt{3}x$, $x < 0$; $y = 0$, $x > 0$; $y = -\sqrt{3}x$, $x < 0$. As can be seen from (2.16), these lines are just the coincidence lines $x_1 = x_2$, $x_2 = x_2$, and $x_3 = x_1$, respectively. Denoting the region bounded by the $x_1 = x_2$ and $x_1 = x_3$ coincidence lines as region 1, that bounded by the $x_2 = x_1$ and $x_2 = x_3$ coincidence lines as region 2, and that bounded by the $x_3 = x_1$ and $x_3 = x_2$ coincidence lines as region 3, the energy $\epsilon(x, y)$ in each region, neglecting the rounding of the edges, is[15]

$$\epsilon = \frac{A}{\sqrt{6}}(2x) \qquad \text{in region 1,}$$

$$\epsilon = -\frac{A}{\sqrt{6}}(x - \sqrt{3}y) \qquad \text{in region 2,}$$

$$\epsilon = -\frac{A}{\sqrt{6}}(x + \sqrt{3}y) \qquad \text{in region 3.} \tag{3.4}$$

The rounding of the edges is illustrated by the expression for the potential $\epsilon(x, y)$ in regions 2 and 3 in the limit of $x^2 + y^2 \gg J\sqrt{6}/A$ (but at distances greater than $J\sqrt{6}/A$ from the $x_1 = x_2$ and $x_1 = x_3$ coincidence lines), namely:

$$\epsilon(x, y) = -\frac{Ax}{\sqrt{6}} - J\left[3\left(\frac{Ay}{J\sqrt{6}}\right)^2 + 1\right]^{1/2}, \tag{3.5}$$

which reduces to the formulae of (3.4) for regions 2 and 3 for $|y| \gg J\sqrt{6}/A$; this is far from the rounded region. In addition, in the vicinity of the origin ($x^2 + y^2 \ll J\sqrt{6}/A$) the analytic expression for $\epsilon(x, y)$ may be approximated by its Taylor expansion about the origin:

$$\epsilon(x, y) \simeq -2J\left[1 + \frac{1}{3}\left(\frac{A}{J\sqrt{6}}\right)^2 (x^2 + y^2) - \frac{1}{9}\left(\frac{A}{J\sqrt{6}}\right)^3 (x^2 - 3y^2)x\right]. \tag{3.6}$$

This expansion manifests the fact that the maximum value of $\epsilon(x, y)$ is its value at the origin, explicitly $-2J$.

The potential in the Hamiltonian (2.19) is made up of two terms, namely $(M/2)\omega_0^2(x^2 + y^2)$ and $\epsilon(x, y)$. The vibrational terms is an increasing quadratic function of x and y, while $\epsilon(x, y)$ decreases linearly with distance from the origin. Thus, as illustrated by the crosses in Fig. 2, there is one minimum in each of the

[15] Since the edges of the triangular pyramid are rounded within the characteristic distance $J\sqrt{6}/A$, we see that $\epsilon(x, y)$ with its rounding neglected is just $\epsilon(x, y)$ in the limit of $J = 0$.

three regions, each with potential energy $-A^2/3M\omega_0^2$: In particular, the minima are located at[16]

$$\left(\frac{-2A}{\sqrt{6}\,M\omega_0^2}, 0\right), \quad \left(\frac{A}{\sqrt{6}\,M\omega_0^2}, \frac{-\sqrt{3}\,A}{\sqrt{6}\,M\omega_0^2}\right), \quad \text{and} \quad \left(\frac{A}{\sqrt{6}\,M\omega_0^2}, \frac{\sqrt{3}\,A}{\sqrt{6}\,M\omega_0^2}\right).$$

Having established the general behavior of $\epsilon(x, y)$, we note from (2.17) and (2.10) that in region 1 but not in the vicinity of a coincidence line $X \sim J$, $Y \sim (A/\sqrt{6})(3x - \sqrt{3}y)$, and $Z \sim (A/\sqrt{6})(3x + \sqrt{3}y)$. Utilizing these results in Eqs. (2.11), we note that, away from the coincidence lines

$$\left|\frac{C_3}{C_1}\right|^2 \sim \left|\frac{J}{(A/\sqrt{6})(3x + \sqrt{3}\,y)}\right|^2 \sim \frac{J}{(A^2/M\omega_0^2)} \ll 1,$$

$$\left|\frac{C_2}{C_1}\right|^2 \sim \left|\frac{J}{(A/\sqrt{6})(3x - \sqrt{3}\,y)}\right|^2 \sim \left|\frac{J}{A^2/M\omega_0^2}\right|^2 \ll 1, \quad \text{and} \quad |C_1|^2 \sim 1.$$

Thus in the well of region 1 the electron is considered localized on site 1. Similarly, for values of x and y in the vicinity of the minimum of region 2 or region 3 the electron is considered localized on site 2 or site 3, respectively.

The effective magnetic field, $H(x, y)$, is calculated in Appendix E, yielding the expression

$$H(x, y) = H_0 \frac{3^3}{2} \frac{(-\epsilon/J)}{[(\epsilon/J)^2 - (A/J\sqrt{6})^2 (x^2 + y^2) - 1]^3}, \tag{3.7}$$

where $H_0 = \mathbf{H} \cdot \mathbf{A}_{321}(A/J\sqrt{6})^2 (2/3)^3 (1/\sqrt{3})$ is the field at its peak, the origin. Since $H(x, y)$ obviously possesses the threefold symmetry of $\epsilon(x, y)$ we can infer the general behavior of $H(x, y)$ from its behavior in regions 2 and 3 between the lines $y = \sqrt{3}x$ and $y = -\sqrt{3}x$. At large distances from the origin ($x^2 + y^2 \gg J\sqrt{6}/A$) in this sector of the $x - y$ plane approximation (3.5) is valid and we may write

$$H(x, y) = \frac{H_0}{2}\left(\frac{3}{2}\right)^3 \frac{(Ax/J\sqrt{6}) + [3(Ay/J\sqrt{6})^2 + 1]^{1/2}}{\{(Ax/J\sqrt{6})[3(Ay/J\sqrt{6})^2 + 1]^{1/2} + (Ay/J\sqrt{6})^2\}^3}. \tag{3.8}$$

From (3.8) we can see that at large distances from the origin $H(x, y)$ falls off as the inverse fifth power of the distance from the origin for $x \sim y$, while for $x \gg y$

$$H(x, y) \simeq \frac{H_0}{2}\left(\frac{3}{2}\right)^3 \frac{1}{(Ax/J\sqrt{6})^2\,[1 + 3(Ay/J\sqrt{6})^2]^{3/2}}, \tag{3.9}$$

[16] In finding the minima of the lattice potential energy we have taken $\epsilon(x, y)$ to be given by the expression (3.4). To justify this procedure we first note that (3.4) is valid at distances from the coincidence lines which are greater than $J\sqrt{6}/A$ while the minima we have found are a distance of $(\sqrt{3}A)/(\sqrt{6}M\omega_0^2)$ from the nearest coincidence lines. Therefore the minima which we have found will be correct provided that $1 \gg (J\sqrt{6}/A)/[(\sqrt{3}A)/(\sqrt{6}M\omega_0^2)] \sim J/(A^2/4M\omega_0^2)$—a condition which we assume to be fulfilled in our small-polaron treatment.

that is, $H(x, y)$ falls off as the inverse square of the distance in the limited region along the $x_2 = x_2$ coincidence line $| y | < J\sqrt{6}/A$, while falling off more rapidly at greater distances from the coincidence line ($| y | > J\sqrt{6}/A$). In addition, we can elucidate the behavior of $H(x\ y)$ in the vicinity of the origin ($x^2 + y^2 \ll J\sqrt{6}/A$) by inserting the expansion (3.6) into the general expression (3.7) to obtain the following approximation for $H(x, y)$ in the vicinity of the origin:

$$H(x, y) = H_0 \left[1 - \frac{4}{3}\left(\frac{A}{J\sqrt{6}}\right)^2 (x^2 + y^2) + \frac{7}{9}\left(\frac{A}{J\sqrt{6}}\right)^3 (x^2 - 3y^3)x\right], \quad (3.10)$$

where H_0 is seen to be the magnitude of $H(x, y)$ at the origin.

The upshot of these results is that $H(x, y)$ is sharply peaked about the origin, falling off in the direction of the minima as the inverse fifth power of the distance from the origin and as the inverse square of the distance along a coincidence line.[17]

IV. FIELD-DEPENDENCE OF THE HOPPING PROBABILITY

In this section a general expression for the (magnetic) field-dependent part of the elementary two-site transition probability will be developed.

As shown in the previous section—in particular, in the text between equations (3.6) and (3.7)—the three regions into which the x, y configurational-coordinate plane is subdivided (cf. Fig. 2) are each associated with a definite site-occupancy of the charge-carrier (as indicated by the numerical index in each such region). From this observation it follows that, in a classical adiabatic theory, a transition from e.g., site 1 to site 3, occurs via trajectories which "originate" in region 1 and, after traversing one or more coincidence lines (e.g., the coincidence line $x_1 = x_3$, or successively the lines $x_1 = x_2$ and $x_2 = x_3$) "terminate" in region 3.

> [Here, as noted in Ref. II (especially pages 386-389 and footnote 37), the existence of vibrational dispersion [arising from the second sum of the vibrational Hamiltonian, (1.1)] plays a vital role. Namely, in its absence, one would have to be concerned with "ringing" effects, in which trajectories could reverse themselves in a time of the order of a vibrational period, $2\pi/\omega_0$. The existence of nonvanishing dispersion, giving rise as it does to spatial propagation of vibrational energy, has the effect of dissipating vibrational excitation momentarily concentrated in (molecular) sites 1, 2, and 3, so that the likelihood of an immediate reversal (within a

[17] The fact that $H(x, y)$ falls off as r^{-2} in the small sector in the vicinity of coincidence lines [$\Delta\theta \sim (J\sqrt{6}/A)/r$] and faster away from the coincidence lines leads to the conclusion that the total flux through the $x - y$ plane, $\int dx \int dy\, H(x, y) = \int dr\, r \int d\theta\, H(r, \theta)$ is finite. It is explicitly calculated in Appendix F and found to be equal to the quantity $\mathbf{H} \cdot \mathbf{A}_{321}$ defined in (1.7).

time $2\pi/\omega_0$) is negligible. Eventually, of course, according to general dynamical principles, such a reversal will occur; however, within the framework of a statistical kinetic treatment, the two trajectories are to be considered as uncorrelated. It is in this sense that the text statement concerning trajectories "originating" in one region and "terminating" in another, is to be understood.]

Now, from the results obtained in the two previous sections (in particular, Eqs. (2.20), (2.22), together with (3.7) and subsequent text), it is clear that, in the presence of the external magnetic field, there exists a Lorentz type force which, in general, produces a net deflection of all trajectories in a given (angular) direction. If this direction were, e.g., counter-clockwise, certain trajectories which in zero field terminate in region 2, would be deflected into region 3; another group would be correspondingly deflected from region 3 into region 1. The difference in the contributions of the two groups of trajectories to the overall probability of transitions between regions 1 and 3 constitutes the *net field-induced change* in this transition probability (i.e., the basic quantity of interest to us).

A feature of decisive importance for the treatment of the problem is the circumstance that, as shown in the concluding paragraphs of Sec. III, the equivalent magnetic field is essentially localized within a region of linear dimensions $\sim J\sqrt{6}/A$ surrounding the triple-coincident point ($x = 0$, $y = 0$). If then (cf. Fig. 3) one draws a vertical "reference" line far enough to the left of the triple-coincidence

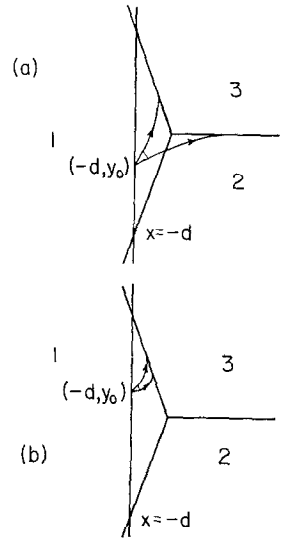

FIG. 3. Figures 3a shows a typical pair of limiting trajectories at high energies $E > -2J$. Figure 3b shows the low-energy limiting trajectories ($E < -2J$).

point—specifically a line $x = -d$, where $d \gg J\sqrt{6}/A$—one may assume that the a priori probability of a trajectory which originates in region 1 crossing this line within a given differential range of the configurational coordinate y_0, direction θ, and energy E[18] *is independent of the magnetic field.*

[Here a qualifying remark is in order. Strictly speaking, the equivalent magnetic field vanishes only in the limit $x^2 + y^2 \to \infty$[$\sim 1/(x^2 + y^2)$ along a coincidence line and $\sim 1/(x^2 + y^2)^{5/2}$ in other directions]. The question as to whether small but nonvanishing values of the field at large distances from the triple-coincidence point have any appreciable effect may, however, be decided a posteriori, simply by going to the limit $d \to \infty$. It will be seen that the condition $d \gg J\sqrt{6}/A$ is in fact sufficient. An additional remark: For finite d, there exist trajectories which pass from region 1 to region 3 without crossing the reference line; however, the effect of the magnetic field on such trajectories may concomitantly be expected to be negligible (as is also established below, in Sec. VI).]

This basic approach is utilized as follows. As illustrated in Fig. 3, those trajectories of energy E which originate in region 1, cross the reference line at a "height" y_0, and terminate in region 3, generally lie within a range of incident angles defined by limits, $\theta^{\max}$ and $\theta^{\min}$.[19] From the previous paragraph, it follows that the occurrence probability of trajectories within *fixed* angular limits is independent of the magnetic field; the effect of the field manifests itself solely in the alteration of the "limiting" angles, i.e., $\theta^{\max}$ and $\theta^{\min}$ are functions of the magnetic field. This functional dependence plays a crucial role in the treatment.

With these orienting preliminaries out of the way, let us now proceed to obtain an expression for the probability per unit time of a trajectory crossing the reference line and passing from region 1 to region 3. As an initial step, one notes that because of the vibrational coupling of the three sites of interest to the remainder of the lattice [via the dispersion term of (1.1)], it is appropriate to assume that the occurrence probability of the parameters y_0, E, and θ (characterizing the trajectories at the reference line) corresponds to conditions of statistical equilibrium. It then follows that, since a "particle" whose x-coordinate lies between $x = -(d + v_x\, dt)$ and $x = -d$ at $t = 0$ will cross the reference line within the time interval dt, we

[18] It is also possible to define trajectories by the parameters y_0, v_x, and v_y; here the Cartesian components of velocity along a trajectory are given by $v_x = v\cos\theta$ and $v_y = v\sin\theta$ with $v = \{2[E - V(-d, y_0)]/M\}^{1/2}$. In the interest of convenience, we shall utilize whichever set of parameters appears most appropriate at a given point in the exposition.

[19] A discussion of the "limiting" trajectories for both $E > -2J$ and $E < -2J$ is given in Appendix G. An important result of the treatment therein is that trajectories whose energy is less than $-2J$ (i.e., trajectories which are energetically incapable of attaining the triple-coincidence point) cannot pass from region 1 to region 3 *via region* 2; hence the group of trajectories which are deflected from region 2 to region 3 by a magnetic field does not occur for $E < -2J$.

may write the probability of a trajectory crossing the reference line between times t and $t + dt$ with an x-component of velocity between v_x and $v_x + dv_x$, a y-component of velocity between v_y and $v_y + dv_y$, and an ordinate between y_0 and $y_0 + dy_0$ as

$$(v_x\, dt)\, dv_x\, dv_y\, dy_0 \frac{\exp[-E(v_x, v_y, y_0)/kT}{Z}, \tag{4.1}$$

where

$$Z = \int_{-\infty}^{\infty} dv_x \int_{-\infty}^{\infty} dv_y \int dx \int dy \exp[-E(v_x, v_y, x, y)/kT].$$
$$\text{region 1}$$

The probability per unit time of such a crossing is then

$$\frac{e^{-E/kT}}{Z} v_x\, dv_x\, dv_y\, dy_0 . \tag{4.2}$$

We may eliminate the variables v_x and v_y in (4.2) in favor of the variables E (the energy) and θ (the angle between the trajectory and the x-axis) by utilizing the transformation:

$$\begin{aligned} v_x &= v \cos\theta \\ v_y &= v \sin\theta \\ v &= \left\{\frac{2[E - V(-d, y_0)]}{M}\right\}^{1/2}. \end{aligned} \tag{4.3}$$

In that the Jacobian of such a transformation is M^{-1}, (4.2) becomes

$$\frac{e^{-E/kT}}{MZ} v\, dE\, dy_0 \cos\theta\, d\theta.$$

Therefore between energies E and $E + dE$, the number of trajectories which cross the reference line between y_1 and y_2 and pass from region 1 to region 3 is

$$W_{13}(E)\, dE = \frac{e^{-E/kT}}{MZ} \int_{y_1}^{y_2} dy_0 v \int_{\sin\theta^{\min}}^{\sin\theta^{\max}} d(\sin\theta)\, dE, \tag{4.4}$$

where $\theta^{\min}$ and $\theta^{\max}$ are the limiting angles between which trajectories of energy E and ordinate y_0 pass from region 1 to region 3. The angular integration can be performed immediately to yield

$$W_{13}(E) = \frac{e^{-E/kT}}{MZ} \int_{y_1}^{y_2} dy_0 v\{\sin\theta^{\max} - \sin\theta^{\min}\}. \tag{4.5}$$

When a magnetic field is applied the classical trajectories are deflected causing the limiting angles to be altered. The new limiting angles are denoted by

$$\theta_H^{\max} = \theta^{\max} + \Delta\theta^{\max}$$
$$\theta_H^{\min} = \theta^{\min} + \Delta\theta^{\min}, \tag{4.6}$$

where the $\Delta\theta$'s are regarded as arbitrarily small in view of the arbitrary smallness of the magnetic field.[20] Utilizing this arbitrary smallness one may write

$$\sin\theta_H^{\max} - \sin\theta^{\max} = (\cos\theta^{\max})\,\Delta\theta^{\max},$$
$$\sin\theta_H^{\min} - \sin\theta^{\min} = (\cos\theta^{\min})\,\Delta\theta^{\min}. \tag{4.7}$$

Therefore the alteration of $W_{13}(E)$ by the magnetic field [to be designated by the notation $W_{13}^H(E)$] is

$$W_{13}^H(E) = \frac{e^{-E/kT}}{MZ}\int_{y_1}^{y_2} dy_0[\cos\theta^{\max} v\Delta\theta^{\max} - \cos\theta^{\min} v\Delta\theta^{\min}], \tag{4.8}$$

where y_1 and y_2 are chosen so that (4.8) includes the contribution of all trajectories from region 1 which are shifted into region 3 by the magnetic field.

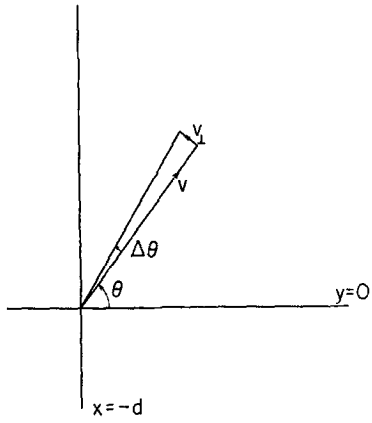

FIG. 4. As depicted above, an arbitrarily small increment $\Delta\theta$ of a limiting angle corresponds to the addition of an arbitrarily small component of velocity $v_\perp$ perpendicular to the original velocity v.

[20] The assumption of arbitrary smallness of field has already been introduced in Sec II. It is adequate for the calculation of the lowest order Hall effect (linear in the field).

[In general the limits $y_1(E)$ and $y_2(E)$ are chosen to be the values of y_0 between which trajectories that cross the reference line can originate in region 1 and reach region 3. However, it will be demonstrated in Sec. VI that each field-induced change of a limiting angle, $\Delta\theta^{\min}(y_0, E)$ or $\Delta\theta^{\max}(y_0, E)$, is only nonzero for a finite range of values of y_0 which is contained between the above mentioned limits. In addition, it will be shown that the nonzero range of $\Delta\theta^{\max}(y_0, E)$ is contained within that of $\Delta\theta^{\min}(y_0, E)$. Thus, by choosing $y_1(E)$ and $y_2(E)$ to be values of y_0 outside of which $\Delta\theta^{\min}(y_0, E)$ is zero, we insure that all trajectories that are shifted into region 3 are counted in $W_{13}^H(E)$.]

As shown in Fig. 4, the $\Delta\theta$'s may be rewritten as

$$\Delta\theta^{\max} = \frac{v_\perp^{\max}}{v}, \qquad \Delta\theta^{\min} = \frac{v_\perp^{\min}}{v}, \tag{4.9}$$

where the $v_\perp$'s are the components of the initial velocity of the limiting trajectories perpendicular to the zero-field limiting trajectories at $(-d, y_0)$. Equation (4.8) may therefore be rewritten as

$$W_{13}^H(E) = \frac{e^{-E/kT}}{MZ} \int_{y_1}^{y_2} dy_0 [\cos\theta^{\max} v_\perp^{\max} - \cos\theta^{\min} v_\perp^{\min}]. \tag{4.10}$$

Recalling that the angles $\theta^{\max}$ and $\theta^{\min}$ of Eq. (4.10) are the angles between the zero-field limiting trajectories and the x-axis, we observe in Fig. 5 that $\theta^{\max}$ and

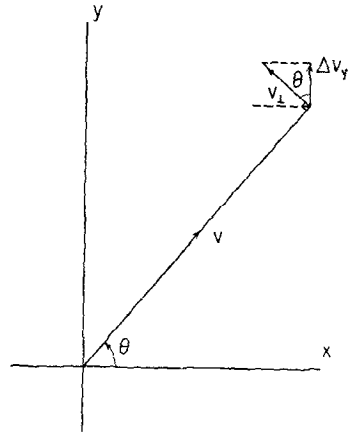

FIG. 5. The angular relationships between v, Δv_y, and $v_\perp$ are illustrated above.

$\theta^{\min}$ are also the angles between the y-direction and $v_\perp^{\max}$ and $v_\perp^{\min}$, respectively. Hence (cf. Fig. 5)

$$v_\perp^{\max} \cos \theta^{\max} = \Delta v_y^{\max},$$
$$v_\perp^{\min} \cos \theta^{\min} = \Delta v_y^{\min}, \tag{4.11}$$

where $\Delta v_y^{\max}$ and $\Delta v_y^{\min}$ are the changes of the initial velocity components in the y-direction due to the magnetic field.[21] Therefore we have

$$W_{13}^H(E) = \frac{e^{-E/kT}}{MZ} \int_{y_1}^{y_2} dy_0 [\Delta v_y^{\max} - \Delta v_y^{\min}]. \tag{4.12}$$

V. A USEFUL FLUX THEOREM

It is now our task to evaluate (4.12). To this end, we shall prove a theorem concerning the integral of Δv_y along the reference line, where Δv_y refers to either $\Delta v_y^{\min}$ or $\Delta v_y^{\max}$. The theorem, illustrated in Fig. 6, is: The integral of Δv_y between any two points y_1 and y_2 on the reference line is equal to $-e/Mc$ multiplied by the magnetic flux Φ enclosed within the region which is bounded by the reference line between y_1 and y_2 and by those limiting trajectories (trajectories tangent to

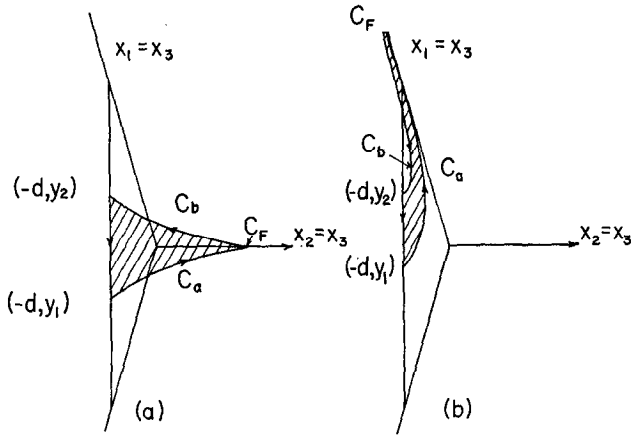

FIG. 6. The contour of integration and the corresponding flux is shown for trajectories which are tangent to the $x_2 = x_3$ coincidence line [in (a)] and to the $x_1 = x_3$ coincidence line [in (b)].

[21] To first order in the magnetic field, the field produces no change in the velocity component along the zero-field trajectory, that is, $\Delta \mathbf{v} \cdot \mathbf{v} = 0$. This is a manifestation of the fact that the kinetic energy associated with a particle of energy E at a given point is unaffected by the application of a magnetic field, that is $[\Delta(\mathbf{v} \cdot \mathbf{v})]/2 = \Delta \mathbf{v} \cdot \mathbf{v} = 0$ to first order. It then follows that Δv_y is proportional to $\Delta v_\perp$ as given by Eq. (4.11).

either the $x_1 = x_3$ or $x_3 = x_2$ coincidence lines) which pass through the reference line at the points $(-d, y_1)$ and $(-d, y_2)$ respectively, thus

$$\int_{y_1}^{y_2} dy_0 \Delta v_y = -\frac{e}{Mc}\Phi. \tag{5.1}$$

With the aid of this theorem, $W_{13}^{H}(E)$ will be expressed in terms of fluxes through regions of appropriate geometrical forms.

As a first step toward proving the above theorem the following lemma is proved: For a given solution of the Hamiltonian–Jacobi equation, the line integral of the change of the velocity field,[22] due to the magnetic field, along any closed path is equal to e/Mc multiplied by the flux enclosed by the contour of integration, that is

$$\oint \Delta \mathbf{v} \cdot d\mathbf{l} = \frac{e}{Mc}\Phi, \tag{5.2}$$

where Φ is the enclosed flux.

In the presence of a magnetic field, the Hamilton–Jacobi equation associated with (2.19) may be written as

$$\frac{1}{2M}[\mathrm{grad}_{\mathbf{r}}(S_0 + S_1) + (e/c)\mathbf{A}]^2 + V(x, y) = E, \tag{5.3}$$

where S_0 is a solution of the field free Hamilton–Jacobi equation:

$$\frac{1}{2M}[\mathrm{grad}_{\mathbf{r}} S_0]^2 + V = E. \tag{5.4}$$

The velocity at any point in space is given by

$$\mathbf{v} = \frac{\mathrm{grad}_{\mathbf{r}} S + (e/c)\mathbf{A}}{M} = \frac{\mathrm{grad}_{\mathbf{r}} S_0}{M} + \frac{\mathrm{grad}_{\mathbf{r}} S_1 + (e/c)\mathbf{A}}{M}, \tag{5.5}$$

where $\mathrm{grad}_{\mathbf{r}} S_0/M$ is the velocity field in the absence of a magnetic field. The field-induced change in this velocity is then[23]

$$\Delta \mathbf{v} = \frac{\mathrm{grad}_{\mathbf{r}} S_1 + (e/c)\mathbf{A}}{M}. \tag{5.6}$$

[22] The velocity field $\mathbf{v}(x, y)$ corresponding to a solution of the Hamilton–Jacobi equation $S(x, y)$ is explicitly $[\mathrm{grad}_{\mathbf{r}} S(x, y) + (e/c)\,\mathbf{A}(x, y)]/M$. It is the velocity associated with a trajectory at the point (x, y), the trajectory belonging to the class of non-intersecting trajectories derived from a particular solution of the Hamilton–Jacobi equation $S(x, y)$.

[23] Subtracting (5.4) from (5.3) we have, to first order in the magnetic field

$$(\mathrm{grad}_{\mathbf{r}} S_0/M) \cdot ([\mathrm{grad}_{\mathbf{r}} S_1 + (e/c)\mathbf{A}]/M) = 0$$

where S_1 and $\mathbf{A}$ are considered as infinitesimals proportional to the magnetic field. This equation may be rewritten as $\mathbf{v} \cdot \Delta \mathbf{v} = 0$ [by use of (5.6)], confirming the conclusion of footnote 21.

Integrating $\Delta\mathbf{v}$ about an arbitrary closed path, we have (with the use of Stokes Theorem)

$$\oint \Delta\mathbf{v} \cdot d\mathbf{l} = \iint \operatorname{curl} \frac{\operatorname{grad}_r S_1 + (e/c)\mathbf{A}}{M} \cdot d\mathbf{a}$$
$$= \frac{e}{Mc} \iint \mathbf{H} \cdot d\mathbf{a} = \frac{e}{Mc} \Phi, \tag{5.2}$$

where Φ is the flux enclosed by the path of integration.

In order to apply Lemma (5.2) to the proof of (5.1) it is necessary to confirm that a family of limiting trajectories—specifically, the totality of those trajectories of energy E which pass through the reference line and approach tangency to a coincidence line ($x_1 = x_3$ or $x_2 = x_3$) as $r = x^2 + y^2 \to \infty$[24]—is described by a single solution of the Hamilton–Jacobi equation. We shall demonstrate this fact by formally constructing such a solution. We proceed by recalling that at a given energy E the two families of limiting curves are uniquely defined by their respective limiting angles $\theta^{\min}(y_0)$ and $\theta^{\max}(y_0)$.[25] Restricting our attention to either of these families of limiting trajectories of energy E we may unambiguously[26] construct a well-behaved solution of the Hamilton–Jacobi equation, the trajectories of which comprise the desired limiting family. In particular, we construct the envelope solution

$$S(x, y) = \int_{(-d, y_0)}^{(x, y)} \mathbf{p}(x', y') \cdot d\mathbf{s}' + \mathscr{S}(y_0),$$

where a) $\mathbf{p}(x', y')$ is the momentum vector directed along the appropriate limiting trajectory passing through (x', y') [that is, belonging to one of the two classes defined by $\theta^{\min}(y_0)$ or $\theta^{\max}(y_0)$], $\mathbf{p}(x', y')$ being a continuous function of x' and y'; b) y_0 is the function of x and y determined by the requirement that y_0 be the ordinate at the point of intersection where the limiting trajectory passing through

[24] The fact that trajectories approach tangency asymptotically follows from the fact that the force [the gradient of the potential energy $(M/2)\omega_0^2(x^2 + y^2) + \epsilon(x, y)$] at any point on any coincidence line, possesses no component perpendicular to the line itself; it is directed radially outward along the coincidence line.

[25] Specifically, stipulation of the energy E and the direction $\theta(y_0)$ of the fictitious particle at the point $(-d, y_0)$ uniquely defines a trajectory crossing the reference line. Furthermore, ignoring the peculiar situation in which limiting trajectories of a family may intersect one another (referred to in footnote 26), we note that for a given family of limiting trajectories we may uniquely associate each point (x, y) with an ordinate y_0 and a direction $\theta(y_0)$ at $x = -d$.

[26] Strictly speaking, the action function $S(x, y)$ may be multivalued; this complication arises when the trajectories are bent in such a way so as to span the same region of space more than once. In such a situation the above theorems are to be applied to each sheet of $S(x, y)$ (and the concomitant trajectories) individually. Further discussion of this point is found in the final two paragraphs of this section.

(x, y) crosses the reference line; c) $\mathscr{S}(y_0)$ is constructed so that the envelope condition $\partial S/\partial y_0 = 0$ is satisfied,[27] i.e.,

$$\mathscr{S}(y_0) = \int_0^{y_0} p_y(-d, y_0')\, dy_0' .$$

The proof of (5.1) now follows. If we choose either of the two paths of integration depicted in Fig. 6, corresponding to trajectories which are tangent to the $x_2 = x_3$ and $x_1 = x_3$ lines, respectively, we may write

$$\oint \Delta\mathbf{v} \cdot d\mathbf{l} = \int_{y_2}^{y_1} \Delta v_y\, dy_0 + \int_{C_a} \Delta\mathbf{v} \cdot d\mathbf{s} + \int_{C_b} \Delta\mathbf{v} \cdot d\mathbf{s} + \int_{C_F} \Delta\mathbf{v} \cdot d\mathbf{s}, \quad (5.7)$$

where C_a is the tangential trajectory from $(-d, y_1)$ in the absence of the magnetic field, and C_b is a similar trajectory from $(-d, y_2)$. The final contribution is from a curve, C_F, which intersects C_a and C_b far from the origin. The velocity along either C_a or C_b is just $(\text{grad}_r S_0)/M$. Since to the first order in the magnetic field $(\text{grad}_r S_0) \cdot [\text{grad}_r S_1 + (e/c)\mathbf{A}] = 0$, we see that

$$\frac{1}{M}[\text{grad}_r S_1 + (e/c)\mathbf{A}]_a = 0, \qquad \frac{1}{M}[\text{grad}_r S_1 + (e/c)\mathbf{A}]_b = 0, \quad (5.8)$$

where the subscripts designate the component of the bracketed expression along the curves C_a and C_b, respectively. In that the expressions (5.8) are just the components of Δv along the curves C_a and C_b, respectively, we may write

$$\oint \Delta\mathbf{v} \cdot d\mathbf{l} = \int_{y_2}^{y_1} dy_0\, \Delta v_y + \int_{C_F} \Delta\mathbf{v} \cdot d\mathbf{s}. \quad (5.9)$$

$\Delta v\,|_{C_F}$ may be taken as zero by choosing the curve C_F sufficiently far from the origin. This is because the trajectories in the presence of the magnetic field are chosen so that they merge with nonmagnetic limiting trajectories at large distance along the coincidence line, i.e., $\Delta\mathbf{v} = 0$ for distances greater than a distance $r^{\max}$ beyond which the magnetic field is neglected. Thus

$$\int_{y_1}^{y_2} dy_0\, \Delta v_y = -\frac{e}{Mc}\Phi, \quad (5.1)$$

where Φ is the flux enclosed by the contour of integration shown in Fig. 6.

[27] For a discussion of the properties of first order partial differential equations and the Hamilton–Jacobi equation in particular, the reader is referred to R. Courant and D. Hilbert, "Methods of Mathematical Physics," (Interscience Publishers, New York, 1962), Vol. II, Sec. II, p. 62.

In the previous discussion it has been tacitly assumed that from a solution of the Hamilton–Jacobi equation S_0 we can find the equation of an entire (zero-field) trajectory. This is not always true. In particular, we have focused our attention on regions of space in which the solutions of the Hamilton–Jacobi equation are real. However, for bounded motion there are regions in which the solutions are complex. These correspond to regions which are classically inaccessible for the trajectories associated with a particular solution. The boundary between the purely real and the complex regime is the locus of the "turning points" of the classical motion. In general two different solutions of the Hamilton–Jacobi equation are needed to describe the trajectories which encounter such turning points. For example, in the case of a body thrown upward into the air, one solution describes the "upward" motion and the other describes the "downward" trajectories.

Pursuing the correspondence between Hamilton–Jacobi Theory and geometrical optics, we recall that the curves of constant S correspond to wavefronts and classical trajectories correspond to rays perpendicular to the wave fronts. The locus of "turning points" corresponds to a reflecting surface. Just as the wavefronts before and after reflection are described by different solutions to the eikonal equation, so the surfaces of constant S are described by different solutions of the Hamilton–Jacobi equation.

We shall see that at sufficiently low energies, trajectories which are tangent to the $x_1 = x_3$ line may "fall back" into region 1, as illustrated in Fig. 7. Each of these trajectories pass through a turning point.

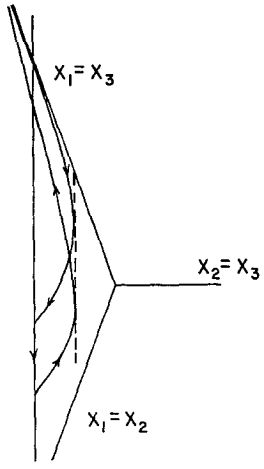

FIG. 7. The dotted line is the locus of the turning points. The contour of integration is depicted by the arrows.

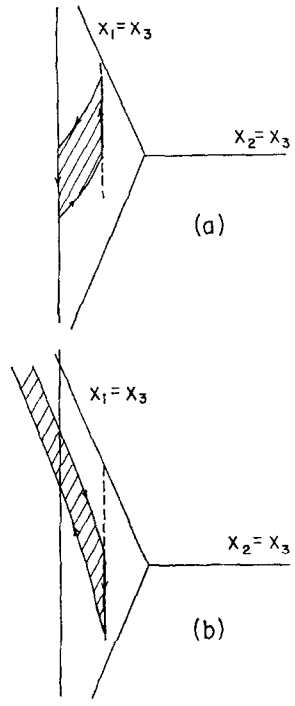

FIG. 8. Figures 8a and 8b show the contours of integration for the integrals $\oint_1 \Delta\mathbf{v} \cdot d\mathbf{l}$ and $\oint_2 \Delta\mathbf{v} \cdot d\mathbf{l}$, respectively.

To establish (5.2) for such a situation, we consider

$$\oint \Delta\mathbf{v} \cdot d\mathbf{l} = \oint_1 \Delta\mathbf{v} \cdot d\mathbf{l} + \oint_2 \Delta\mathbf{v} \cdot d\mathbf{l}, \tag{5.10}$$

where the contours 1 and 2 are shown in Fig. 8. Each of the two integrals involves only one branch of $S(\mathbf{r})$ and hence is equal to the flux enclosed within the corresponding region, Φ_1 or Φ_2, respectively. Thus

$$\oint \Delta\mathbf{v} \cdot d\mathbf{l} = \Phi_1 + \Phi_2 . \tag{5.11}$$

Noting that the area that is shared by both integrals gives cancelling contributions to the total flux, we see that

$$\Phi_1 + \Phi_2 = \Phi, \tag{5.12}$$

where Φ is the flux enclosed by the original contour C. Thus formula (5.1) is established. Q.E.D.

VI. DERIVATION OF FLUX EXPRESSION FOR W_{13}^H

Before proceeding to evaluate (4.12) with the aid of the theorem (5.1), it is necessary to elucidate the nature of the limiting trajectories. This task is performed in Appendix G; the conclusions are given here.[28]

As shown in Fig. 9, for energies above that of the peak, $-2J$, the maximum and minimum limiting trajectories from a point on the line $x = -d$ are trajectories which are tangent to the $x_1 = x_3$ and the $x_3 = x_2$ coincidence lines, respectively. As the energy of such trajectories decreases the distance of closest approach to the origin decreases. For energies less than $-2J$ (the "peak" energy) it is not possible for a trajectory which is tangent to the $x_3 = x_2$ line to originate in region 1 [cf., Appendix G, Eq. (G.6)].

Several pairs of limiting trajectories of energy E, less than $-2J$ are shown in Fig. 10. Trajectories, from a given point on the reference line, which lie between the two limiting trajectories from that point (both tangent to the $x_1 = x_3$ line) cross to region 3. Those not included between the two limiting trajectories are confined to region 1. As shown in Fig. 10, as the crossing point descends the two limiting trajectories tend to merge. At $y_0 = y_m(E)$ the maximum and minimum limiting trajectories coincide. For values of y_0 below $y_m(E)$ no trajectory can reach region 3.

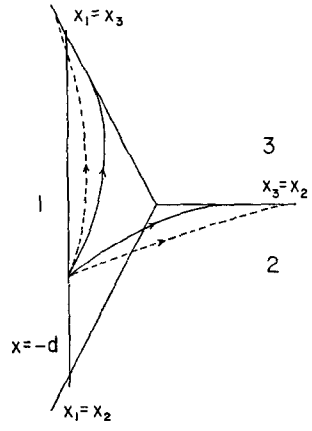

FIG. 9. Two pairs of illustrative limiting trajectories for energies above $-2J$. The dotted line trajectories are of higher energy than the solid line trajectories.

[28] Although the equations of motion for the exact potential, $\epsilon(x, y)$, have not been solved exactly, several models which approximate the exact potential have been studied. All of these models predict the behavior described below. Thus the trajectories described in words and figures are to be considered as "illustrative" of what we believe to be the behavior of the trajectories and not the result of an exact solution of the equations of motion.

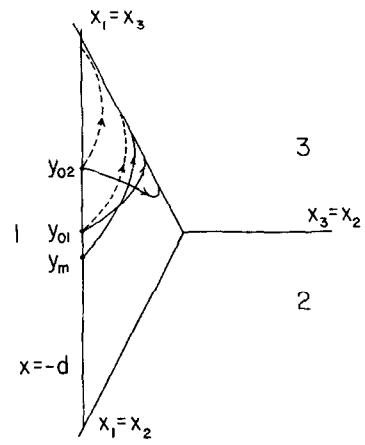

FIG. 10. Illustrative pairs of trajectories for an energy below $-2J$ from various points (y_{01}, y_{02}, and y_m) on the line $x = -d$. At $y_0 = y_m$ the two limiting trajectories have merged into one. For y_0 less than y_m there are no trajectories which reach the coincidence line at this energy.

As the energy approaches $-2J$ from below, $y_m(E)$ drops until it lies on the $x_1 = x_2$ coincidence line [$y_m(-2J) = -\sqrt{3}d$].

Let us first evaluate (4.12) for energies above that of the peak, $-2J$. In this regime $\Delta v_y^{\min}$ is the difference in the y-component of the velocity at $(-d, y_0)$ between

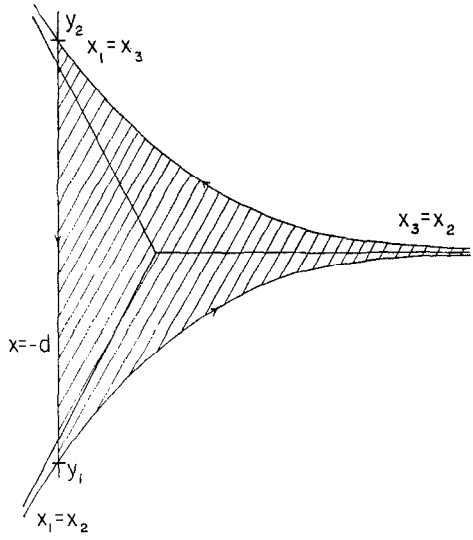

FIG. 11. The limiting trajectories corresponding to $\Delta v_y^{\min}$ at the limiting values y_1 and y_2 for an energy above that of the peak, $E > -2J$. The shaded area denotes the flux $\Phi_{\min}$.

trajectories which are tangent to the $x_2 = x_3$ line with and without the presence of a magnetic field. The limits of integration y_2 and y_1 (shown in Fig. 11) are chosen so that only trajectories originating in region 1 are counted. As depicted in Fig. 11, y_1 is the point at which the trajectory which is tangent to both the $x_3 = x_2$ and $x_1 = x_2$ lines intersects the reference line; correspondingly, y_2 is the point at which the trajectory which is tangent to both the $x_3 = x_2$ and $x_1 = x_3$ lines intersects the reference line.[29] For values of y_0 not between y_1 and y_2, trajectories which are tangent to the $x_3 = x_2$ coincidence line will not originate in region 1. Thus, recalling (5.1), one has

$$\int_{y_1}^{y_2} dy_0 \, \Delta v_y^{\min}(y_0, E) = -\frac{e}{Mc} \Phi_{\min}(E), \tag{6.1}$$

where $\Phi_{\min}(E)$ is the flux enclosed between the two doubly tangent trajectories and the reference line, i.e., the shaded region of Fig. 11.

To discuss the contribution of the $\Delta v_y^{\max}$ term of (4.12), let us examine Fig. 12. The trajectory which is tangent to both the $x_1 = x_2$ and $x_1 = x_3$ lines intersects the reference line at y_1'. For $y_1' > y_0 > y_1$ the maximum value of v_y is determined by the requirement that the trajectory originate in region 1.

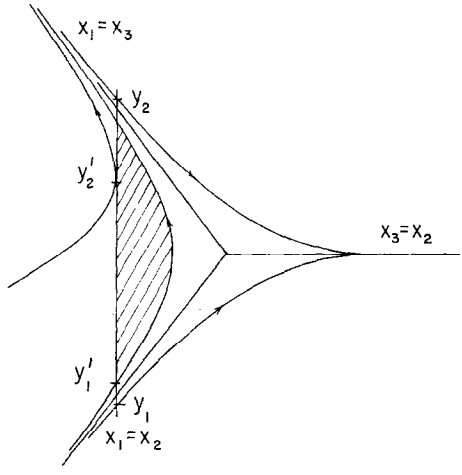

FIG. 12. The limiting trajectories for $\Delta v_y^{\max}$ are shown in addition to those for $\Delta v_y^{\min}$, for $E > -2J$. y_1' and y_2' are the limiting values of y_0 involved in the evaluation of the integral (6.5). The shaded area denotes the flux $\Phi_{\max}$.

[29] $\Delta v_y^{\min} = 0$ for $y_0 > y_2$ since the restriction which determines the direction of the minimum trajectory at $(-d, y_0)$ for this range of y_0 values (namely, that the trajectories originate in region 1) does not involve the magnetic field.

It then follows that $v_y^{\max}$ is not a function of H, i.e.,

$$\Delta v_y^{\max}(-d, y_0) = 0 \tag{6.2}$$

for $y_1' > y_0 > y_1$.

We label the ordinate at which a trajectory which is tangent to the $x_1 = x_3$ line achieves tangency to the reference line as y_2'; such a trajectory is illustrated in Fig. 12. For $y_0 > y_2'$, $\theta^{\max} = \pi/2$, corresponding to trajectories originating in region 1 and achieving tangency to the $x = -d$ line at $(-d, y_0)$. Therefore the corresponding maximum value of $v_y(-d, y_0)$ for this range of y_0 is

$$v_y^{\max}(-d, y_0) = \left| \frac{2[E - V(-d, y_0)]}{M} \right|^{1/2}. \tag{6.3}$$

Since the magnetic field does not affect the relation (6.3),

$$\Delta v_y^{\max}(-d, y_0) = 0 \tag{6.4}$$

for $y_0 > y_2'$.

When $y_2' > y_0 > y_1'$ the trajectory characterized by $v_y^{\max}(-d, y_0, E)$ is tangent to the $x_1 = x_3$ line. The value of $v_y^{\max}(-d, y_0, E)$ for this range of y_0 is shifted by the magnetic field and

$$\int_{y_1}^{y_2} dy_0 \, \Delta v_y^{\max}(y_0, E) = \int_{y_1'}^{y_2'} dy_0 \, \Delta v_y^{\max}(y_0, E) = \frac{-e\Phi_{\max}(E)}{Mc}, \tag{6.5}$$

where $\Phi_{\max}(E)$ is the flux enclosed by the two trajectories of energy E which are tangent to $x_1 = x_3$ and pass through $y_1'(E)$ and $y_2'(E)$ and the reference line between these two points of intersection. Since the magnetic field is assumed to be zero for $x < -d$, $\Phi_{\max}(E)$ is equal to the flux enclosed between the doubly tangent trajectory of energy E and the reference line (shown by the shaded area of Fig. 12).

Inserting the above results into Eq. (4.12), we have for $E > -2J$

$$\begin{aligned} W_{13}^H(E) &= \frac{e^{-E/kT}}{MZ} (e/Mc)[\Phi_{\min}(E) - \Phi_{\max}(E)] \\ &= \frac{e^{-E/kT}}{MZ} (e/Mc)\, \Phi(E), \end{aligned} \tag{6.6}$$

where $\Phi(E)$ is the flux enclosed between the three trajectories which are each tangent to two coincidence lines, as represented by the shaded area of Fig. 13.[30]

[30] One may include the pieces of this area to the left of the reference line since they contribute nothing to the flux.

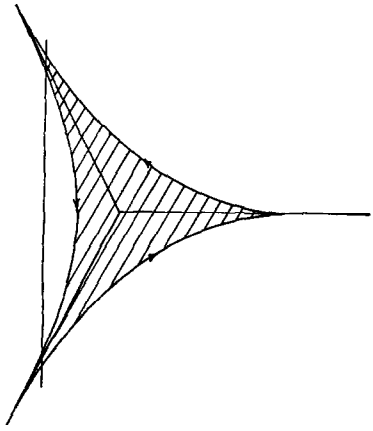

FIG. 13. The shaded area illustrates $\Phi(E)$ for $E > -2J$, the energy of the peak.

To evaluate (4.12) for energies below $-2J$, we recall that the limiting trajectories are those described earlier and illustrated in Fig. 10. Thus in this energy regime $\Delta v_y^{\max}(y_0, E)$ and $\Delta v_y^{\min}(y_0, E)$ are the differences in the initial y-component of velocity of each of the pair of trajectories from $(-d, y_0)$ that are tangent to the $x_1 = x_3$ line with and without the presence of a magnetic field.

As there are no tangential trajectories from region 1 for $y_0 < y_m(E)$ or $y_0 > \sqrt{3}d$, Eq. (4.12) becomes

$$W_{13}^H(E) = \frac{e^{-E/kT}}{MZ} \int_{y_m(E)}^{\sqrt{3}d} dy_0[\Delta v_y^{\max} - \Delta v_y^{\min}]. \tag{6.7}$$

Using the theorem (5.1), the integration of $-\Delta v_y^{\min}$ yields the flux depicted by the shaded area of Fig. 14,[31] namely that enclosed by the limiting trajectory from $(-d, y_m)$, the limiting trajectory from $(-d, \sqrt{3}d)$, and the reference line between $y_0 = \sqrt{3}d$ and $y_0 = y_m$.

In order to find the upper limit of integration for the $\Delta v_y^{\max}$ term, it is noted that for large enough y_0 [greater than a maximum value labeled by $y_{\pi/2}(E)$] trajectories tangent to the $x_1 = x_3$ line have an initial angle greater than $\pi/2$.[32] Since the trajectories originating in region 1 are being counted as they cross $x = -d$ with $v_x > 0$

[31] The situation that is illustrated in Fig. 14 is for limiting trajectories from $(-d, y_m)$ and $(-d, \sqrt{3}\,d - \delta)$, where δ is a small positive quantity. When $\delta = 0$, the case in evaluating (6.7), the smaller shaded region to the right of the $x = -d$ line vanishes. Thus for $\delta = 0$, the enclosed flux to the right of the $x = -d$ line is that bounded by the limiting trajectory from $(-d, y_m)$ and the reference line.

[32] We can see that such a situation will not arise for those tangential trajectories which are considered in the integration of $\Delta v_y^{\min}(y_0)$ by observing that as y_0 is increased from y_m, θ decreases monotonically from an angle less than $\pi/2$ to a minimum of $-(\pi/3)$ at the $x_1 = x_3$ coincidence line ($y_0 = \sqrt{3}d$).

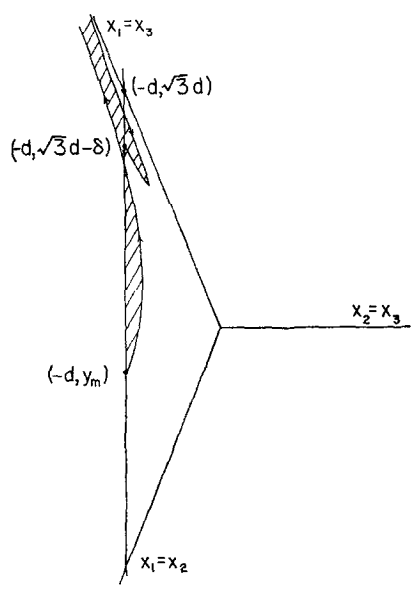

FIG. 14. The contribution of the $\Delta v_y^{\min}$ term to the integral of (6.7) is proportional to the magnetic flux through the shaded region in the limit $\delta = 0$.

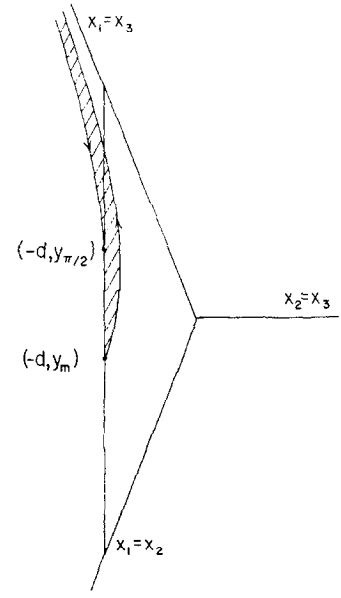

FIG. 15. The contribution of the $\Delta v_y^{\max}$ term to the integral of (6.7) is proportional to the magnetic flux through the shaded region.

those trajectories with $\theta > \pi/2$ are not to be considered. Therefore, for sufficiently large y_0 the "maximum" limiting trajectory has $\theta = \pi/2$ ($v_x = 0$). As before, $\Delta v_y^{\max} = 0$ for these trajectories as there is no field-induced shift in $v_y^{\max}$ when $v_y^{\max}$ is determined by the condition $v_x^{\max}(-d, y_0) = 0$.

Therefore the evaluation of the integral of $\Delta v_y^{\max}$ yields the negative of the flux enclosed between the single limiting trajectory from y_m, the limiting trajectory from $y_{\pi/2}$, and the reference line between y_m and $y_{\pi/2}$ as illustrated by the shaded portion of Fig. 15. In that the field is assumed zero for $x < -d$, the flux involved in both the integration of $\Delta v_y^{\min}$ and that of $\Delta v_y^{\max}$ is just the flux enclosed by the limiting trajectory from y_m and the reference line. Thus the difference of the two fluxes is just zero. Hence there is no net contribution to $\Phi(E)$ for $E < -2J$, the energy of the peak.

The upshot of the preceding evaluation is that

$$\begin{aligned} W_{13}^H(E) &= \frac{e^{-E/kT}}{MZ}(e/Mc)\,\Phi(E), \qquad E \geqslant -2J \\ &= 0, \qquad\qquad\qquad\qquad\quad E \leqslant -2J, \end{aligned} \tag{6.8}$$

where $\Phi(E)$ is the flux enclosed by the three trajectories of energy E which are each tangent to two coincidence lines, as represented by the shaded area of Fig. 13.

VII. HIGH ENERGY BEHAVIOR OF $\Phi(E)$

In this section let us examine the high energy, $J/(E + 2J) \ll 1$, behavior of the flux $\Phi(E)$. As a first step, let us recall from Sec III that the effective magnetic field $H(x, y)$ [given by (3.7)] is sufficiently localized so that the total magnetic flux through the $x - y$ plane is finite. In fact the total flux is found (in Appendix F) to be equal to $\mathbf{H} \cdot \mathbf{A}_{321}$, the magnetic flux associated with the area defined by three lattice sites g_1, g_2, and g_3 depicted in Fig. 1. We shall proceed by assuming that we may expand the flux $\Phi(E)$ in powers of $J/(E + 2J)$ about its value at arbitrarily high energy, namely $\mathbf{H} \cdot \mathbf{A}_{321}$:

[The validity of this assumption is automatically tested by the procedure of evaluating the coefficients of the expansion. If, for example, the lowest-order correction in the parameter $\gamma \equiv [J/(E + 2J)]$ were proportional to $\gamma^{1/2}$ or to $\gamma \ln \gamma$, the evaluation of $(\partial\Phi(E)/\partial\gamma)|_{\gamma\to 0}$ (carried out below) would yield an infinite result. Since only the first derivative is evaluated here, we are not able at this time to exclude the possibility of occurrence of higher-order singular terms, e.g. of the form $\gamma^{3/2}$ or $\gamma^2 \ln \gamma$.]

$$\phi(E) = \mathbf{H} \cdot \mathbf{A}_{321} + \frac{d\Phi(E)}{d[J/(E + 2J)]}\Big|_{J/(E+2J)=0} [J/(E + 2J)] + \cdots . \tag{7.1}$$

Rewriting (7.1) as

$$\Phi(E) = \mathbf{H} \cdot \mathbf{A}_{321} - [(E + 2J)/J]^2 \frac{d\Phi(E)}{d(E/J)}\Big|_{E+2J=\infty} [J/(E + 2J)] + \cdots , \tag{7.2}$$

we are led to focus our attention on the derivative of the flux with respect to energy.

It will be convenient for us to utilize the symmetry of the problem and express the enclosed flux, $\Phi(E)$, as six times the flux enclosed by the lines $y = 0$ and $y = \sqrt{3}x$ and the trajectory which is tangent to the coincidence lines, $y = 0$ and $y = -\sqrt{3}x$. The shaded portion of Fig. 16 illustrates the difference between this flux at energy $E + dE$ and at energy E. Denoting $(x_i, y_i = \sqrt{3}x_i)$ as the point at which the doubly tangent trajectory crosses the line $y = \sqrt{3}x$, the difference in the enclosed flux $\Delta\Phi$ at energies $E + dE$ and E (to first order in dE) is

$$6 \int_0^{y_i(E)} dy \int_{x(y,E)}^{x(y,E+dE)} dx\, H(x, y), \tag{7.3}$$

where $x(y, E)$ is the equation of the doubly tangent trajectory and $H(x, y)$ is the effective magnetic field. Writing

$$x(y, E + dE) = x(y, E) + \frac{\partial x(y, E)}{\partial E}\, dE$$

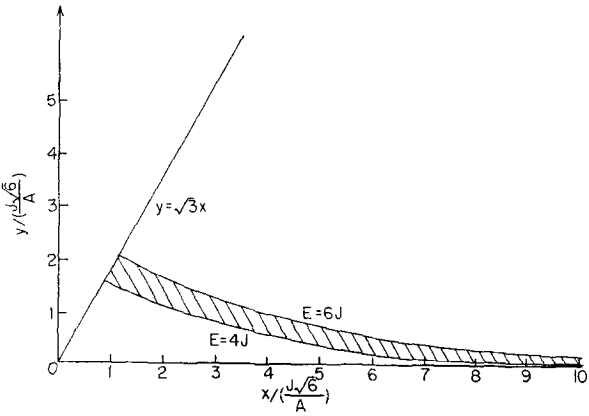

FIG. 16. The shaded region represents one-sixth of the difference in the enclosed flux $\Phi(6J) - \Phi(4J)$. The doubly tangent trajectories shown above are calculated from the potential (3.5) at energies $E = 6J$ and $E = 4J$.

and preceeding to the limit of an arbitrarily small energy increment dE, we may write

$$\frac{d\Phi}{dE} = 6 \int_0^{y_i(E)} dy\, H[x(y, E), y] \frac{\partial x(y, E)}{\partial E}. \tag{7.4}$$

Our task is now to evaluate (7.4) as the energy becomes arbitrarily large. Since for arbitrarily large energy the ratio $[x(y, E)]/[(J6^{1/2})/A]$ becomes arbitrarily large for values of y between 0 and y_i, the potential $\epsilon(x, y)$ in this region is given by the expression (3.5):

$$\epsilon(x, y) = -[x + (1 + 3y^2)^{1/2}], \tag{3.5}$$

where the coordinates x and y are measured in units of $J\sqrt{6}/A$ and the energy $\epsilon(x, y)$ is measured in units of J.[33] Noting that the potential is separable, we may write

$$E_x = \frac{M}{2} v_x^2 - x, \tag{7.5a}$$

$$E_y = \frac{M}{2} v_y^2 - (1 + 3y^2)^{1/2}, \tag{7.5b}$$

where

$$E = E_x + E_y. \tag{7.5c}$$

[33] We shall see that the chief contribution to (7.4) comes from $y \lesssim 1$ and therefore we must utilize (3.5) rather than the corresponding pyramidal expression $\epsilon(x, y) = -[x + \sqrt{3}y]$.

We can see from (7.5b) that for a trajectory to be tangent to the $y = 0$ line, that is, $v_y = 0$ at $y = 0$, we must have

$$E_y = -1. \tag{7.6}$$

Furthermore, since we shall consider only arbitrarily large energies, $E \gg 1$, we shall replace $E_x = E + 1$ by E in all that follows. From Eqs. (7.5a), (7.5b), and (7.6), we may write

$$\frac{-dy}{[(1 + 3y^2)^{1/2} - 1]^{1/2}} = \frac{dx}{(E + x)^{1/2}}, \tag{7.7}$$

where dy/dx is taken to be negative. Integrating (7.7) to find the equation of a trajectory from $(x_i, \sqrt{3}x_i)$ which is tangent to $y = 0$, we find

$$2(E + x)^{1/2}\Big|_{x_i}^{x} = (-1/\sqrt{3}) \left\{ \frac{1}{\sqrt{2}} \ln \left(\frac{[1 + (1 + 3y^2)^{1/2}]^{1/2} - \sqrt{2}}{[1 + (1 + 3y^2)^{1/2}]^{1/2} + \sqrt{2}} \right) + 2[1 + (1 + 3y^2)^{1/2}]^{1/2} \right\} \Big|_{\sqrt{3}x_i}^{y}. \tag{7.8}$$

To find the value of x_i corresponding to a trajectory of energy E that is tangent to $y = -\sqrt{3}x$ as well as being tangent to $y = 0$, we impose the symmetry condition that the trajectory be perpendicular to $y = \sqrt{3}x$ at $(x_i, \sqrt{3}x_i)$, namely,

$$\left.\frac{dy}{dx}\right|_i = -\frac{[(1 + 9x_i^2)^{1/2} - 1]^{1/2}}{[E + x_i]^{1/2}} = -\frac{1}{\sqrt{3}}. \tag{7.9}$$

Solving (7.9) for x_i we find

$$x_i = \frac{(E + 3) + [3^4(E^2 + 6E) + 3^2]^{1/2}}{3^4 - 1}, \tag{7.10}$$

which for arbitrarily large E becomes

$$x_i = E/8. \tag{7.11}$$

To calculate the expression $(\partial x(y, E)/\partial E)$, we differentiate (7.8) implicitly with respect to E and x holding y constant and utilize the condition (7.9) to find

$$\frac{\partial x(y, E)}{\partial E} = [(E + x)/(E + x_i)]^{1/2} [4(dx_i/dE) + 1] - 1, \tag{7.12}$$

which for arbitrarily large E becomes

$$\frac{\partial x(y, E)}{\partial E} = \left[\frac{2(E + x)}{E}\right]^{1/2} - 1, \tag{7.13}$$

where (7.11) has been used.

The magnetic field, in units of $(\mathbf{H}\cdot\mathbf{A}_{321})/(J\sqrt{6}/A)^2$, is found by substituting the expression for ϵ, (3.5), into the general expression for the field, (3.7):

$$H(x,\,y)=\frac{4}{\sqrt{3}}\left\{\frac{-\epsilon}{[\epsilon^2-(x^2+y^2+1)]^3}\right\}$$
$$=\frac{1}{2\sqrt{3}}\left\{\frac{x+(1+3y^2)^{1/2}}{[x(1+3y^2)^{1/2}+y^2]^3}\right\}. \tag{7.14}$$

Inserting (7.13) and (7.14) into (7.4) we obtain

$$\frac{d\Phi}{dE}=\sqrt{3}\int_0^{y_i}dy\,\frac{[x+(1+3y^2)^{1/2}]\{[2(E+x)/E]^{1/2}-1\}}{[x(1+3y^2)^{1/2}+y^2]^3}, \tag{7.15}$$

where x is given by

$$x=-E+\left\{(2E)^{1/2}-\frac{1}{\sqrt{3}}[1+(1+3y^2)^{1/2}]^{1/2}\right.$$
$$\left.-\frac{1}{2\sqrt{6}}\ln\left(\frac{[1+(1+3y^2)^{1/2}]^{1/2}-\sqrt{2}}{[1+(1+3y^2)^{1/2}]^{1/2}+\sqrt{2}}\right)\right\}^2. \tag{7.16}$$

Equation (7.16) is derived by taking x_i, y_i, and E very much larger than unity in the expression (7.8).

The expression (7.16) indicates that x is of the order of E except for values of y which are sufficiently small so that the size of the logarithmic term is much greater than $\sqrt{2}E$.[34] Ignoring, for the present, these arbitrarily small values of y and considering x to be of the order of E, we see that for $E\sqrt{3}/8\geq y\gg 1$, the integrand of (7.15) is roughly $[E(1+y/E)]/[(Ey)^3(1+y/E)^3]\sim E^{-2}y^{-3}$ while for $y\lesssim 1$ the integrand is of order $1/E^2$. Therefore, for arbitrarily large values of E we see that the dominant contribution to the integral (7.15) comes from the regime in which y is less than the order of E: i.e., $y\ll x\sim E$. Thus we may write[35]

$$\frac{d\Phi}{dE}=\sqrt{3}\int_0^{y_i}dy\,\frac{(2(E+x)/E)^{1/2}-1}{x^2(1+3y^2)^{3/2}}. \tag{7.17}$$

Furthermore, for $y\ll x$, E (7.16) may be rewritten as

$$x=-E+\left[(2E)^{1/2}-\frac{1}{2\sqrt{6}}\ln\frac{3y^2}{16}\right]^2. \tag{7.18}$$

[34] Such small values of y are characteristically much less than $e^{-2\sqrt{3}E}$, which in turn is much less than unity.

[35] Since ultimately we shall focus our attention on $\lim_{E\to\infty}E^2(d\Phi/dE)$, corrections to (7.17), being of lower order than E^{-2}, are of no consequence and may be safely ignored.

where it has been noted that the logarithmic term only manifests itself for extremely small values of y: $y \lesssim \exp[-2\sqrt{3E}]$. Since the contribution to (7.17) from $y \lesssim \exp[-2\sqrt{3E}]$ falls off with energy at least as fast as $\exp[-2\sqrt{3E}]$, we can ignore it as it makes no contribution to $\lim_{E\to\infty} E^2(d\Phi/dE)$. Thus in the integral (7.17) the logarithmic term of (7.18) may be ignored and $(d\Phi/dE)$ rewritten as

$$\frac{d\Phi}{dE} = \sqrt{3}\int_0^{\sqrt{3E}/8} dy \frac{1}{E^2(1+3y^2)^{3/2}} = \frac{1}{E^2}\frac{3E/8}{[(3E/8)^2+1]^{1/2}}. \tag{7.19}$$

Therefore the coefficient is readily evaluated:

$$\lim_{E\to\infty} \frac{E^2\, d\Phi}{dE} = \lim_{E\to\infty} \frac{3E/8}{[(3E/8)^2+1]^{1/2}} = 1 \tag{7.20}$$

in dimensionless units (the flux being expressed in units of $\mathbf{H}\cdot\mathbf{A}_{321}$). Keeping the first two terms of the expansion, (7.2) may now be rewritten

$$\Phi(E) = \mathbf{H}\cdot\mathbf{A}_{321}\left[1 - \frac{J}{(E+2J)}\right], \tag{7.21}$$

where the appropriate dimensions have been reintroduced.

VIII. $\Phi(E)$ AT LOW ENERGIES, $(E+2J)/J \lesssim 1$

In order to calculate the low energy, $(E+2J)/J \lesssim 1$, behavior of $\Phi(E)$, we must find the equation of a low energy doubly tangent trajectory. In particular, if we consider the doubly tangent trajectory which is tangent to both the x-axis, and the $y = -\sqrt{3}x$ line, as shown in Fig. 17, we see that the total enclosed flux is just six times that enclosed by the trajectory, the x-axis and the $y = \sqrt{3}x$ line. Thus we need only find the equation of a doubly tangent trajectory between its intersections with the $y = \sqrt{3}x$ line and the x-axis.

At a sufficiently low energy such a doubly tangent trajectory lies close to the x-axis for positive x; that is, $y \leqslant 1$ for $x > 0$ (where distances are measured in units of $J6^{1/2}/A$). In light of this we are led to expand the potential $\epsilon(x, y)$ about $\epsilon(x, 0)$ and keep only the first y-dependent term:

$$\epsilon(x, y) = \epsilon(x, 0) - y^2\epsilon_1(x), \tag{8.1}$$

where $\epsilon_1(x)$ is positive.[36] The range of validity of (8.1) will be discussed later.

[36] ϵ_1 is equal to $-\frac{1}{2}(\partial^2\epsilon(x, y)/\partial y^2)$. The second partial derivative is readily evaluated by repeated use of (C.4) yielding $\epsilon_1 = (2x - \epsilon(x, 0))/(\epsilon^2(x, 0) - x^2 - 1)$, a positive quantity which for positive x is of the order of unity.

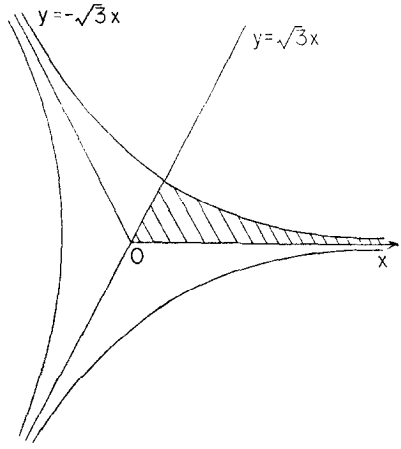

FIG. 17. The shaded area is enclosed by the x-axis, the $y = \sqrt{3}x$ line, and the trajectory which is tangent to both the x-axis and the $y = -\sqrt{3}x$ line. It is one-sixth of the area enclosed by the three doubly tangent trajectories.

With $\epsilon(x, y)$ of (8.1) as the potential energy, the Hamilton–Jacobi equation may be written as

$$(\partial S/\partial x)^2 + (\partial S/\partial y)^2 = 2M[E - \epsilon(x, 0) + y^2\epsilon_1(x)]. \tag{8.2}$$

Motivated by the smallness of y and the concomitant smallness of $p_y = \partial S/\partial y$ for low energy limiting trajectories at positive x, let us write $S(x, y)$ as a series in powers of y^2, viz.:

$$S(x, y) = S_0(x) + (y^2/2)\, S_1(x) + (y^4/4)\, S_2(x) + \cdots, \tag{8.3}$$

where it should be noted that the requirement for tangency to the x-axis, namely that $p_y = 0$ when $y = 0$, is automatically met since p_y is proportional to y. Inserting (8.3) into (8.2), we have to the lowest three orders in y^2, respectively,[37]

$$(dS_0/dx)^2 = 2M[E - \epsilon(x, 0)] \tag{8.4a}$$

$$(dS_1/dx)(dS_0/dx) + S_1^2 = 2M\epsilon_1 \tag{8.4b}$$

$$\tfrac{1}{2}(dS_2/dx)(dS_0/dx) + 2S_1S_2 + \tfrac{1}{4}(dS_1/dx)^2 = 0. \tag{8.4c}$$

At this point let us approximate (8.3) by its first two terms, i.e.,

$$S(x, y) \cong S_0(x) + (y^2/2)\, S_1(x). \tag{8.5}$$

[37] These equations have to be supplemented by appropriate boundary conditions, to be given later for each equation successively.

This approximation will be justified below by showing that, for relevant values of the y-coordinate, $y^4S_2(x)/4$ is negligible. Before solving for $S_0(x)$ and $S_1(x)$ explicitly, let us obtain expressions for the limiting trajectories, as given by (8.5). One has

$$dy/dx = p_y/p_x = [yS_1(x)]/[p_x(x)], \tag{8.6}$$

which may be rearranged to read

$$dy/y = \{[S_1(x)]/[p_x(x)]\}\, dx, \tag{8.7}$$

where $p_x(x) = \partial S/\partial x$ is the x-component of momentum. Formally integrating (8.7), we have

$$y = y_i \exp\left[\int_{x_i}^{x} \frac{S_1(x')}{p_x(x')}\, dx'\right] \tag{8.8}$$

where the choice of the point (x_i, y_i) determines the particular tangential trajectory. We are interested in the trajectory which in addition to being tangent to the x-axis is perpendicular to the $y = \sqrt{3}x$ line. We therefore choose the point (x_i, y_i) to be the point of intersection of the doubly tangent trajectory with the $y = \sqrt{3}x$ line with the stipulation that the trajectory have a slope equal to $-1/\sqrt{3}$ at (x_i, y_i). Explicitly, x_i and y_i are found from the conditions:

$$\begin{aligned} y_i &= \sqrt{3}x_i\,, \\ (dy/dx)_i &= [y_iS_1(x_i)]/[p_x(x_i)] = -1/\sqrt{3}. \end{aligned} \tag{8.9}$$

Having found formulae for the limiting trajectory, namely (8.8) and (8.9), we must now solve the differential equation (8.4b) for $S_1(x)$.[38] Let us rewrite (8.4b) as

$$dS_1/dx = -[S_1^2 - 2M\epsilon_1]/p_0\,, \tag{8.10}$$

where $p_0(x)$ is the x-component of momentum for motion on the x-axis:

[This equation may be converted to a second order linear differential equation by the substitution $S_1 = [dy/dx][p_0(x)/y]$. The resulting equation is

$$p_0(x)\frac{d}{dx}\left[\frac{p_0(x)}{M}\frac{dy}{dx}\right] = 2y\epsilon_1(x),$$

which may be recognized to be Newton's equation of motion for the y-direction, where the y-dependence of the x-component of force is ignored in writing $p_0(x)$ for $p_x(x)$.]

$$p_0(x) = (dS_0/dx) = \{2M[E - \epsilon(x, 0)]\}^{1/2}. \tag{8.11}$$

[38] From (8.4b), (8.8), and the fact the $p_x = \partial S/\partial x$, it is clear that $S_0(x)$ need not be obtained explicitly; knowledge of dS_0/dx [as given by (8.4a) directly] is sufficient.

In order to formulate the approximate boundary condition for the solution of (8.10) we consider the motion of a tangential trajectory as x becomes large enough for $\epsilon_1(x)$ to approach the constant $\epsilon_1(\infty)$.[39] If ϵ_1 is a constant, the potential (8.2) is separable and the associated equations of motion are uncoupled. In particular, for the y-component of the motion we find the differential equation

$$\ddot{y} = [(2\epsilon_1(\infty))/M]\, y, \tag{8.12}$$

which, with the condition that at $t = \infty$, $y = 0$ and $v_y = 0$, has the solution

$$y = y_0 \exp\{-[(2\epsilon_1(\infty))/M]^{1/2}\, t\} \tag{8.13}$$

where y_0 is the ordinate at $t = 0$. From (8.13) we find that at arbitrarily large values of x the ratio p_y/y is given by

$$p_y/y = Mv_y/y = -[2M\epsilon_1(\infty)]^{1/2}, \tag{8.14}$$

while we know in general from (8.5) that

$$p_y/y = S_1(x). \tag{8.15}$$

From (8.14) and (8.15), it becomes clear that the appropriate ideal boundary condition to be attached to (8.10) is

$$S_1(x) \underset{x\to\infty}{\to} -[2M\epsilon_1(\infty)]^{1/2}. \tag{8.16a}$$

However, for a numerical solution of (8.10) (as has been carried out in the present treatment) (8.16a) requires some modification. What has been done is to replace it by the "practical" boundary condition

$$S_1(a) = -[2M\epsilon_1(a)]^{1/2}, \tag{8.16b}$$

where a is chosen to be a sufficiently large positive value of x so that $(1/\epsilon_1)(d\epsilon_1/dx)_{x=a} \ll 1$. Although the value of $S_1(a)$ given by (8.16) is not strictly correct for a finite value of a,[40] its use as an initial value is tenable if $S_1(x)$ is insensitive to changes in the value of $S_1(a)$ about $-[2M\epsilon_1(a)]^{1/2}$.

Numerical solutions of (8.10) with the initial value given by (8.16) have been found for several values of the energy E. A few of these solutions are plotted in Fig. 18 with the function $-[2M\epsilon_1(x)]^{1/2}$. It is observed that $S_1(x)$ closely follows

[39] As x becomes arbitrarily large, $\epsilon(x, 0)$ approaches $-[x + 1]$. Substituting $\epsilon(x, 0) = -[x + 1]$ into the expression for ϵ_1 in footnote 36, we obtain $\epsilon_1 = 3(1 + 1/3x)/2$, which asymptotically approaches 3/2 as x becomes very large compared with unity.

[40] $S_1(x) = -[2M\epsilon_1(x)]^{1/2}$ is not a solution of (8.10) when ϵ_1 is not strictly a constant.

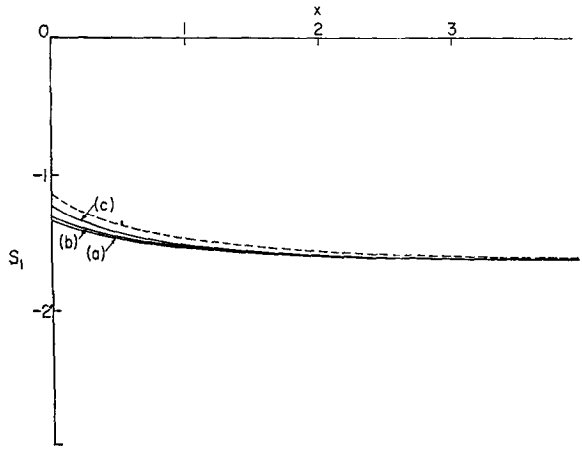

FIG. 18. Curves (a), (b), and (c) are plots of $S_1(x)$ for energies $-1.00J$, $-1.50J$, and $-1.95J$, respectively. x is expressed in units of $J\sqrt{6}/A$ while S_1 is in units of $(JM)^{1/2}/(J\sqrt{6}/A)$. The dashed curve is a plot of $-[2M\epsilon_1(x)]^{1/2}$.

$-[2M\epsilon_1(x)]^{1/2}$, manifesting a mild energy dependence. Furthermore we found that major deviations of $S_1(a)$ from $-[2M\epsilon_1(a)]^{1/2}$ produce only very minor changes in $S_1(x)$ away from a; $S_1(x)$ rapidly approaches $-[2M\epsilon_1(x)]^{1/2}$ from its initial value, $S_1(a)$.[41] Thus the use of the boundary condition (8.16) in the solution of (8.10) is justified.

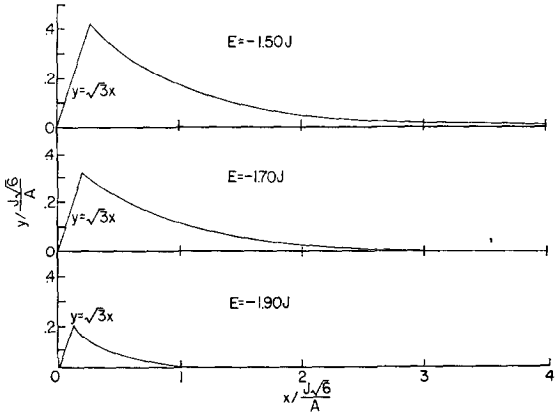

FIG. 19. Trajectories for the energies $-1.90J$, $-1.70J$, and $-1.50J$ are shown above, where x and y expressed in units of $J\sqrt{6}/A$. The interval in the y-direction is twice that of the x-direction.

[41] Quantitatively we found that a 25 % change in S_1 ($a = 6$) produced about a 1 % change in $S_1(x)$ at $x = 4$ and a much smaller alteration of $S_1(x)$ for smaller values of x; the curves of Fig. 18 are essentially unaffected by such a change in $S_1(a)$.

The doubly tangent trajectories, some of which are plotted in Fig. 19, are calculated from (8.8), where x_i and y_i are found from (8.9).

[Having found $S_1(x)$ we can find the x-component of momentum as a function of x, y, and E for each trajectory of interest, that is,

$$p_x^2 = \{2M[E - \epsilon(x, y)] - p_y^2\}^{1/2}$$
$$= \{2M[E - \epsilon(x, 0)] - [S_1^2(x) - 2M\epsilon_1(x)]\, y^2\}^{1/2},$$

where, consistent with our approximations, $p_y = yS_1$ and $\epsilon(x, y)$ is given by (8.1). The above expression for p_x is used in (8.9) in finding x_i and y_i. Furthermore, in integrating (8.8) numerically at a particular energy E, the value of $p_x(x')$ appropriate to the interval between $x' + dx'$ and x' is found by substituting the value of y at x' in the above expression for p_x.]

The degree of authenticity of such trajectories is determined from the range of validity of the approximations involved in their calculation. The two approximations which have been made are contained in Eqs. (8.1) and (8.5): the truncated expansion of $\epsilon(x, y)$ about $\epsilon(x, 0)$ and the truncated expansion of $S(x, y)$ in powers of y^2, respectively.

To investigate the validity of the latter assumption we shall estimate the relative magnitude of the first two y-dependent terms in the expansion, namely $(y^2S_1)/2$ and $(y^4S_2)/4$. Having already calculated $S_1(x)$ we focus our attention on $S_2(x)$. $S_2(x)$ is the solution of the differential Eq. (8.4c), rewritten here as

$$\frac{dS_2}{dx} = \frac{-4S_1(x)}{p_0(x)}\left[S_2 + \frac{1}{8S_1(x)}\left(\frac{dS_1}{dx}\right)^2\right] \tag{8.17}$$

with the boundary condition that $\lim_{x\to\infty} S_2(x) = 0$.[42] Introducing the notation

$$F(x) = -\int_0^x \frac{4S_1(x')}{p_0(x')}\,dx' = \int_0^x \frac{4\,|\,S_1(x')|}{p_0(x')}\,dx', \tag{8.18a}$$

one may write the solution of (8.17) [together with the boundary condition $S_2(\infty) = 0$] as the manifestly positive quantity

$$S_2(x) = e^{F(x)}\int_x^\infty dx'\,\frac{e^{-F(x')}}{2p_0(x')}\left(\frac{dS_1}{dx'}\right)^2$$
$$= e^{F(x)}\int_x^\infty dx'\,e^{-F(x')}F'(x')\left[\frac{1}{8\,|\,S_1(x')|}\left(\frac{dS_1}{dx'}\right)^2\right] \tag{8.18b}$$

[42] We have already shown that for arbitrarily large x, $\epsilon_1(x)$ is essentially constant and $p_y/y = (1/y)(\partial S/\partial y) = -[2M\epsilon_1(\infty)]^{1/2}$. Since for arbitrarily large x, $(1/y)(\partial S/\partial y)$ is independent of y, we see from the expansion $(1/y)(\partial S(x, y)/\partial y) = S_1(x) + y^2S_2(x) + \ldots$ that $S_2(x)$, as well as coefficients of higher powers of y^2, must vanish at arbitrarily large values of x.

[cognizance having been taken of the fact that $S_1(x) = -|S_1(x)|$ for all values of x]. Let us now note that (cf. Fig. 18) the square bracketed factor in the integrand of (8.18b) is a monotonically diminishing function of x; one therefore has [with $F'(x')$ positive]

$$S_2(x) \leqslant \frac{1}{8\,|\,S_1(x)|}\left(\frac{dS_1}{dx}\right)^2 \int_x^\infty e^{F(x)-F(x')}F'(x')\,dx'$$

$$= \frac{1}{8\,|\,S_1(x)|}\left(\frac{dS_1}{dx}\right)^2 \tag{8.18c}$$

[the last equality following by virtue of the fact that, with $F'(x \to \infty) \sim x^{-1/2}$, $F(x \to \infty) \sim x^{1/2}$, one has $\exp[-F(x \to \infty)] = 0$].

Now the maximum value of $(1/|\,8S_1\,|)(dS_1/dx)^2$ for positive x is near $x = 0$ where $(1/|\,8S_1\,|)(dS_1/dx)^2 = .005$. The ratio of the first two y-dependent terms in (8.3), $y^2S_2/2S_1$, is then of the order of $[y^2(dS_1/dx)^2]/16S_1^2$ which has an upper limit of .003 y^2. Anticipating that we shall be restricted to values of y less than unity, we see that we are justified in ignoring the contribution of $[y^4S_2(x)]/4$ to $S(x, y)$ compared with that of $[y^2S_1(x)]/2$. Assuming that none of the still higher order corrections are anomalously large, it is clear that truncating the expansion of $S(x, y)$ after the first y-dependent term is justified for $y < 1$.

All the analysis of this section has been based on the potential $\epsilon(x, y)$ as approximated by (8.1). The potential (8.1) is only a good estimate of the true potential for small values of y^2: $y^2 \ll 1$. For larger values of y, the y-dependence of $\epsilon(x, y)$ is no longer quadratic but approaches linearity.[43] Hence the magnitude of the component of force in the y-direction derived from (8.1), $|\,2\epsilon_1(x)\,y\,|$, increases with increasing y while the magnitude of the true component of force approaches a constant. Thus the approximation (8.1) produces an overestimation of the magnitude of the y-component of the force. As a result of this overestimation, the calculated trajectories tangent to the x-axis *and* perpendicular to the $y = \sqrt{3}x$ line must underestimate $y(x)$, that is, lie too close to the x-axis. Such an underestimate of $y(x)$ produces an underestimate of the shaded area of Fig. 17 and hence of the flux $\Phi(E)$. Furthermore, the underestimation of the flux associated with the calculated doubly tangent trajectories becomes increasingly large as the energy increases, since increasing energies are associated with trajectories which involve increasingly large values of y.

The calculated low energy flux is plotted as a function of $(E + 2J)/J$ in Fig. 20;

[43] The breakdown of the quadratic approximation is especially easy to see at large values of x for which $\epsilon(x, y) = -[x + (1 + 3y^2)^{1/2}]$. At small values of y^2, $3y^2 \ll 1$, a quadratic dependence is manifested: $\epsilon(x, y) = -[x + 1] - 3y^2/2$, while for $3y^2 \gg 1$, a linear y-dependence is seen: $\epsilon(x, y) = -[x + \sqrt{3}\,|\,y\,|]$.

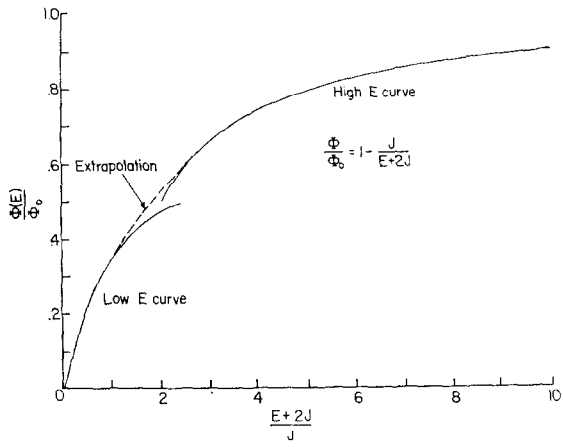

FIG. 20. $\Phi(E)/\mathbf{H} \cdot \mathbf{A}_{321}$ is plotted against $(E + 2J)/J$.

included on the graph is a plot of the high energy expression for the flux. The dashed curve is an extrapolation between the two limiting regimes.

[An estimate of the underestimation of the flux inherent in the approximation (8.1) can be found by first noting that the inclusion of the next order term in (8.1), $\epsilon_2(x)y^4$, produces an additional driving term in (8.17), namely $M\epsilon_2(x)/S_1(x)$. Following an analogous procedure to that used in discussing (8.17), one finds an upper limit of S_2 [when the additional driving term is included in (8.17)] of $M\epsilon_2(x)/S_1(x)$—this term being an order of magnitude greater than $(dS_1/dx)^2/8 \mid S_1 \mid$ and at least an order of magnitude smaller than $\mid S_1 \mid /y^2$. With the inclusion of $y^4S_2(x)/4$ in the expansion for $S(x, y)$ we find that $p_y = yS_1 + y^3S_2$. With the additional term y^3S_2 in the expression for p_y, the point (x_i, y_i) (found from the condition $p_y/p_x \mid_i = -1/\sqrt{3}$) and the trajectories (found from an approximate solution to the differential equation $p_y/p_x = dy/dx$ based on the assumptions that $y^2S_2/S_1 \ll 1$ and that the relative change in the trajectories is small, i.e., $\Delta y(x)/y(x) \sim y^2S_2/S_1 \ll 1$) are obtained. It is further observed that since $\Delta y(x)/y(x) \sim \Delta y_i/y_i \sim y_i^2S_2(x_i)/\mid S_1(x_i)\mid$ and the y-dependence of $H(x, y)$ is ignorable for small values of y, $y \ll 1$, the relative change of the flux $\Delta\Phi/\Phi$ is roughly $y_i^2S_2(x_i)/\mid S_1(x_i)\mid \sim y_i^2/12$ (in dimensionless units). Therefore we are able to use our computer calculation of $y_i(E)$ to estimate the error in the flux and thereby justify our extrapolation of Fig. 20.]

IX. THE HALL MOBILITY: RESULTS AND DISCUSSION

At this point in our exposition we can calculate the linearly field-dependent contribution to the jump rate from site 1 to site 3, namely,

$$w_{13}^{H} = \int_{-\infty}^{\infty} dE\, W_{13}^{H}(E). \tag{9.1}$$

Inserting the results (6.8) in (9.1) we find

$$\begin{aligned} w_{13}^{H} &= \frac{e}{Mc}\left(\frac{1}{MZ}\right)\int_{-2J}^{\infty} dE\, e^{-E/kT}\Phi(E) \\ &= \frac{e\mathbf{H}\cdot\mathbf{A}_{321}}{c}\left(\frac{kT}{M^2Z}\right)F(T)\, e^{2J/kT}, \end{aligned} \tag{9.2}$$

where $F(T)$ is the dimensionless function of temperature defined by

$$F(T) = \int_{-2J}^{\infty} d(E/kT)\, e^{-(E+2J)/kT}\frac{\Phi(E)}{\mathbf{H}\cdot\mathbf{A}_{321}} \tag{9.3}$$

and plotted in Fig. 21 as a function of J/kT. With the introduction of an explicit expression for Z given by Eq. (H.3), (9.2) becomes

$$w_{13}^{H} = [e/c\mathbf{H}\cdot\mathbf{A}_{321}](\omega_0/2\pi)^2\frac{\exp[-(\epsilon_3 - 2J)/kT]}{kT}F(T), \tag{9.4}$$

where

$$\epsilon_3 \equiv \frac{A^2}{3M\omega_0{}^2}.$$

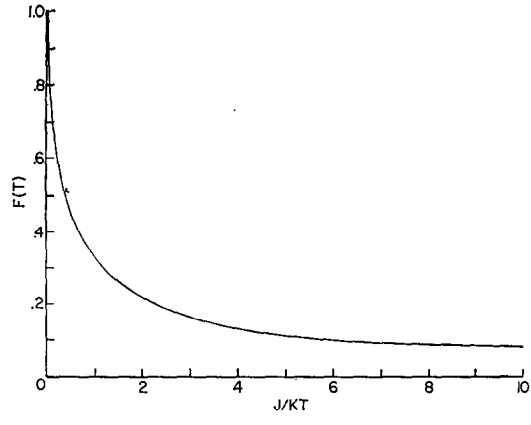

FIG. 21. $F(T)$ is plotted against J/kT.

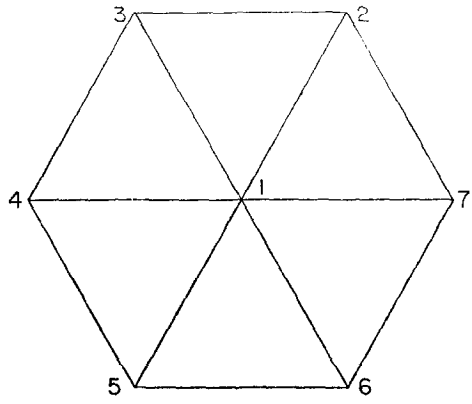

FIG. 22. The triangular lattice structure.

In Sec. IV of Ref. III, the Hall and drift mobilities are calculated for the triangular lattice structure shown in Fig. 22, yielding the results

$$\mu_H = \frac{2}{\sqrt{3}} \frac{c}{H} \frac{w_{13}^H}{w_{13}^0}$$

$$\mu_D = \frac{3}{2} \frac{ea^2}{kT} w_{13}^0 , \tag{9.5}$$

where a is the intersite distance and w_{13}^0 is the jump rate from site 1 to site 3 in the absence of an external field. In Appendix I of this work, w_{13}^0 is calculated yielding

$$w_{13}^0 = (\omega_0/2\pi) \exp[-(\epsilon_2 - J)/kT], \tag{9.6}$$

where

$$\epsilon_2 \equiv \frac{A^2}{4M\omega_0^2} .$$

Introducing the results (9.4) and (9.6) into the formulae (9.5) we find

$$\mu_H = \frac{ea^2}{2J} \left(\frac{\omega_0}{2\pi}\right)\left(\frac{J}{kT}\right) F(T) \exp[-(1/kT)(\epsilon_2/3 - J)] \tag{9.7a}$$

$$\mu_D = \frac{ea^2}{2J} \left(\frac{\omega_0}{2\pi}\right)\left(\frac{3J}{kT}\right) \exp[-(1/kT)(\epsilon_2 - J)], \tag{9.7b}$$

where we have replaced the area of the equilateral triangle A_{321} by $\sqrt{3}\, a^2/4$ in the

expression for the Hall mobility. Furthermore, we may utilize (9.7) to calculate the Hall coefficient

$$R_3 \equiv \frac{-1}{nec}\left(\frac{\mu_H}{\mu_D}\right) = \frac{-1}{nec}\left(\frac{F(T)}{3}\right)\exp\left(\frac{2}{3}\epsilon_2/kT\right). \tag{9.8}$$

We shall now compare our results for the Hall and drift mobilities and the Hall coefficient with those obtained by Friedman and Holstein in III. In particular, they found [Eqs. (4.10) and (4.12) of their paper]

$$\mu_H^{(FH)} = \frac{ea^2}{2J}\left(\frac{\omega_0}{2\pi}\right)\left(\frac{J\pi}{\hbar\omega_0}\right)\left(\frac{J^2\pi}{kT\epsilon_2}\right)^{1/2}\exp[-\epsilon_2/3kT] \tag{9.9a}$$

$$\mu_D^{(FH)} = \frac{ea^2}{2J}\left(\frac{\omega_0}{2\pi}\right)\left(\frac{3J}{kT}\right)\left(\frac{J\pi}{\hbar\omega_0}\right)\left(\frac{J^2\pi}{kT\epsilon_2}\right)^{1/2}\exp[-\epsilon_2/kT] \tag{9.9b}$$

and hence

$$R_3^{(FH)} \equiv \frac{-1}{nec}\left(\frac{\mu_H^{(FH)}}{\mu_D^{(FH)}}\right) = \frac{-1}{nec}\left(\frac{kT}{3J}\right)\exp\left(\frac{2}{3}\epsilon_2/kT\right). \tag{9.10}$$

The temperature dependence of $\mu_H^{(FH)}$, $\mu_D^{(FH)}$, and $R_3^{(FH)}$ is almost totally due to the respective exponential temperature dependent factors in these three quantities. Furthermore we observe that the activation energy associated with the Friedman–Holstein Hall mobility is one-third that associated with their drift mobility. Turning our attention to the mobilities in the adiabatic theory [given specifically by (9.7a) and (9.7b)], we note that the activation energies of both μ_H and μ_D are each lower than their Friedman–Holstein counterparts by an amount J. The appearance of J in the activation energy of μ_D will produce no major changes in the temperature dependence of μ_D, since ϵ_2 is substantially larger than J (as may be seen by recalling from Ref. I that the condition for the existence of the small polaron is $A^2/2M\omega_0^2 \gg 2J$). However, the presence of J in the activation energy for the adiabatic Hall mobility may produce a major difference between the temperature dependences of μ_H and $\mu_H^{(FH)}$ since $\epsilon_2/3$ may be of the order of J.

[Recalling from the paper of Friedman and Holstein that the activation energies in w_{13}^0 and w_{13}^H are the minimum potential energies, in excess of the binding energy, required to establish two and three site coincidences, respectively, we deduce that the exact three-site activation energy must be greater than or equal to the exact two-site activation energy since the establishment of a triple coincidence imposes a greater constraint on

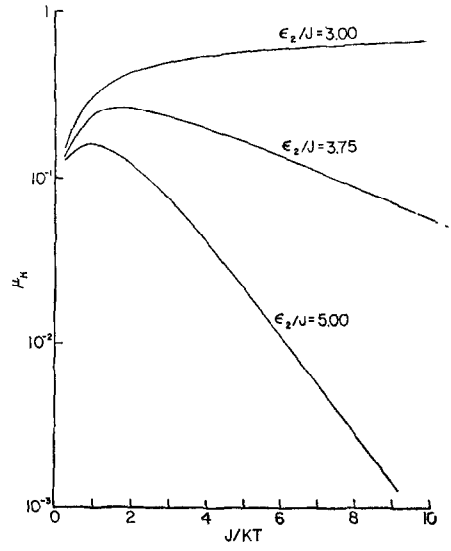

FIG. 23. The Hall mobility in the adiabatic approximation [in units of $(ea^2/2J)(\omega_0/2\pi)$] versus J/kT for three values of the parameter ϵ_2/J.

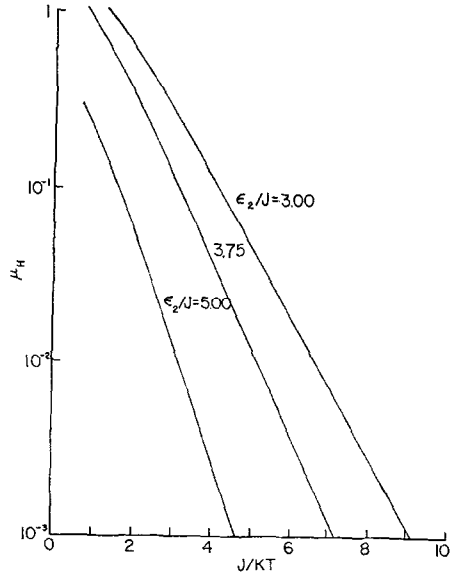

FIG. 24. The Hall mobility of the theory of Friedman and Holstein [in units of $(ea^2/2J)(\omega_0/2\pi)$] versus J/kT for three values of ϵ_2/J. For the purpose of these plots we have chosen $J = \hbar\omega_0$.

the system than the establishment of a double coincidence. Therefore the exact Hall-mobility activation energy, the difference of the three- and two-site activation energies [as seen from (9.5)] must be positive definite. In light of this fact, the case $\epsilon_2/3 = J$ (for which the exponent of (9.7a) formally vanishes) must be considered as an upper limit for the physical meaningfulness of the present results.]

The temperature dependences of μ_H and $\mu_H^{(FH)}$ are explicitly displayed in Figs. 23 and 24, respectively, where the Hall mobility is plotted as a function of J/kT for various values of the parameter ϵ_2/J.

[The curves of Fig. 24 are drawn for a particular choice of $(J/h\omega_0)$ in Eq. (9.9a), namely, $J/h\omega_0 = 1$. Noting that $\mu_H^{(FH)}$ is being plotted on a logarithmic scale we can see from (9.9a) that the particular choice of the factor $J/h\omega_0$ does not alter the temperature dependence of $\mu_H^{(FH)}$ as it only contributes a constant, $\ln(J/h\omega_0)$, to $\ln \mu_H^{(FH)}$. However, the curves derived in the adiabatic theory, specifically, the plots of μ_H [in units of $(ea^2/2J(\omega_0/2\pi))$] *vs.* J/kT found in Fig. 23, are independent of the ratio $J/h\omega_0$ as may be seen from (9.7a).]

We should like to stress the fact, apparent from Fig. 23, that the Hall mobility in the hopping model need not be an exponentially decreasing function of reciprocal temperature. In fact, the Hall mobility in the hopping regime may even be an increasing function of reciprocal temperature over a significant temperature range. However, as is shown in Fig. 25, the drift mobility in the adiabatic theory does possess an activated temperature dependence which further manifests itself in the three site Hall coefficient plotted in Fig. 26.

In that all of the preceding calculation and discussion has been limited to a triangular lattice structure, we would like to point out that for other lattice structures a term proportional to J may also occur in the Hall mobility activation energy. In particular, preliminary consideration of a two-dimensional lattice in which the lattice sites form a square array yields the following drift and Hall mobility activation energies, $E_D{}^4$ and $E_H{}^4$ respectively,

$$E_D{}^4 = \epsilon_2 - J = \epsilon_2 \left[1 - \frac{J}{\epsilon_2}\right],$$

$$E_H{}^4 = \frac{\epsilon_2}{3} - (\sqrt{2} - 1)J = \frac{\epsilon_2}{3}\left[1 - 3(\sqrt{2} - 1)\frac{J}{\epsilon_2}\right]. \tag{9.11}$$

Since the J-dependent term of $E_H{}^4$ is less than half that of the comparable term of the triangular lattice Hall activation energy its effect on the Hall mobility of the square lattice will be of less consequence.

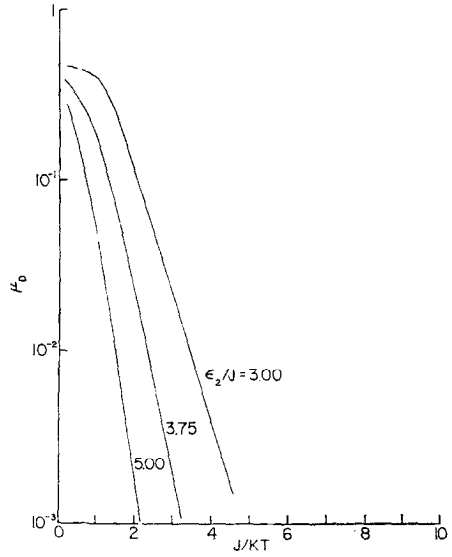

FIG. 25. The drift mobility in the adiabatic approximation [in units of $(ea^2/2J)(\omega_0/2\pi)$] for three values of the ratio ϵ_2/J.

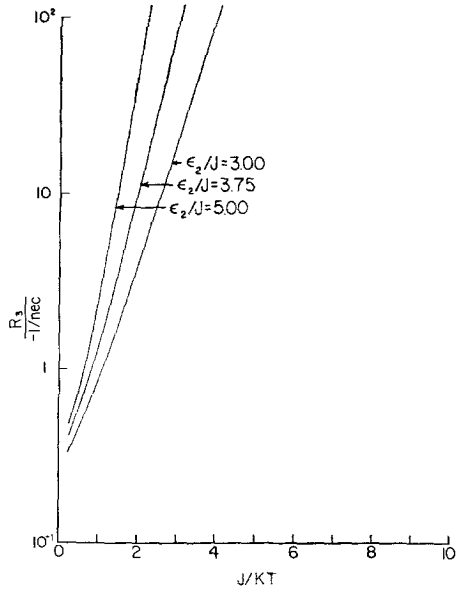

FIG. 26. Temperature dependence of the three site Hall coefficient, $R_3/(-1/nec)$.

However, to put the matter in proper perspective, it should be recalled that the small polaron picture is only strictly correct for $J \ll \epsilon_2$. For values of J which approach the order of magnitude of ϵ_2 the polaron increases in size, that is, the lattice distortion at sites which are adjacent to the site about which the polaron is localized experience a substantial distortion. One feature of this regime, that of the semi-small polaron, $J \lesssim \epsilon_2$, is the further J-dependent reduction of the energy required to achieve double and triple coincidences. In particular, in lowest order the spreading out of the polaron is associated with corrections to the Hall and drift mobility activation energies which are of the order of J^2/ϵ_2. Thus, since these corrections to the activation energies may be substantial for $J \sim \epsilon_2/3$ the activation energies of Eqs. (9.7) are not to be taken literally for such values of the parameters but rather are to be viewed as illustrative of a possible trend in the semi-small polaron regime, i.e., hopping characterized by a very weakly activated Hall mobility.[44]

Some discussion of the behavior of μ_H in the "transition" region—between the domains of validity of the adiabatic approach of the present paper and the small-J theory of FH—is now in order. As shown in II [cf. Eq. (103)], this region is characterized by the condition

$$J \sim J_{tr} \equiv \left(\frac{2kT\epsilon_2}{\pi}\right)^{1/4} \left(\frac{\hbar\omega_0}{\pi}\right)^{1/2}; \tag{9.12}$$

for $J \ll J_{tr}$, non-adiabatic transitions between different potential energy surfaces are of major importance, whereas for $J \gg J_{tr}$ these processes are negligible and the adiabatic theory is valid.

Now, when $J \sim J_{tr}$ (and for $J_{tr} \ll kT$[45]) the non-adiabatic two site hopping probability [given by (79) of II: the factor $\hbar^2$ in the denominator of that expression should be replaced by $\hbar$] is comparable in magnitude to its adiabatic counterpart [(9.6) of the present paper]; because of the proportionality of the two-site hopping probability to the drift mobility μ_D the latter quantity also exhibits this behavior [as is easily verified by comparison of (9.7b) and (9.9b) for $J \sim J_{tr}$]. One may then infer that the variation of μ_D as a function of bandwidth parameter J is of a simple

[44] In fact, the inclusion of the lowest order correction term in the activation energies of (9.7) does not substantially alter our conclusions concerning the temperature dependence of the mobilities for the triangular lattice structure. In addition, a preliminary calculation carried out for the square lattice structure indicates that the lowest order corrections to (9.11) further reduces the ratio E_H^4/E_D^4.

[45] The discussion of Appendix III of II, which established (9.12) as the transition region between the domains of validity of the two approaches, was based on the assumption that the nuclear motion could be treated purely classically. The validity-condition for this assumption is given by the first inequality on page 385 of II, namely $kT \gg \frac{1}{4}[(3A^2/M\omega_0^2)(\hbar\omega_0)^2]^{1/3} = [\frac{3}{16}\epsilon_2(\hbar\omega_0)^2]^{1/3}$, eliminating $\hbar\omega_0$ by use of (9.12), one obtains $kT \gg J_{tr}$. Q.E.D.

monotonic type in which μ_D rises with increasing J ($\propto J^2$ in the non-adiabatic regime) to an asymptotic upper limit given by the adiabatic theory.

It has now to be remarked that this relatively simple behavior is *not* exhibited by the Hall mobility. In particular, the right hand sides of (9.7a) and (9.9a), which give the adiabatic and FH Hall mobilities, are *not* of comparable order in the transition region, $J \sim J_{tr}$. In fact, upon dividing (9.7a) by (9.9a), setting J equal to J_{tr}, and with the use of (9.11), one has

$$\frac{\mu_H}{\mu_H^{(FH)}} = \left(\frac{1}{2}\right)^{1/2} \frac{J_{tr}}{kT} F(T)\, e^{J_{tr}/kT}$$

which, in the relevant limit, $J_{tr}/kT \ll 1$, becomes

$$\frac{\mu_H}{\mu_H^{(FH)}} \simeq \left(\frac{1}{2}\right)^{1/2} \frac{J_{tr}}{kT} \ll 1.$$

From this result it is apparent that the J-variation of μ_H in the transition region is more complicated than that of μ_D; in particular, it is not likely to be of the simple monotonic type discussed above.

A definitive resolution of the question would appear to require a full treatment of the three-site problem in the transition region itself. In the absence of such a treatment, the following brief remarks concerning the physical origin of the order-of-magnitude discrepancy between μ_H and $\mu_H^{(FH)}$ in the transition region are, in the opinion of the present authors, pertinent and perhaps ultimately useful.

As may be observed from the text on pages 508–510 in FH's Sec. II [especially Eq. (2.18)], contributions to the FH Hall Effect arise, more or less uniformly, from all trajectories which pass through the immediate vicinity of the triple-coincidence point. On the other hand, as is shown in the present paper (especially in the first few paragraphs of Sec. IV), only differentially small groups of trajectories—in the vicinity of the so-called "limiting" trajectories—contribute to the adiabatic Hall effect. In the domain of $J \ll kT$, relevant to the present discussion, these trajectories are—to within a differentially small angle ($\propto H$)—nearly parallel to the coincidence line between regions 2 and 3, i.e., nearly parallel to the x-axis of Fig. 2. It is then apparent that, in contrast to the two-site hopping process in which essentially only one type of trajectory is involved (characterized by crossing the appropriate coincidence line: cf. Fig. 2 of II), the transition from the small-J to the adiabatic regime must, as far as the three-site Hall effect is concerned, be of a highly non-uniform character. Specifically, as J is increased, two quite different physical processes must occur:

(1) Contributions to $W_{13}^{(H)}$ from the main group of trajectories, not parallel to the x-axis of Fig. 2, must become negligible—possibly in a manner similar to the

disappearance of non-adiabatic transitions (as described, e.g., by III-7 of Appendix III of II), and

(2) the contributions of trajectories which, within the above-described differential angle, are parallel to the x-axis, and which since they are differential in number contribute insignificantly to $W_{13}^{(H)}$ in the small-J regime, must grow in importance, ultimately assuming the dominant role in the adiabatic regime.

From these rather brief remarks, it is clear that the J-variation of $W_{13}^{(H)}$ and, hence, of μ_H, is inherently more complicated than that of quantities (such as μ_D) which are determined by the elementary two-site hopping process. An investigation along lines indicated by the above discussion should (hopefully) be undertaken in the not too distant future.

X. SUMMARY

A theoretical treatment, based on the *adiabatic approximation*, is given for the Hall-mobility of the small polaron in the hopping regime. It is shown that, in the presence of an external magnetic field, the usual vibrational Hamiltonian of adiabatic theory is augmented by terms linearly dependent on the magnetic field and on the vibrational momenta. The differential effect of these terms on the elementary (intersite) hopping probability of small polarons in a two-dimensional triangular lattice is computed. The result leads directly to an expression for the Hall-mobility, μ_H, which can be compared (a) to the drift mobility, μ_D, and (b) to the non-adiabatic expression for μ_H, obtained in the earlier work of Friedman and one of the present authors (T. Holstein).

A principal feature of the new results is that, for reasonable values of the physical parameters, the activation behavior of μ_H is much weaker than that of μ_D; in fact, μ_H may diminish with increasing temperature over a significant temperature range. In addition, it has been found that, contrary to the predictions of non-adiabatic theory, the magnitude of μ_H is less than that of μ_D at sufficiently high temperatures.

ACKNOWLEDGMENT

One of the authors (T. Holstein) is pleased to acknowledge an important conversation with C. Herring, which took place a number of years ago. In this conversation, Dr. Herring remarked that, in an adiabatic theory (in which the electronic wavefunction is fixed by the vibrational coordinates), one would expect the $\mathbf{A} \cdot \mathbf{v}$ term of the electronic Lagrangian to contribute to the *vibrational* Lagrangian terms linearly proportional to both the magnetic field and to the *time-derivatives* of the *vibrational coordinates*; such terms would then embody the mechanism through which the magnetic field affects the dynamics of adiabatic hopping transitions. The reader will recognize that the basic approach of our treatment, as contained in Section II, in essence constitutes the realization—in Hamiltonian form—of the above-described idea.

APPENDIX A. PROOF OF THE IDENTITY (2.6)

Consider the term

$$\sum_p C_p^* \frac{\partial^2 C_p}{\partial x_g^2}. \tag{A.1}$$

Writing

$$C_p = R_p \exp[i\theta_p], \tag{A.2}$$

where R_p and θ_p are real functions of x, we note that

$$\frac{\partial}{\partial x_g}(R_p \exp[i\theta_p]) = \left(\frac{\partial R_p}{\partial x_g} + i\frac{\partial \theta_p}{\partial x_g} R_p\right) \exp[i\theta_p] \tag{A.3}$$

and

$$\begin{aligned}\frac{\partial^2}{\partial x_g^2}(R_p \exp[i\theta_p]) = &\left[\frac{\partial^2 R_p}{\partial x_g^2} - R_p\left(\frac{\partial \theta_p}{\partial x_g}\right)^2\right] \exp[i\theta_p] \\ &+ i\left(\frac{2\partial\theta_p}{\partial x_g}\frac{\partial R_p}{\partial x_g} + \frac{\partial^2\theta_p}{\partial x_g^2} R_p\right) \exp[i\theta_p].\end{aligned} \tag{A.4}$$

Hence

$$\begin{aligned} i \operatorname{Im}\left(\sum_p C_p^* \frac{\partial^2 C_p}{\partial x_g^2}\right) &= i\sum_p \left[\frac{\partial\theta_p}{\partial x_g}\frac{\partial R_p^2}{\partial x_g} + R_p^2 \frac{\partial}{\partial x_g}\left(\frac{\partial\theta_p}{\partial x_g}\right)\right] \\ &= i\frac{\partial}{\partial x_g}\left(\sum_p \frac{\partial\theta_p}{\partial x_g} R_p^2\right). \end{aligned} \tag{A.5}$$

However, from (A.2) and (A.3) and the normalization condition

$$\sum_p |C_p|^2 = \sum_p R_p^2 = 1$$

we find that

$$\begin{aligned}\sum_p C_p^* \frac{\partial C_p}{\partial x_g} &= \sum_p \left(\frac{1}{2}\frac{\partial R_p^2}{\partial x_g} + i\frac{\partial\theta_p}{\partial x_g} R_p^2\right) \\ &= \frac{1}{2}\frac{\partial}{\partial x_g}\left(\sum_p R_p^2\right) + i\sum_p \frac{\partial\theta_p}{\partial x_g} R_p^2 \\ &= i\sum_p \frac{\partial\theta_p}{\partial x_g} R_p^2. \end{aligned} \tag{A.6}$$

Inserting (A.6) into (A.5), we obtain the relationship (2.6), namely,

$$i \operatorname{Im}\left(\sum_p C_p^* \frac{\partial^2 C_p}{\partial x_g}\right) = \frac{\partial}{\partial x_g}\left(\sum_p C_p^* \frac{\partial C_p}{\partial x_g}\right). \tag{A.7}$$

APPENDIX B. THE ELECTRONIC ENERGY $\epsilon(x, y)$

In this appendix we shall study the lowest energy solution $\epsilon(x, y)$[46] of the three solutions of the cubic equation (2.15), namely,

$$\begin{aligned}
\epsilon &= 2\sqrt{a}\cos[(\phi/3) + (2\pi/3)] = -\sqrt{a}[\cos(\phi/3) + \sqrt{3}\sin(\phi/3)] \\
\epsilon' &= 2\sqrt{a}\cos[(\phi/3) - (2\pi/3)] = -\sqrt{a}[\cos(\phi/3) - \sqrt{3}\sin(\phi/3)] \\
\epsilon'' &= 2\sqrt{a}\cos(\phi/3),
\end{aligned} \tag{B.1}$$

where

$$\cos\phi = \frac{-b}{a^{3/2}}, \qquad 0 \leqslant \phi \leqslant \pi \tag{B.2}$$

and

$$\begin{aligned}
a &\equiv J^2[(A/J\sqrt{6})^2(x^2 + y^2) + 1] \\
b &\equiv J^3[(A/J\sqrt{6})^3(3y^2 - x^2)x + 1].
\end{aligned} \tag{B.3}$$

Before proceeding further we find it useful to express a and b in terms of the polar coordinates r and θ via the transformation

$$\begin{aligned}
x &= r\cos\theta \\
y &= r\sin\theta, \qquad 0 \leqslant \theta \leqslant 2\pi
\end{aligned}$$

that is,

$$\begin{aligned}
a &= J^2[(Ar/J\sqrt{6})^2 + 1] \\
b &= J^3[-(Ar/J\sqrt{6})^3\cos 3\theta + 1],
\end{aligned} \tag{B.4}$$

where the identity

$$\cos 3\theta = \cos\theta[\cos^2\theta - 3\sin^2\theta] \tag{B.5}$$

has been used in finding (B.4).

Let us first consider the energy surface $\epsilon(x, y)$ in the limit in which $J \to 0$. In this limit we find that

$$\begin{aligned}
a &= (Ar/\sqrt{6})^2 \\
b &= -(Ar/\sqrt{6})^3\cos 3\theta
\end{aligned}$$

[46] Bearing in mind that $\phi/3$ is restricted to lie between 0 and $\pi/3$ (so that $\cos\phi/3$ and $\sin\phi/3$ are both positive quantities), it becomes clear from (B.1) that $\epsilon \leqslant \epsilon' \leqslant \epsilon''$ ($\epsilon = \epsilon'$ for $\phi/3 = 0$ and $\epsilon' = \epsilon''$ for $\phi/3 = \pi/3$). In addition it can be shown that ϵ never equals ϵ' (that is, that $\phi/3 > 0$) by noting from (B.4) that $\cos\phi = -b/a^{3/2} < 1$.

and

$$\phi = \cos^{-1}(\cos 3\theta). \tag{B.6}$$

Observing that the eigenvalue of interest to us,

$$\epsilon = (2Ar/\sqrt{6})\cos[(\phi + 2\pi)/3], \tag{B.7}$$

possesses the property of being unaffected by the replacement of ϕ by $2\pi - \phi$: i.e.,

$$\cos\left(\frac{2\pi - \phi + 2\pi}{3}\right) = \cos\left(\frac{4\pi - \phi}{3}\right) = \cos\left(\frac{\phi - 4\pi}{3}\right) = \cos\left(\frac{\phi + 2\pi}{3}\right),$$

we see that we may allow ϕ, the solution of (B.6), to have values between 0 and 2π without affecting the eigenvalue ϵ. Bearing this in mind, the solution of (B.6) is

$$\begin{aligned}
&\phi = 3\theta && \text{for} \quad 0 \leqslant \theta < 2\pi/3 \quad \text{(region 3)} \\
&\phi = 3\theta - 2\pi && \text{for} \quad 2\pi/3 \leqslant \theta < 4\pi/3 \quad \text{(region 1)} \\
&\phi = 3\theta - 4\pi && \text{for} \quad 4\pi/3 \leqslant \theta < 2\pi \quad \text{(region 2).}
\end{aligned} \tag{B.8}$$

Inserting these results into the expression for ϵ (B.7), we have

$$\begin{aligned}
&\epsilon = -(A/\sqrt{6})(x + \sqrt{3}y), && \text{region 3} \\
&\epsilon = 2Ax/\sqrt{6}, && \text{region 1} \\
&\epsilon = -(A/\sqrt{6})(x - \sqrt{3}y), && \text{region 2.}
\end{aligned} \tag{B.9}$$

Geometrically the surface $\epsilon(x, y)$ defined by (B.9) is a triangular pyramid with its edges on the lines $\theta = 0$ ($y = 0, x > 0$), $\theta = 2\pi/3$ ($y = -\sqrt{3}x, x < 0$), and $\theta = 4\pi/3$ ($y = \sqrt{3}x, x < 0$).

We shall now proceed to verify that for $r \gg J\sqrt{6}/A$ and $-2\pi/3 < \theta < 2\pi/3$,

$$\epsilon = -(Ax/\sqrt{6}) - J[3(Ay/J\sqrt{6})^2 + 1]^{1/2}. \tag{3.5}$$

Rewriting (3.5) in polar coordinates as

$$\epsilon = (2Ar/\sqrt{6})[1 + (J\sqrt{6}/Ar)^2]^{1/2}\left\{-\frac{1}{2}\frac{[\cos\theta + (3\sin^2\theta + (J\sqrt{6}/Ar)^2)^{1/2}]}{[1 + (J\sqrt{6}/Ar)^2]^{1/2}}\right\} \tag{B.10}$$

and noting the general relation [inserting the expression for a (B.4) into (B.1)],

$$\epsilon = (2Ar/\sqrt{6})[1 + (J\sqrt{6}/Ar)^2]^{1/2}\cos[(\phi + 2\pi)/3], \tag{B.11}$$

we observe that we can verify (3.5) by showing that in the limit as $(J\sqrt{6}/Ar) \to 0$, with $-2\pi/3 < \theta < 2\pi/3$, $\cos[(\phi + 2\pi)/3]$ approaches

$$\zeta \equiv -\frac{1}{2}\frac{[\cos\theta + (3\sin^2\theta + (J\sqrt{6}/Ar)^2)^{1/2}]}{[1 + (J\sqrt{6}/Ar)^2]^{1/2}}. \tag{B.12}$$

Let us now observe that the trigonometric identity [equivalent to (B.5)]

$$\cos\phi = \cos[(\phi + 2\pi)/3][4\cos^2((\phi + 2\pi)/3) - 3] \tag{B.13}$$

will be satisfied by the exact expressions for $\cos[(\phi + 2\pi)/3]$ and $\cos\phi$. Upon inserting the exact expression for $\cos\phi$:

$$\cos\phi = \frac{\cos 3\theta - (J\sqrt{6}/Ar)^3}{[1 + (J\sqrt{6}/Ar)^2]^{3/2}} \tag{B.14}$$

[obtained by inserting (B.4) into (B.2)] into (B.13), we may regard (B.13) as an equation for $\cos[(\phi + 2\pi)/3]$. Let us now introduce the ansatz $\cos[(\phi + 2\pi)/3]$ only differs slightly from its assumed limiting value ζ. Explicitly let us write

$$\cos[(\phi + 2\pi)/3] = \zeta + \delta,$$

where ζ is defined in (B.12) and δ is deemed arbitrarily small, so that to first order in δ (B.13) becomes

$$\cos\phi - \zeta[4\zeta^2 - 3] = \delta[12\zeta^2 - 3]. \tag{B.15}$$

Furthermore, one can show by use of (B.12) that

$$[12\zeta^2 - 3] = \frac{6\{\sin^2\theta + \cos\theta[3\sin^2\theta + (J\sqrt{6}/Ar)^2]^{1/2}\}}{[1 + (J\sqrt{6}/Ar)^2]} \tag{B.16}$$

and that, with (B.12) and (B.14)

$$\cos\phi - \zeta[4\zeta^2 - 3] = -(J\sqrt{6}/Ar)^2\frac{\{(J\sqrt{6}/Ar) + [3\sin^2\theta + (J\sqrt{6}/Ar)^2]^{1/2}\}}{[1 + (J\sqrt{6}/Ar)^2]^{3/2}} \tag{B.17}$$

Utilizing (B.16), (B.17), and (B.12) in (B.15), we finally find

$$\frac{\delta}{\zeta} = \frac{\frac{1}{3}(J\sqrt{6}/Ar)^2\{(J\sqrt{6}/Ar) + [3\sin^2\theta + (J\sqrt{6}/Ar)^2]^{1/2}\}}{\{\sin^2\theta + \cos\theta[3\sin^2\theta + (J\sqrt{6}/Ar)^2]^{1/2}\}\{\cos\theta + [3\sin^2\theta + (J\sqrt{6}/Ar)^2]^{1/2}\}}$$

$$= \frac{\frac{1}{3}(J\sqrt{6}/Ar)^2\{(J\sqrt{6}/Ar) + [3\sin^2\theta + (J\sqrt{6}/Ar)^2]^{1/2}\}}{\{4\sin^2\theta\cos\theta + [3\sin^2\theta + (J\sqrt{6}/Ar)^2]^{1/2} + (J\sqrt{6}/Ar)^2\cos\theta\}}. \tag{B.18}$$

At large distances from the origin ($J\sqrt{6}/Ar \ll 1$) and for finite angles, $\sin\theta \gg (J\sqrt{6}/Ar)$,

$$\frac{\delta}{\zeta} \sim \frac{\frac{1}{3}(J\sqrt{6}/Ar)^2\,[3\sin^2\theta]^{1/2}}{\{4\sin^2\theta\cos\theta + [3\sin^2\theta]^{1/2}\}}$$

$$= \frac{\frac{1}{3}(J\sqrt{6}/Ar)^2}{\frac{4}{\sqrt{3}}\cos\theta[\sin^2\theta]^{1/2} + 1}. \tag{B.19}$$

The denominator of (B.19) is nonzero for $-2\pi/3 < \theta < 2\pi/3$ (having its zeros at $\theta = 2\pi/3$ and $\theta = -2\pi/3$, the $x_1 = x_3$ and $x_1 = x_2$ coincidence lines, respectively). Furthermore for $J\sqrt{6}/Ar \lesssim |\theta| \ll 2\pi/3$,[47]

$$\frac{\delta}{\zeta} \sim \frac{1}{3}(J\sqrt{6}/Ar)^2.$$

To complete our verification of the fact that δ/ζ vanishes in regions 2 and 3 (away from the $x_1 = x_2$ and $x_1 = x_3$ lines) as $J\sqrt{6}/Ar \to 0$, we note from (B.18) that for small angles, $|\sin\theta| \sim |\theta| \lesssim J\sqrt{6}/Ar$,

$$\frac{\delta}{\zeta} \lesssim \frac{2}{3}(J\sqrt{6}/Ar)^2.$$

Hence we have verified that (3.5) is an approximate eigenvalue of (2.15) in regions 2 and 3 for $r = [x^2 + y^2]^{1/2} \gg J\sqrt{6}/A$. Since (3.5) yields the pyramidal results (3.4) in regions 2 and 3 in the limit as J tends to zero, we can state that (3.5) is the large r approximation to the desired eigenvalue $\epsilon(x, y)$ in these two regions.

To expand $\epsilon(x, y)$ about the origin in powers of $Ar/J\sqrt{6}$ it is convenient to rewrite $\epsilon(x, y)$ as

$$\epsilon = 2J[1 + (Ar/J\sqrt{6})^2]^{1/2}\cos[(\phi + 2\pi)/3], \tag{B.20}$$

where

$$\cos\phi = \frac{(Ar/J\sqrt{6})^3\cos[3\theta] - 1}{[1 + (Ar/J\sqrt{6})^2]^{3/2}}. \tag{B.21}$$

It is clear from (B.21) that for $r = 0$ we have $\cos\phi = -1$; hence $\phi = \pi$ and $\cos[(\phi + 2\pi)/3] = -1$. With this in mind we shall write

$$\cos[(\phi + 2\pi)/3] = -1 + \delta \tag{B.22}$$

[47] Near the $x_1 = x_3$ and $x_1 = x_2$ lines, $\theta \sim \pm 2\pi/3 \mp (J\sqrt{6}/Ar)$, the denominator becomes $J\sqrt{6}/Ar$ and $\delta/\zeta \sim (J\sqrt{6}/Ar)$.

and assume that near the origin ($Ar/J\sqrt{6} \ll 1$) $\delta \ll 1$, so that we may keep only the lowest order term in δ when (B.22) is inserted in the identity (B.13), that is, we have, with (B.21),

$$\cos\phi = \frac{(Ar/J\sqrt{6})^3\cos(3\theta) - 1}{[1 + (Ar/J\sqrt{6})^2]^{3/2}} = (-1 + \delta)[4(-1 + \delta)^2 - 3] \simeq -1 + 9\delta. \tag{B.23}$$

Proceeding to expand the left hand side of (B.23) about $Ar/J\sqrt{6} = 0$ and keeping terms up to the third power of $Ar/J\sqrt{6}$, we find[48]

$$\delta = \tfrac{1}{6}(Ar/J\sqrt{6})^2 + \tfrac{1}{9}(Ar/J\sqrt{6})^3\cos 3\theta. \tag{B.24}$$

Finally, to find ϵ in the vicinity of the origin we expand the square root of (B.20) about unity and insert the ansatz (B.22) and result (B.24) into (B.20), yielding the third order in $Ar/J\sqrt{6}$,[49]

$$\epsilon = -2J[1 + \tfrac{1}{3}(Ar/J\sqrt{6})^2 - \tfrac{1}{9}(Ar/J\sqrt{6})^3\cos 3\theta]. \tag{B.25}$$

Expressing the expansion (B.25) in Cartesian coordinates, we readily obtain the expansion (3.6).

APPENDIX C. CALCULATION OF $(\partial\epsilon/\partial x) + (A/\sqrt{6})$ AND $\partial\epsilon/\partial y$

It is the purpose of this appendix to calculate the partial derivatives $(\partial/\partial x)\,\epsilon(x, y)$ and $(\partial/\partial y)\,\epsilon(x, y)$ which arise in the calculations of Appendices D and E. We can proceed to accomplish this task in a formal way by rewriting the eigenvalue equation (2.15) with the definitions of a and b found in (3.3) as

$$\epsilon^3 - 3a\epsilon + 2b = 0. \tag{C.1}$$

If we partially differentiate (C.1) with respect to x and y, respectively, we find

$$\begin{aligned} 3(\epsilon^2 - a)\frac{\partial\epsilon}{\partial x} - 3\epsilon\frac{\partial a}{\partial x} + 2\frac{\partial b}{\partial x} &= 0 \\ 3(\epsilon^2 - a)\frac{\partial\epsilon}{\partial y} - 3\epsilon\frac{\partial a}{\partial y} + 2\frac{\partial b}{\partial y} &= 0. \end{aligned} \tag{C.2}$$

[48] If we were to include terms of higher powers of $Ar/J\sqrt{6}$ in (B.24) consistency would require that we retain higher powers of δ in (B.23).

[49] A Taylor expansion of $\epsilon(x, y)$ about $\epsilon(0, 0) = -2J$ (with repeated use of the derivative formulas of Appendix C) yields the identical result.

Equation (C.2) may be solved for the partial derivatives $\partial\epsilon/\partial x$ and $\partial\epsilon/\partial y$ with the result that

$$\frac{\partial\epsilon}{\partial x} = \frac{3\epsilon(\partial a/\partial x) - 2(\partial b/\partial x)}{3(\epsilon^2 - a)}$$
$$\frac{\partial\epsilon}{\partial y} = \frac{3\epsilon(\partial a/\partial y) - 2(\partial b/\partial y)}{3(\epsilon^2 - a)}. \tag{C.3}$$

Inserting the definitions of a and b from (3.3) into (C.3), we readily find that

$$\frac{\partial\epsilon}{\partial x} = \frac{-A}{3(\epsilon^2 - a)}\left[\frac{A^2}{\sqrt{6}}(y^2 - x^2) - \epsilon Ax\right]$$
$$\frac{\partial\epsilon}{\partial y} = \frac{-A}{3(\epsilon^2 - a)}\left[\frac{2A^2}{\sqrt{6}}xy - \epsilon Ay\right]. \tag{C.4}$$

In anticipation of the use of these derivatives in Appendices D and E we proceed to express the quantities $(\partial/\partial y)\epsilon(x, y)$ and $(\partial/\partial x)\epsilon(x, y) + A/\sqrt{6}$ in terms of the quantities X_0, Y_0, and Z_0 [the quantities defined in (2.10) in the limit of $\alpha = 0$]. That is, utilizing (2.10) and the results (2.17), we may write

$$\frac{\partial\epsilon}{\partial y} = \frac{-A}{3(\epsilon^2 - a)}[-Ay][\epsilon - (2Ax/\sqrt{6})]$$
$$= \frac{-A}{3(\epsilon^2 - a)}[(Y_0 - Z_0)/\sqrt{2}][X_0 + J]. \tag{C.5}$$

Furthermore, we use the definition of a (3.3), the result (C.4), (2.10), and (2.17) in writing

$$\frac{\partial\epsilon}{\partial x} + \frac{A}{\sqrt{6}} = \frac{-A}{3(\epsilon^2 - a)}\left[\frac{A^2}{\sqrt{6}}(y^2 - x^2) - \epsilon Ax - \frac{3(\epsilon^2 - a)}{\sqrt{6}}\right]$$
$$= \frac{A}{3(\epsilon^2 - a)}\frac{3}{\sqrt{6}}\left[\epsilon^2 + \frac{2Ax}{\sqrt{6}}\epsilon + \left(\frac{A}{\sqrt{6}}\right)^2(x^2 - 3y^2) - J^2\right]$$
$$= \frac{A}{\sqrt{6}(\epsilon^2 - a)}[Y_0Z_0 + J(Y_0 + Z_0)]. \tag{C.6}$$

At this point we introduce the eigenvalue equation (2.15) expressed in terms of X_0, Y_0, and Z_0:

$$X_0Y_0Z_0 + J[X_0Y_0 + Y_0Z_0 + Z_0X_0] = 0. \tag{C.7}$$

Utilizing (C.7) we may rewrite (C.6) and (C.5) as

$$\frac{\partial \epsilon}{\partial x} + \frac{A}{\sqrt{6}} = \frac{-A}{(\epsilon^2 - a)\sqrt{6}} \left(\frac{JY_0Z_0}{X_0} \right)$$

$$\frac{\partial \epsilon}{\partial y} = \frac{A}{3(\epsilon^2 - a)} \left(\frac{Y_0 - Z_0}{\sqrt{2}} \right) \left[\frac{J(Y_0 + Z_0) X_0}{Y_0Z_0} \right]$$

$$= \frac{A}{3(\epsilon^2 - a)} \left(\frac{J(Y_0^2 - Z_0^2) X_0}{\sqrt{2}\, Y_0Z_0} \right). \tag{C.8}$$

In order to express $3(\epsilon^2 - a)$ in terms of X_0, Y_0, and Z_0 we note the identity [which may be verified by utilizing (2.10) and (2.17) to express ϵ^2 and a in terms of X_0, Y_0, and Z_0]:

$$3(\epsilon^2 - a) = (X_0Y_0 + Y_0Z_0 + Z_0X_0) + 2J(X_0 + Y_0 + Z_0). \tag{C.9}$$

Utilizing the eigenvalue equation (C.7) and the identity

$$X_0^2Y_0^2 + Y_0^2Z_0^2 + Z_0^2X_0^2 = (X_0Y_0 + Y_0Z_0 + Z_0X_0)^2 - 2X_0Y_0Z_0(X_0 + Y_0 + Z_0),$$

we may write

$$X_0^2Y_0^2 + Y_0^2Z_0^2 + Z_0^2X_0^2$$

$$= \left(-\frac{X_0Y_0Z_0}{J} \right) [X_0Y_0 + Y_0Z_0 + Z_0X_0 + 2J(X_0 + Y_0 + Z_0)]. \tag{C.10}$$

Inserting (C.9) in (C.10) we find

$$\frac{1}{3(\epsilon^2 - a)} = \left(-\frac{X_0Y_0Z_0}{J} \right) \frac{1}{(X_0^2Y_0^2 + Y_0^2Z_0^2 + Z_0^2X_0^2)}. \tag{C.11}$$

With the aid of (C.11) we may finally write the equations (C.8) as

$$\frac{\partial \epsilon}{\partial x} + \frac{A}{\sqrt{6}} = \left(\frac{3A}{\sqrt{6}} \right) \frac{Y_0^2Z_0^2}{(X_0^2Y_0^2 + Y_0^2Z_0^2 + Z_0^2X_0^2)}$$

$$\frac{\partial \epsilon}{\partial y} = \left(\frac{\sqrt{3}\, A}{\sqrt{6}} \right) \frac{X_0^2(Z_0^2 - Y_0^2)}{(X_0^2Y_0^2 + Y_0^2Z_0^2 + Z_0^2X_0^2)}. \tag{C.12}$$

APPENDIX D. CALCULATION OF THE VECTOR POTENTIAL $\mathbf{A}(x, y)$

In this appendix we shall first demonstrate that although the ratios (2.11) and the requirement that

$$\sum_p | C_p |^2 = 1$$

do not completely specify the C_p's, no physically significant arbitrariness results since, as we shall show, the arbitrariness in the choice of the C_p's is equivalent to the choice of the gauge of the vector potential and hence does not affect the effective magnetic field $\mathbf{H}(x, y) = \text{curl } \mathbf{A}(x, y)$. We shall then proceed to calculate the vector potential for a particularly convenient choice of gauge.

To begin, let us write

$$C_p = R_p \exp(i\theta_p), \tag{D.1}$$

where R_p and θ_p are real functions of x and y. The vector potential (2.20) is then

$$\begin{aligned} \mathbf{A} &= \frac{1}{i}\left(\frac{c\hbar}{e}\right) \sum_{p=1}^{3} C_p^* \operatorname{grad}_r C_p \\ &= \frac{1}{i}\left(\frac{c\hbar}{e}\right) \sum_{p=1}^{3} (\tfrac{1}{2} \operatorname{grad}_r R_p^2 + iR_p^2 \operatorname{grad}_r \theta_p). \end{aligned} \tag{D.2}$$

Noting that

$$\sum_p | C_p |^2 = \sum_p R_p^2 = 1,$$

the summation and differentiation may be reversed to yield

$$\mathbf{A} = \frac{c\hbar}{e} \sum_{p=1}^{3} R_p^2 \operatorname{grad}_r \theta_p , \tag{D.3}$$

which is manifestly real. Now defining the relative phases

$$\phi_{pp'} \equiv \theta_p - \theta_{p'} , \tag{D.4}$$

we have

$$\mathbf{A} = \frac{c\hbar}{e} \sum_p (R_p^2 \operatorname{grad}_r \phi_{pp'}) + \frac{c\hbar}{e} \operatorname{grad}_r \theta_{p'} . \tag{D.5}$$

Therefore the magnetic field, curl $\mathbf{A}$, depends only on the relative phases of the C_p's, the choice of $\theta_{p'}$ being equivalent to the choice of a gauge.

We shall now proceed to demonstrate that choosing C_1 to be real, that is $\theta_1 = 0$, corresponds to the choice of a vector potential in which the x-component of A vanishes: $A_x = 0$. We begin by investigating the relative phases ϕ_{21} and ϕ_{31} which we find from (2.11) to satisfy the following equations:

[In fact, the ratios of the C_p's (2.11) may be written as

$$\frac{C_2}{C_1} = \frac{|X|}{|Y|}\left[\frac{XY}{|X||Y|}\frac{\exp(i\alpha_{23})}{\exp(i\alpha_{13})}\right],$$
$$\frac{C_3}{C_1} = \frac{|X|}{|Z|}\left[\frac{X^*Z^*}{|X||Z|}\frac{\exp(i\alpha_{32})}{\exp(i\alpha_{12})}\right]. \text{]}$$

$$\exp[i(\phi_{21} + \alpha_{13} - \alpha_{23})] = \frac{XY}{|XY|}$$
$$\exp[i(\phi_{31} + \alpha_{12} - \alpha_{32})] = \frac{X^*Z^*}{|XZ|}. \tag{D.6}$$

To proceed, we note that the transformation

$$x \to x, \qquad y \to -y \tag{D.7}$$

produces the following replacements:

$$X \to X, \qquad Y \to Z, \qquad Z \to Y. \tag{D.8}$$

Furthermore, discarding the constant contributions to ϕ_{21} and ϕ_{31}, since they do not affect A (D.5), we see from (D.6) that the replacement of y by $-y$ converts ϕ_{21} to $-\phi_{31}$ and ϕ_{31} to $-\phi_{21}$. Introducing this transformation (y to $-y$) into (D.5) with $\theta_1 = 0$, we find that the components of the vector potential satisfy the relations

$$A_x(x, y) = -A_x(x, -y)$$
$$A_y(x, y) = A_y(x, -y). \tag{D.9}$$

From these relationships it follows that the magnetic field $\mathbf{H}(x, y)$, oriented in the positive z-direction with the magnitude[50]

$$H(x, y) = \frac{\partial A_y(x, y)}{\partial x} - \frac{\partial A_x(x, y)}{\partial y}, \tag{D.10}$$

[50] It may be recalled from Sec. II that C_p is independent of z and hence, as is immediately clear from (D.2), $A_z = 0$. Furthermore the fact that the C_p's are independent of z implies that A_x and A_y are only functions of x and y, i.e., $\partial A_x/\partial z = \partial A_y/\partial z = 0$. Therefore the magnetic field $\mathbf{H} = \text{curl } \mathbf{A}$ has only the z-component given by (D.10).

is an even function of y, i.e., $H(x, y) = H(x, -y)$. Therefore if we observe the field in the inverted coordinate system (obtained by rotating our coordinate system by π about the x-axis) that is, the system in which

$$x_r = x, \qquad y_r = -y, \qquad z_r = -z \tag{D.11}$$

(where the subscript r refers to the rotated coordinate system), the magnetic field will be directed in the positive z_r-direction with the magnitude $H_r = -H$. We further note that the components of **A** in the rotated coordinate system obey the relations

$$\begin{aligned} A_{x_r}(x_r, y_r) &= A_x(x, -y) \\ A_{y_r}(x_r, y_r) &= -A_y(x, -y). \end{aligned} \tag{D.12}$$

We may utilize the symmetry relationships (D.9) to rewrite (D.12) as

$$\begin{aligned} A_{x_r}(x_r, y_r) &= -A_x(x, y) \\ A_{y_r}(x_r, y_r) &= -A_y(x, y). \end{aligned} \tag{D.13}$$

In the rotated system the z_r-component of the magnetic field, curl **A**, is

$$H_r = (\partial A_{y_r}/\partial x_r) - (\partial A_{x_r}/\partial y_r),$$

which with (D.11) and (D.13) becomes

$$H_r = -(\partial A_y/\partial x) - (\partial A_x/\partial y). \tag{D.14}$$

Requiring that $H_r = -H$ we conclude that $(\partial A_x/\partial y) = 0$ for all x and y, that is, A_x must be independent of y. However, we have already shown by (D.9) that A_x must be odd in y. The only way to meet both of these requirements is for A_x to vanish, i.e.,

$$A_x = 0.$$

In proceeding to calculate A_y with this choice of gauge, we write

$$C_2 = \beta_2 C_1, \qquad C_3 = \beta_3 C_3, \tag{D.15}$$

where

$$C_1^2 = \frac{1}{1 + |\beta_2|^2 + |\beta_3|^2}$$

and

$$\beta_2 = \frac{X}{Y^*}\frac{\exp(i\alpha_{23})}{\exp(i\alpha_{13})}, \qquad \beta_3 = \frac{X^*}{Z}\frac{\exp(i\alpha_{32})}{\exp(i\alpha_{12})}. \tag{D.16}$$

Noting that the vector potential is real, we may proceed to write

$$\begin{aligned} A_y &= \left(\frac{e\hbar}{ci}\right)\sum_{p=1}^{3} C_p^*\frac{\partial C_p}{\partial y} = \left(\frac{e\hbar}{c}\right)\mathrm{Im}\left(\sum_{p=1}^{3} C_p^*\frac{\partial C_p}{\partial y}\right) \\ &= \left(\frac{e\hbar}{c}\right)\mathrm{Im}\left[C_1^2\left(\beta_2^*\frac{\partial\beta_2}{\partial y} + \beta_3^*\frac{\partial\beta_3}{\partial y}\right)\right], \end{aligned} \tag{D.17}$$

where the totally real term $(\partial C_1^2/\partial y)/2C_1^2$ has been dropped from the square brackets. Inserting the explicit expressions for the β's, we find

$$\begin{aligned} A_y &= \left(\frac{c\hbar}{e}\right)C_1^2\,\mathrm{Im}\left[\frac{X^*}{Y}\frac{\partial}{\partial y}\left(\frac{X}{Y^*}\right) + \frac{X}{Z^*}\frac{\partial}{\partial y}\left(\frac{X^*}{Z}\right)\right] \\ &= \left(\frac{c\hbar}{e}\right)C_1^2\,\mathrm{Im}\left(\frac{X^*}{|Y|^2}\frac{\partial X}{\partial y} + \frac{X}{|Z|^2}\frac{\partial X^*}{\partial y} - \frac{|X|^2}{|Y|^4}\frac{Y\partial Y^*}{\partial y} - \frac{|X|^2}{|Z|^4}\frac{Z^*\partial Z}{\partial y}\right). \end{aligned} \tag{D.18}$$

In order to evaluate (D.18) we recall from (2.10) and (2.17) that

$$\begin{aligned} X &= \epsilon(x, y) - \frac{A}{\sqrt{6}}(2x) - Je^{-i\alpha} \\ Y &= \epsilon(x, y) + \frac{A}{\sqrt{6}}(x - \sqrt{3}y) - Je^{-i\alpha} \\ Z &= \epsilon(x, y) + \frac{A}{\sqrt{6}}(x + \sqrt{3}y) - Je^{-i\alpha} \end{aligned} \tag{D.19}$$

and furthermore that

$$\begin{aligned} \frac{\partial X}{\partial y} &= \frac{\partial\epsilon}{\partial y} \\ \frac{\partial Y}{\partial y} &= \frac{\partial\epsilon}{\partial y} - \frac{A\sqrt{3}}{\sqrt{6}} \\ \frac{\partial Z}{\partial y} &= \frac{\partial\epsilon}{\partial y} + \frac{A\sqrt{3}}{\sqrt{6}}. \end{aligned}$$

Noting in addition that

$$\mathrm{Im}(X) = \mathrm{Im}(Y) = \mathrm{Im}(Z) = J\sin\alpha,$$

we rewrite (D.18) as

$$A_y = \left(\frac{c\hbar}{e}\right) C_1^2 J \sin\alpha \left[\frac{\partial\epsilon}{\partial y}\left(\frac{1}{|Z|^2} - \frac{1}{|Y|^2} + \frac{|X|^2}{|Z|^4} - \frac{|X|^2}{|Y|^4}\right)\right.$$
$$\left. + \frac{A\sqrt{3}}{\sqrt{6}}\left(\frac{|X|^2}{|Y|^4} + \frac{|X|^2}{|Z|^4}\right)\right]$$
$$= \left(\frac{c\hbar}{e}\right) C_1^2 J \sin\alpha \left\{\frac{\partial\epsilon}{\partial y}\left(\frac{|Y|^2 - |Z|^2}{|Y|^4 |Z|^4}\right)(|Y|^2|Z|^2 + |X|^2|Y|^2 + |X|^2|Z|^2)\right.$$
$$\left. + \frac{A\sqrt{3}}{\sqrt{6}}\left[\frac{|X|^2(|Z|^4 + |Y|^4)}{|Y|^4|Z|^4}\right]\right\}. \tag{D.20}$$

Since α is proportional to the infinitesimal magnetic field, $\sin\alpha$ may be replaced by α outside the curly brackets and α set equal to zero within the curly brackets. In Appendix C it is shown that

$$\frac{\partial\epsilon}{\partial y} = \left(\frac{A\sqrt{3}}{\sqrt{6}}\right)\frac{X_0^2(Z_0^2 - Y_0^2)}{X_0^2Y_0^2 + Y_0^2Z_0^2 + Z_0^2X_0^2} \tag{C.12}$$

where the subscript zero denotes the fact that α has been set equal to zero. Inserting (C.12) into (D.20) we obtain

$$A_y = \left(\frac{c\hbar\alpha}{e}\right)\left(J\frac{A\sqrt{3}}{\sqrt{6}}\right) C_1^2 \left(\frac{2X_0^2}{Y_0^2Z_0^2}\right). \tag{D.21}$$

Noting from (D.15) that

$$C_1^2 = \frac{Y_0^2Z_0^2}{X_0^2Y_0^2 + Y_0^2Z_0^2 + Z_0^2X_0^2},$$

we may finally rewrite (D.21) as

$$A_y = \left(\frac{c\hbar\alpha}{e}\right)(JA\sqrt{2})\left(\frac{X_0^2}{X_0^2Y_0^2 + Y_0^2Z_0^2 + Z_0^2X_0^2}\right). \tag{D.22}$$

APPENDIX E. Calculation of the Effective Magnetic Field $H(x, y)$

Using the results of Appendix D, we can readily calculate the magnetic field, $\mathbf{H}(x, y) = \text{curl } \mathbf{A}$. Choosing the gauge in which $A_x = 0$, it is simply

$$H(x, y) = \frac{\partial A_y}{\partial x}(x, y), \tag{E.1}$$

where A_v is given by (D.22). Performing the differentiation we find

$$H(x, y) = \left(\frac{c\hbar\alpha}{e}\right)(JA\sqrt{2})\left[\frac{2}{[X_0^2Y_0^2 + Y_0^2Z_0^2 + Z_0^2X_0^2]^2}\right] \times \left[X_0Y_0^2Z_0^2\frac{\partial X_0}{\partial x} - X_0^2Y_0(X_0^2 + Z_0^2)\frac{\partial Y_0}{\partial x} - X_0^2Z_0(X_0^2 + Y_0^2)\frac{\partial Z_0}{\partial x}\right]. \tag{E.2}$$

Equation (E.2) may be further simplified by noting from (D.19) that

$$\frac{\partial Y_0}{\partial x} = \frac{\partial Z_0}{\partial x} = \frac{\partial \epsilon}{\partial x} + \frac{A}{\sqrt{6}}$$

and

$$\frac{\partial X_0}{\partial x} = \frac{\partial Y_0}{\partial x} - \frac{3A}{\sqrt{6}},$$

and hence from (C.12) that

$$\frac{\partial X_0}{\partial x} = -\left(\frac{3A}{\sqrt{6}}\right)\frac{X_0^2[Y_0^2 + Z_0^2]}{[X_0^2Y_0^2 + Y_0^2Z_0^2 + Z_0^2X_0^2]}$$

$$\frac{\partial Y_0}{\partial x} = \left(\frac{3A}{\sqrt{6}}\right)\frac{Y_0^2Z_0^2}{[X_0^2Y_0^2 + Y_0^2Z_0^2 + Z_0^2X_0^2]},$$

to yield

$$H(x, y) = \left(\frac{c\hbar\alpha}{e}\right)(JA\sqrt{2})\left[\frac{-2(X_0Y_0Z_0)^2}{[X_0^2Y_0^2 + Y_0^2Z_0^2 + Z_0^2X_0^2]^3}\right]\left(\frac{3A}{\sqrt{6}}\right) \times \{X_0(Y_0^2 + Z_0^2) + Y_0(X_0^2 + Z_0^2) + Z_0(X_0^2 + Y_0^2)\}$$

$$= \left(\frac{c\hbar\alpha}{e}\right)(JA^2\sqrt{3})\left[\frac{-2(X_0Y_0Z_0)^2}{(X_0^2Y_0^2 + Y_0^2Z_0^2 + Z_0^2X_0^2)^3}\right] \times \{X_0Y_0(X_0 + Y_0) + Y_0Z_0(Y_0 + Z_0) + Z_0X_0(Z_0 + X_0)\}. \tag{E.3}$$

From (D.19) we observe the identity

$$X_0 + Y_0 + Z_0 = 3(\epsilon - J),$$

which when inserted into the curly bracketed term of (E.3) transforms it to

$$\{3[(X_0Y_0 + Y_0Z_0 + Z_0Y_0)(\epsilon - J) - X_0Y_0Z_0]\}.$$

Furthermore, observing that the eigenvalue equation, (2.15), when rewritten in terms of X_0, Y_0, and Z_0, is

$$X_0Y_0 + Y_0Z_0 + Z_0X_0 = -\frac{X_0Y_0Z_0}{J},$$

the curly bracketed term becomes

$$\frac{-3\epsilon(X_0Y_0Z_0)}{J}.$$

The magnetic field may now be written as

$$H(x, y) = \mathbf{H} \cdot \mathbf{A}_{321}(6\sqrt{3}A^2)(-\epsilon)\left(\frac{-X_0Y_0Z_0}{X_0^2Y_0^2 + Y_0^2Z_0^2 + Z_0^2X_0^2}\right)^3. \quad \text{(E.4)}$$

Finally, using the identity (C.11) with the definition of a (3.3), we have for the effective magnetic field:

$$H(x, y) = \mathbf{H} \cdot \mathbf{A}_{321}\left(\frac{A}{J\sqrt{6}}\right)^2\left(\frac{2^2}{\sqrt{3}}\right)\frac{(-\epsilon/J)}{[(\epsilon/J)^2 - (A/J\sqrt{6})^2(x^2 + y^2) - 1]^3}. \quad \text{(3.7)}$$

[$H(x, y)/\mathbf{H} \cdot \mathbf{A}_{321}$ is a finite positive definite quantity as may be seen by noting that ϵ is always negative (hence the numerator $-\epsilon/J$ is positive) and that the denominator of (3.7) may be rewritten [with the aid of (3.1) and (3.3)] as the positive definite quantity

$$a^3\left[4\cos^2\left(\frac{\phi}{3} + \frac{2\pi}{3}\right) - 1\right]^3,$$

where $0 < \phi \leqslant \pi$. (The fact that $\phi > 0$ can be seen from (3.2) when it is noted from (B.4) that $a^{3/2} > -b$ for all x and y.)]

APPENDIX F. Calculation of the Total Flux Through the xy-Plane

The results of Appendix D are now used in the calculation of the total flux through the xy-plane, namely,

$$\int dx \int dy\, H(x, y) = \oint \mathbf{A} \cdot d\mathbf{l}. \quad \text{(F.1)}$$

Choosing the rectangular contour shown in Fig. 27, the total flux Φ^{total} is given by

$$\Phi^{\text{total}} = \lim_{d\to\infty}\left[\int_{\sqrt{3}d}^{-\sqrt{3}d} dy\, A_y(-d, y) + \int_{-\sqrt{3}d}^{\sqrt{3}d} dy\, A_y(d, y)\right]. \quad \text{(F.2)}$$

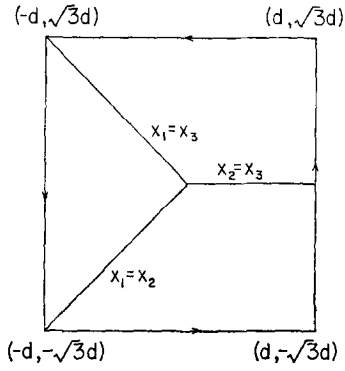

FIG. 27. Contour for the calculation of the total flux through the $x - y$ plane.

To proceed with the calculation let us first note from (D.19) that we may write

$$X_0 = \epsilon - \frac{A}{\sqrt{6}}(2x) - J$$

$$Y_0 = \epsilon + \frac{A}{\sqrt{6}}(x - \sqrt{3}y) - J$$

$$Z_0 = \epsilon + \frac{A}{\sqrt{6}}(x + \sqrt{3}y) - J, \tag{F.3}$$

where the subscript zero denotes the fact that in the expressions for X, Y, and Z, α is taken to be zero. With Eqs. (F.3) we utilize the fact that in region 1 away from the coincidence line ($y^2 \ll 3d^2$) we have

$$\epsilon(x, y) \simeq \frac{A}{\sqrt{6}}(2x)$$

to write that

$$X_0 \simeq -J$$

$$Y_0 \simeq \frac{A}{\sqrt{6}}(3x - \sqrt{3}y) - J$$

$$Z_0 \simeq \frac{A}{\sqrt{6}}(3x + \sqrt{3}y) - J \tag{F.4}$$

in region 1 far from the coincidence lines. Inserting (F.4) in (D.22), we find that in region 1

$$A_y(-d, y) \cong \left(\frac{c\hbar\alpha}{e}\right)(JA\sqrt{2})\frac{2^2J^2}{3^2(Ad)^4[1 - (y^2/3d^2)]^2}. \tag{F.5}$$

In addition, along the coincidence line $y = \pm\sqrt{3}x$ in region 1

$$\epsilon(x, \pm\sqrt{3}x) = \frac{2Ax}{\sqrt{6}} - J,$$

so that

$$A_y(-d, \pm\sqrt{3}d) = \left(\frac{c\hbar\alpha}{e}\right)(JA\sqrt{2})\frac{1}{6(Ad)^2}. \tag{F.6}$$

We can see from (F.5) and (F.6) that as d tends to infinity, A_y decreases sufficiently fast so that

$$\lim_{d\to\infty} \int_{d\sqrt{3}}^{-d\sqrt{3}} A_y(-d, y)\, dy = 0.$$

Proceeding to calculate the other contribution to (F.2), it is recalled [Eq. (3.5)] that for large positive x, $x \gg J\sqrt{6}/A$,

$$\epsilon(x, y) = \frac{-Ax}{\sqrt{6}} - [3(Ay/\sqrt{6})^2 + J^2]^{1/2}.$$

Furthermore, from (F.3) we see that for large positive x, $X_0^2(Y_0^2 + Z_0^2) \gg Y_0^2 Z_0^2$, and therefore we may write that

$$A_y(x, y) = \left(\frac{c\hbar\alpha}{e}\right)(JA\sqrt{2})\frac{1}{Y_0^2 + Z_0^2}, \tag{F.7}$$

where

$$Y_0 = -J\{[1 + (Ay/J\sqrt{2})^2]^{1/2} + (Ay/J\sqrt{2}) + 1\}$$
$$Z_0 = -J\{[1 + (Ay/J\sqrt{2})^2]^{1/2} - (Ay/J\sqrt{2}) + 1\}.$$

Inserting (F.7) in (F.2), the total flux becomes

$$\begin{aligned}\Phi^{\text{total}} &= \left(\frac{c\hbar\alpha}{e}\right)\frac{JA\sqrt{2}}{4J^2}\int_{-\infty}^{\infty}\frac{dy}{\{1 + (Ay/J\sqrt{2})^2 + [1 + (Ay/J\sqrt{2})^2]^{1/2}\}} \\ &= \left(\frac{c\hbar\alpha}{e}\right)\frac{1}{2}\int_{-\infty}^{\infty}\frac{du}{\{1 + u^2 + [1 + u^2]^{1/2}\}} \\ &= \left(\frac{c\hbar\alpha}{e}\right) = \mathbf{H}\cdot\mathbf{A}_{321}.\end{aligned} \tag{F.8}$$

Thus the total flux through the $x - y$ plane is just equal to the total flux through the triangle formed by the three basic lattice sites.

APPENDIX G. LIMITING TRAJECTORIES FOR $E > -2J$ AND $E < -2J$

It is the purpose of this appendix to elucidate the behavior of the limiting trajectories. As a first step, we shall restrict our considerations to the triangular pyramid described by (3.4). This model, henceforth referred to as the pyramidal model, ignores the rounding of the edges of the pyramid. Strictly speaking, the absence of such rounding in the pyramidal model results in an unphysical discontinuity in the force field, $\mathscr{F} = \text{grad}_r\, \epsilon(x, y)$, along the coincidence lines, while the exact potential leads to a completely continuous force field. In fact, the exact expression for $\epsilon(x, y)$ yields no component of the force perpendicular to a coincidence line along such a line, thereby enabling a "particle" once on a coincidence line to remain on the line. With this in mind we shall augment the pyramidal model, described by Eqs. (3.4), by the stipulation that once a limiting trajectory achieves tangency to one of the coincidence lines, it will remain tangent to the coincidence line.[51]

Figure 28 illustrates the class of trajectories which we shall now consider, namely, trajectories which originate in region 1, cross the $x_1 = x_2$ coincidence line, and are tangent to the $x_2 = x_3$ coincidence line. Utilizing the pyramidal expression (3.4) for $\epsilon(x, y)$ in region 2, the energy of a trajectory at (x, y) in region 2 is

$$E = \frac{M}{2}(v_x^2 + v_y^2) - \frac{A}{\sqrt{6}}(x - \sqrt{3}y) \tag{G.1}$$

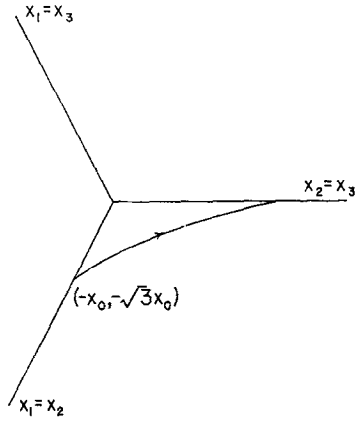

FIG. 28. A typical trajectory which achieves tangency to the $x_2 = x_3$ coincidence line and originates in region 1.

[51] This ansatz will be justified by comparison with a more exact but also more complex treatment of the classical motion.

where v_x and v_y are the velocity components at (x, y). We may rewrite (G.1) as

$$E_x = \frac{M}{2} v_x^2 - \frac{A}{\sqrt{6}} x$$

$$E_y = \frac{M}{2} v_y^2 + \frac{A\sqrt{3}}{\sqrt{6}} y, \tag{G.2}$$

where $E = E_x + E_y$. Restricting our attention to those trajectories which are tangent to the $x_2 = x_3$ coincidence line ($y = 0$), we set $E_y = 0$ so that $v_y = 0$ when $y = 0$. The velocity components of a limiting trajectory at any point in region 2 are[52]

$$v_x = \left\{\frac{2}{M}[E + (Ax/\sqrt{6})]\right\}^{1/2}$$

$$v_y = \left\{\frac{2}{M}[-(A\sqrt{3}/\sqrt{6})y]\right\}^{1/2}. \tag{G.3}$$

At a point $(-x_0, -\sqrt{3}x_0)$, $(x_0 > 0)$ on the $x_1 = x_2$ coincidence line they become

$$v_x = \left\{\frac{2}{M}[E - (Ax_0/\sqrt{6})]\right\}^{1/2}$$

$$v_y = \left\{\frac{2}{M}(3Ax_0/\sqrt{6})\right\}^{1/2}. \tag{G.4}$$

It is clear from (G.4) that the slope of the trajectory $dy/dx = v_y/v_x$ at $(-x_0, -\sqrt{3}x_0)$ increases as the energy E decreases. However, since we are only interested in trajectories originating in region 1 (not in region 2), we demand that

$$\left.\frac{v_y}{v_x}\right|_{(-x_0, -\sqrt{3}x_0)} \leqslant \sqrt{3}, \tag{G.5}$$

where $\sqrt{3}$ is the slope of the $x_1 = x_2$ line, $y = \sqrt{3}\,x$. Thus the trajectory which is tangent to the $x_1 = x_2$ line as well as the $x_2 = x_3$ line possesses the minimum energy with which a trajectory can originate in region 1, cross the $x_1 = x_2$ line at $(-x_0, -\sqrt{3}x_0)$, and be tangent to the $x_2 = x_3$ line. This minimum energy, found by requiring that $v_y/v_x\,|_{(-x_0, -\sqrt{3}x_0)} = \sqrt{3}$, is

$$E_{\min} = \frac{2Ax_0}{\sqrt{6}}. \tag{G.6}$$

[52] These equations may be integrated (and time eliminated as a parameter) to find an explicit expression for a limiting trajectory, which is, in this model, a parabola.

Hence for the pyramidal model the lowest energy trajectory which can originate in region 1 and be tangent to the $x_2 = x_3$ line, passes through the origin and has $E_{\min} = 0$, the potential energy of the peak. For the exact function $\epsilon(x, y)$, the potential energy of the peak, $\epsilon(0, 0) = -2J$, can be seen to be the minimum possible energy for such a limiting curve. Furthermore, in general, as in the case of the pyramidal model, the distance of closest approach for a doubly tangent trajectory increases with energy.

Another class of limiting trajectory, illustrated in Fig. 29, is that which originates in region 1 and achieves tangency to the $x_1 = x_3$ coincidence line. At a given energy E, above the energy of the peak, there is a trajectory which is tangent to both the $x_1 = x_3$ and $x_1 = x_2$ coincidence lines at $(-x_0, \sqrt{3}x_0)$ and $(-x_0, -\sqrt{3}x_0)$, respectively. Such a doubly tangent trajectory is the rotated version (by 120°) of the trajectory which is tangent to the $x_1 = x_2$ and $x_2 = x_3$ lines and has energy $E = 2Ax_0/\sqrt{6}$. Similarly, a doubly tangent trajectory terminating at $(-x_0', \sqrt{3}x_0')$ has an energy equal to $2Ax_0'/\sqrt{6}$. At energies above this energy a tangential trajectory at $(-x_0', \sqrt{3}x_0')$ cannot originate in region 1, while for energies below $2Ax_0'/\sqrt{6}$ it must originate in region 1. Thus at energy $E = 2Ax_0/\sqrt{6}$, $x_0 > 0$ trajectories tangent to the $x_1 = x_3$ line at $(-x_0', \sqrt{3}x_0')$ only originate in region 1 for values of x_0' greater than x_0. In general, the trajectory tangent to both the $x_1 = x_3$ and $x_1 = x_2$ lines bounds the region spanned by trajectories originating in region 1 which are tangent to the $x_1 = x_3$ line and those which, while tangent to the $x_1 = x_3$ line, originate outside of region 1.

We have shown that for a trajectory to be tangent to the $x_2 = x_3$ coincidence line and to originate in region 1, it must have an energy greater than the potential

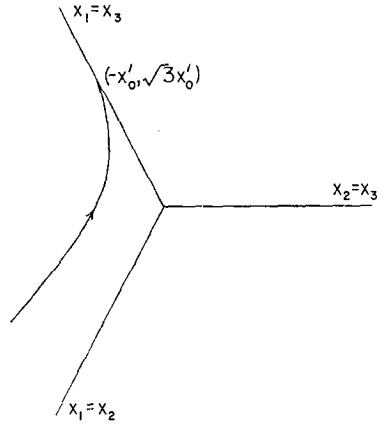

FIG. 29. A typical trajectory which achieves tangency to the $x_1 = x_3$ coincidence line and originates in region 1.

energy of the peak. It is now our task to investigate the limiting trajectories at energies below that of the peak. A trajectory in this energy range can only reach region 3 from region 1 by crossing the $x_1 = x_3$ line. We now proceed to demonstrate, for the pyramidal model, that from a point in region 1 trajectories of energy E below the peak energy which cross into region 3 must lie between two limiting trajectories which are both tangent to the $x_1 = x_3$ line, as shown in Fig. 10.

Let us consider trajectories which pass through a point $(-d, y_0)$ on the reference line $x = -d$, where y_0 is taken so that the point lies in region 1. Taking the negative gradient of the pyramidal expression for $\epsilon(x, y)$ in region 1, namely (3.4), the following equations of motion are found:

$$\begin{aligned} M\ddot{x} &= -Ma' \\ M\ddot{y} &= 0, \end{aligned} \tag{G.7}$$

where $a' \equiv 2A/M\sqrt{6}$. Equations (G.7) are identical with those associated with the classical projectile problem and lead to the following parabolic trajectory:

$$(x + d) = v_{x0}\left(\frac{y - y_0}{v_{y0}}\right) - \frac{a'}{2}\left(\frac{y - y_0}{v_{y0}}\right)^2, \tag{G.8}$$

where the velocity at $(-d, y_0)$ has components v_{x0} and v_{y0}. For this trajectory to cross the $x_1 = x_3$ line, $y = -\sqrt{3}x$, the initial velocities must satisfy the relation (found by substituting $-\sqrt{3}x$ for y in (G.8) and demanding a real solution for x):

$$(v_{x0}\sqrt{3} + v_{y0})^2 - \frac{2 \cdot 3}{\sqrt{3}} a'(\sqrt{3}d - y_0) \geqslant 0, \tag{G.9}$$

while to achieve tangency with the $y = -\sqrt{3}x$ line (that is, to have only one point of intersection with it)

$$(v_{x0}\sqrt{3} + v_{y0}) = \pm\left[\frac{2 \cdot 3}{\sqrt{3}} a'(\sqrt{3}d - y_0)\right]^{1/2}. \tag{G.10}$$

Noting that the energy of any trajectory is given by

$$E = \frac{M}{2}(v_{x0}^2 + v_{y0}^2) - Mad \tag{G.11}$$

and writing the velocities in terms of the energy and the initial angle of the trajectory with the x-axis, (G.10) becomes

$$\sin[\theta_i + (\pi/3)] = \pm\frac{\left[\frac{3}{2\sqrt{3}} a'(\sqrt{3}d - y_0)\right]^{1/2}}{|v|}, \tag{G.12}$$

where

$$v_x = |v| \cos \theta_i$$

$$v_y = |v| \sin \theta_i$$

$$|v| = \left[\frac{2}{M}(E + Ma'd)\right]^{1/2}.$$

The initial slope of a tangential trajectory is given by $\tan \theta_i$. Rewriting (G.12) as

$$\theta_i = -\frac{\pi}{3} \pm \sin^{-1}\frac{u}{|v|}, \tag{G.13}$$

where

$$u \equiv \left[\frac{3}{2\sqrt{3}}a'(\sqrt{3}d - y_0)\right]^{1/2}, \tag{G.14}$$

we find the initial slope:

$$\tan \theta_i = \frac{-\sqrt{3}(v^2 - u^2)^{1/2} \pm u}{(v^2 - u^2)^{1/2} \pm \sqrt{3}u}. \tag{G.15}$$

Thus for $v^2 > u^2$ there are two initial slopes with which a particle with energy E crossing the reference line at $(-d, y_0)$ can achieve tangency to the $x_1 = x_3$ coincidence line,[53] while for $v^2 = u^2$ there is only one such initial slope and for $v^2 < u^2$ there is none. From (G.9) and (G.12) and (G.14) we see that for trajectories to cross the $x_1 = x_3$ line

$$\sin^2[\theta_i + (\pi/3)] > (u/v)^2. \tag{G.16}$$

This restricts the trajectories that cross to a range of initial angles bounded by two tangential trajectories.[54] This situation is illustrated in Fig. 30 in which the limiting trajectories shown display the asymptotic approach to tangency that is associated with the rounding of the edges.

Having discussed the pyramidal model in detail we must now comment about the relationship of the pyramidal model to the exact situation. The basic deficiency of

[53] A unique situation arises for $u = 0$, that is, for the initial point $(-d, \sqrt{3}d)$ lying on the $x_1 = x_3$ coincidence line, since the two initial velocities $[v_{x0} = v/2, v_{y0} = -(\sqrt{3}/2)v$ and $v_{x0} = -v/2, v_{y0} = (\sqrt{3}/2)v]$ correspond to the same tangential trajectory.

[54] Clearly, for $(u/v)^2 = 1$ only one trajectory can be in this range, that for $\theta_i = \pi/6$. For $(u/v)^2 = 0$, $(y_0 = \sqrt{3}d)$ all trajectories except one, $\theta_i = -\pi/3$, cross to region 3.

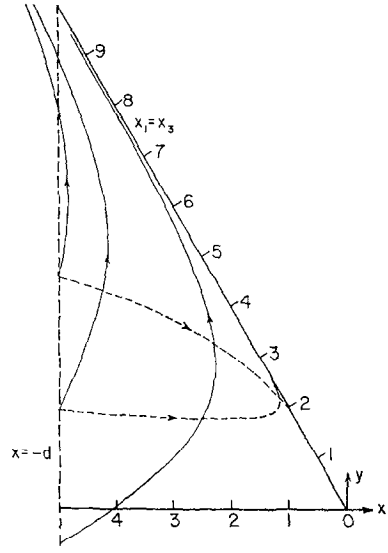

FIG. 30. The limiting trajectories at $E = -3J$ (an energy below the peak energy $-2J$) derived from the potential of (3.5). Length is measured in units of $J\sqrt{6}/A$.

the pyramidal model is the necessity of introducing the ansatz that once a "particle" achieves tangency to a coincidence line it remains on the coincidence line. This is an artificial way of approximating an asymptotic approach to the coincidence line. An improved approximation for $\epsilon(x, y)$ in regions 2 and 3 which permits the asymptotic approach to a coincidence line is[55]

$$\epsilon(x, y) = -\frac{Ax}{\sqrt{6}} - [3(Ay/\sqrt{6})^2 + J^2]^{1/2}. \tag{3.5}$$

With this choice for $\epsilon(x, y)$ in regions 2 and 3 all of the arguments and results of our discussion of the pyramidal model can be maintained. We take this fact as verification of the tangency ansatz of the pyramidal model.

The conclusions that are drawn from the results of this appendix are presented at the beginning of Sec. VI and form the basis of the analysis of that section.

[55] An expression for the associated trajectories which asymptotically approach the $x_2 = x_3$ line ($y = 0$) is given by (7.8). Tangential trajectories obtained from (3.5) for an energy $E = -3J$ (below the potential energy of the peak) are plotted in Fig. 30. Some tangential trajectories at energies above the peak energy are plotted in Fig. 16.

APPENDIX H. CALCULATION OF THE PARTITION FUNCTION Z

We shall evaluate the velocity partition function Z arising from the consideration of motion in the xy plane. In general we may write

$$Z = \int_{-\infty}^{\infty} dv_x \int_{-\infty}^{\infty} dv_y \int_{-\infty}^{0} dx \int_{+\sqrt{3}x}^{-\sqrt{3}x} dy \exp\left\{-\frac{1}{kT}\left[\frac{M}{2}(v_x^2 + v_y^2) + V(x, y)\right]\right\}, \tag{H.1}$$

where

$$V(x, y) = \frac{M}{2}\omega_0^2(x^2 + y^2) + \epsilon(x, y)$$

and $\epsilon(x, y)$ manifests the threefold symmetry of the problem. As mentioned in Sec. 3, the total potential $V(x, y)$ consists of three displaced two-dimensional harmonic oscillator potential wells of depth $A^2/3M\omega_0^2$. For $A^2/2M\omega_0^2 \ll 2J$, the small polaron condition, the effect of the rounding may be neglected so that in region 1 the appropriate potential energy function is

$$\frac{M}{2}\omega_0^2(x^2 + y^2) + \frac{2Ax}{\sqrt{6}} = \frac{M}{2}\omega_0^2\left[\left(x + \frac{2A}{\sqrt{6}\,M\omega_0^2}\right)^2 + y^2\right] - \frac{A^2}{3M\omega_0^2}.$$

Then

$$\begin{aligned} Z = {} & \int_{-\infty}^{\infty}\int dv_x\, dv_y \exp\left\{-\frac{1}{kT}\left[\frac{M}{2}(v_x^2 + v_y^2)\right]\right\} \int_{-\infty}^{\infty} dx \int_{\sqrt{3}x}^{-\sqrt{3}x} dy \\ & \times \exp\left\{-\frac{1}{kT}\left[(M\omega_0^2/2)(x^2 + y^2) + \frac{2Ax}{\sqrt{6}}\right]\right\} \\ = {} & \left(\frac{2\pi kT}{M}\right)\int_{-\infty}^{0} dx \int_{\sqrt{3}x}^{-\sqrt{3}x} dy \exp\left\{-\frac{1}{kT}\frac{M\omega_0^2}{2}\left[\left(x + \frac{2A}{\sqrt{6}\,M\omega_0^2}\right)^2 + y^2\right]\right\} \\ & \times \exp\{(A^2/3M\omega_0^2)/kT\}. \end{aligned} \tag{H.2}$$

For $kT \ll A^2/3M\omega_0^2$ the major contribution to the spatial integrations comes from the vicinity of the bottom of the well. Hence the limits of integration may be extended to include all space yielding

$$Z = \left(\frac{2\pi kT}{M}\right)\left(\frac{2\pi kT}{M\omega_0^2}\right)\exp\{(A^2/3M\omega_0^2)/kT\}. \tag{H.3}$$

In order to incorporate the effects of the electric field **F**, the replacement

$$\frac{2Ax}{\sqrt{6}} \rightarrow \frac{2A}{\sqrt{6}}\left[x - \frac{e\mathbf{F}\cdot(\mathbf{h}_{31}+\mathbf{h}_{21})}{A\sqrt{6}}\right] = \frac{2Ax}{\sqrt{6}} - \frac{e\mathbf{F}\cdot(\mathbf{h}_{31}+\mathbf{h}_{21})}{3}$$

is made in accordance with the prescription introduced in Sec. I. Hence

$$Z = \left(\frac{2\pi kT}{M}\right)\left(\frac{2\pi kT}{M\omega_0{}^2}\right)\exp\left(\frac{A^2/3M\omega_0{}^2}{kT}\right)\exp\left[\frac{e\mathbf{F}\cdot(\mathbf{h}_{31}+\mathbf{h}_{21})}{3kT}\right]. \quad \text{(H.4)}$$

APPENDIX I.

Calculation of the Field Free Jump Rate w_{13}^0 in the Adiabatic Approximation

In order to calculate the field free contribution of the jump rate from site 1 to site 3 in the adiabatic approximation, we follow the procedure of Sec. II and consider the two equations which contain both a_1 and a_3 : [56]

$$i\hbar\frac{\partial a_1}{\partial t} = (H_L - Ax_1)a_1 - Ja_3$$
$$i\hbar\frac{\partial a_3}{\partial t} = (H_L - Ax_3)a_3 - Ja_1 . \quad \text{(I.1)}$$

In the adiabatic approach, we assume that

$$a_1 = C_1(x_1 \cdots x_n)\,\chi(x_1 \cdots x_n, t)$$
$$a_3 = C_3(x_1 \cdots x_n)\,\chi(x_1 \cdots x_n, t), \quad \text{(I.2)}$$

where the C_p's are solutions of the "electronic" equations

$$(\epsilon + Ax_1)C_1 = -JC_3$$
$$(\epsilon + Ax_3)C_3 = -JC_1 \quad \text{(I.3)}$$

subject to the normalization condition

$$C_1{}^2 + C_3{}^2 = 1. \quad \text{(I.4)}$$

[56] During a direct hop of an electron from site 1 to site 3, only a_1 and a_3 will be substantial, of the order of unity, while all other a_g are much smaller, $\sim J/(A/4M\omega_0{}^2)$. Hence only terms in (2.1) involving a_1 and a_3 are retained. In addition, we have noted that in the field free case all of the phase factors $\alpha_{g,g+h}$ are zero.

The "electronic" energy ϵ the lowest eigenvalue of (I.3), is found to be given by the equation,

$$\epsilon = -\frac{A(x_1 + x_3)}{2} - \left[\frac{A^2(x_1 - x_3)^2}{4} + J^2\right]^{1/2}. \tag{I.5}$$

In terms of the new coordinates

$$\eta = \frac{x_3 - x_1}{\sqrt{2}}$$

$$\zeta = \frac{x_3 + x_1}{\sqrt{2}} \tag{I.6}$$

(I.5) may be rewritten as

$$\epsilon = -\frac{A\zeta}{\sqrt{2}} - \left[\left(\frac{A\eta}{\sqrt{2}}\right)^2 + J^2\right]^{1/2}. \tag{I.7}$$

In addition, it is noted that:

$$Ax_1 = \frac{A\zeta}{\sqrt{2}} + \frac{A\eta}{\sqrt{2}}$$

$$Ax_3 = \frac{A\zeta}{\sqrt{2}} - \frac{A\eta}{\sqrt{2}}. \tag{I.8}$$

Thus we see that $\epsilon + Ax_1$ and $\epsilon + Ax_3$ are only functions of the relative coordinate η and hence C_1 and C_3, found from (I.3), are also only functions of η. In particular, for large negative η site 1 is occupied, $|C_1|^2 \gg |C_3|^2$, and for large positive η site 3 is occupied, $|C_1|^2 \ll |C_3|^2$.

[Solving (I.3) for C_1/C_3 and inserting (I.7) and (I.8) into the result, we find

$$\frac{C_1}{C_3} = \frac{-J}{\epsilon + Ax_1} = \frac{-J}{\frac{A\eta}{\sqrt{2}} + \left[\left(\frac{A\eta}{\sqrt{2}}\right)^2 + J^2\right]^{1/2}}.$$

Thus when $\eta^2 \gg 2J^2/A^2$

$$\frac{C_1}{C_3} \simeq \frac{-J}{A\eta\sqrt{2}} \qquad \text{for} \quad \eta > 0$$

and

$$\frac{C_1}{C_3} = \frac{A\eta\sqrt{2}}{J} \qquad \text{for} \quad \eta < 0.]$$

To find the change of the vibrational relative coordinate η with time, we must consider the vibrational Hamiltonian. In the field free adiabatic approximation, the vibrational Hamiltonian is the sum of the lattice Hamiltonian in the absence of

a carrier plus the electronic energy $\epsilon(\zeta, \eta)$ which acts as the additional potential energy term due to the carrier, namely,

$$H_{\text{vib}} = H_{\text{L}} + \epsilon(\zeta, \eta). \tag{I.9}$$

Since we are interested only in the behavior of η we can ignore all terms in H_{vib} which do not involve η. Thus, ignoring (as has been done throughout this work) the dispersive terms of H_{L}, we have

$$H_{\text{vib}} = \frac{P_\eta^2}{2M} + \frac{M}{2}\omega_0^2\eta^2 - \left[\left(\frac{A\eta}{2}\right)^2 + J^2\right]^{1/2}. \tag{I.10}$$

The potential energy of (I.10) possesses two minima, which for J small compared with $A^2/2M\omega_0^2$ (the small polaron condition), are located at $\eta \simeq \pm A^2/(\sqrt{2}\, M\omega_0^2)$ and have a common depth of $-A^2/4M\omega_0^2$. The barrier between these two minima has a peak of height $-J$ at $\eta = 0$. Thus a jump of a carrier from site 1 to site 3 corresponds to an excursion of a fictitious particle of mass M from the well centered at $\eta = -A^2/(\sqrt{2}\, M\omega_0^2)$ across the barrier to the well centered at $\eta = A^2/(\sqrt{2}\, M\omega_0^2)$.

The rate of such excursions is found by noting that all trajectories which lie between $\eta = v_\eta\, dt (v_\eta = P_\eta/M)$ and $\eta = 0$ cross the barrier within the time interval dt. Thus the field free rate with which carriers hop from site 1 to site 3, w_{13}^0, is

$$w_{13}^0 = \frac{\displaystyle\int_0^\infty dv_\eta\, v_\eta \exp\left(-\frac{M}{2}\frac{v_\eta^2}{kT}\right)\exp(J/kT)}{\displaystyle\int_{-\infty}^{\infty} dv_\eta \exp\left(-\frac{M}{2}\frac{v_\eta^2}{kT}\right)\int_{-\infty}^{0} d\eta \exp\left[-\frac{1}{kT}\left\{\frac{M}{2}\omega_0^2\eta^2 - \left[\left(\frac{A\eta}{\sqrt{2}}\right)^2 + J^2\right]^{1/2}\right\}\right]}. \tag{I.11}$$

Performing the velocity integrations, we have

$$w_{13}^0 = \frac{\dfrac{kT}{M}\, e^{J/kT}}{\left(\dfrac{2\pi kT}{M}\right)^{1/2}\displaystyle\int_{-\infty}^{0} d\eta \exp\left[-\frac{1}{kT}\left\{\frac{M}{2}\omega_0^2\eta^2 - \left[\left(\frac{A\eta}{\sqrt{2}}\right)^2 + J^2\right]^{1/2}\right\}\right]}. \tag{I.12}$$

If we ignore the presence of J^2 in the square bracketed term of (I.11), we may rewrite the curly bracketed term as

$$\frac{M\omega_0^2}{2}\left(\eta + \frac{A}{\sqrt{2}\, M\omega_0^2}\right)^2 - \frac{A^2}{4M\omega_0^2},$$

the potential of a harmonic oscillator well which has its equilibrium point at $\eta = -A/\sqrt{2}\, M\omega_0^2$, and (I.12) as

$$w_{13}^0 = \frac{\frac{kT}{M} \exp\left[-\left(\frac{A^2}{4M\omega_0^2} - J\right)/kT\right]}{\left(\frac{2\pi kT}{M}\right)^{1/2} \int_{-\infty}^{0} d\eta \exp\left\{-\frac{1}{kT}\left[\frac{M\omega_0^2}{2}\left(\eta + \frac{A}{\sqrt{2}\, M\omega_0^2}\right)^2\right]\right\}}. \quad \text{(I.13)}$$

Furthermore, by restricting our considerations to sufficiently low temperatures, $kT \ll A^2/4M\omega_0^2$, the upper limit of the η-integration may be extended to infinity, yielding

$$w_{13}^0 = \frac{\frac{kT}{M} \exp\{-[(A^2/4M\omega_0^2) - J]/kT\}}{\left(\frac{2\pi kT}{M}\right)^{1/2}\left(\frac{2\pi kT}{M\omega_0^2}\right)^{1/2}}$$

$$= (\omega_0/2\pi) \exp\{-[(A^2/4M\omega_0^2) - J]/kT\} \quad \text{(I.14)}$$

for the field-free jump rate from site 1 to site 3.

To justify the approximation (I.13) we note that the presence of J^2 in the integrand of (I.12) manifests itself only in the interval $J/A \gtrsim \eta$, within which the error in the integrand is less than $\exp(-J/kT) - 1$. Therefore, we see that the error in the η-integration of (I.12) due to the neglect of J is of the order of

$$\frac{J}{A}(e^{J/kT} - 1),$$

yielding a fractional error in the η-integration of the order of

$$\frac{\frac{J}{A}(e^{J/kT} - 1)}{\left(\frac{2\pi kT}{M\omega_0^2}\right)^{1/2} \exp[(A^2/4M\omega_0^2)/kT]}$$

$$\lesssim \frac{1}{4}\left[\left(\frac{2J}{A^2/2M\omega_0^2}\right)\frac{J}{kT}\right]^{1/2} \exp\{-[(A^2/4M\omega_0^2) - J]/kT\}.$$

For $2J \ll A^2/2M\omega_0^2$, the small polaron condition, and $A^2/4M\omega_0^2 \gg kT \sim J$ we see that the fractional error is much less than unity, thereby justifying the approximation (I.13).

RECEIVED: December 12, 1968